UNIVERSIDADE DE LISBOA

FACULDADE DE CIÊNCIAS

DEPARTAMENTO DE BIOLOGIA VEGETAL

ANIONIC CURRENTS IN POLLEN GRAIN PROTOPLASTS FROM *Arabidopsis thaliana* AND *Lilium longiflorum*

CORRENTES ANIÓNICAS EM PROTOPLASTOS DE GRÃOS DE PÓLEN DE *Arabidopsis thaliana* E *Lilium longiflorum*

Tese orientada pelo Prof. Doutor José Feijó e pela Doutora Ana Bicho

Ana Bárbara Tavares dos Santos

Doutoramento em Biologia

(Biologia do Desenvolvimento)

2011

Correntes Aniónicas em Protoplastos de Grãos de Pólen de *Arabidopsis thaliana* e *Lilium longiflorum*

Resumo: Ao germinar, o grão de pólen forma uma extensão citoplasmática designada por tubo polínico, cujo crescimento é polarizado e apical, podendo atingir os 4 μm s^{-1}. Este crescimento distingue-se por ser oscilatório e por estar intimamente associado a fluxos iónicos através da membrana plasmática e aos gradientes citoplasmáticos que os fluxos originam. Estes fenómenos foram identificados e caracterizados através de técnicas de Imagiologia e de Sondas Vibráteis Auto Referenciáveis. Até à data os iões que se sabem estar envolvidos são o Cloreto (Cl^-), Cálcio (Ca^{2+}), Protão (H^+) e Potássio (K^+), cujos fluxos apicais oscilam com a mesma frequência que o crescimento.

Zonia e colaboradores (2002) identificaram e caracterizaram os fluxos de Cl^- em tubos polínicos de duas espécies, *Lilium longiflorum* e *Nicotiana tabacum*, mostrando que este ião sai do tubo polínico através de um efluxo oscilante no ápice e entra através de um influxo não oscilante nos lados do tubo, e que tem inicio a aproximadamente 15 μm da ponta. Estes autores associaram o efluxo de Cl^- à via de sinalização do Ins(3,4,5,6)P4 (Inositol 3,4,5,6 tetra-*kis*-fosfato). Este composto, conhecido por inibir correntes de Cl^- dependentes de Ca^{2+} e mediadas por receptores, inibiu o crescimento do tubo polínico, induziu o aumento do volume celular e comprometeu o normal efluxo de Cl^-. Outros inibidores de correntes aniónicas também foram testados: o DIDS (ácido 4,4'-di-iso-tiocianato-stilbeno-2,2'-disulfónico), o NPPB (ácido 5-nitro-2-(3-fenil-propil-amino)benzóico) e o ácido niflúmico inibiram completamente o crescimento do tubo polínico, o *streaming* citoplasmático e causaram o aumento do volume celular. No entanto, apenas o DIDS conseguiu destruir os efluxos oscilatórios de cloreto.

Com este artigo, Zonia e colaboradores (2002) mostraram que os fluxos de Cl^- são essenciais ao crescimento do tubo devido ao seu papel na manutenção do volume celular. Esta observação levou à hipótese de que os fluxos de água através da membrana plasmática seguiam os fluxos de Cl^-.

O trabalho desenvolvido durante o meu doutoramento e que conduziu a esta tese prendeu-se com o isolamento e a caracterização das correntes aniónicas em protoplastos de grão de pólen de duas espécies, a *Arabidopsis thaliana* e o *Lilium longiflorum*. A primeira espécie foi escolhida por ser o modelo biológico das plantas e por possuir as

ferramentas moleculares necessárias à identificação dos possíveis canais responsáveis pelos fluxos de Cl^- descritos por Zonia e colaboradores (2002). A segunda espécie foi escolhida não só por ser um modelo recorrentemente utilizado no estudo do desenvolvimento em tubos polínicos, mas também por permitir uma comparação entre o mesmo tipo de correntes em duas espécies tão distintas.

A necessidade de desenvolver protocolos específicos para o isolamento das correntes aniónicas neste sistema surgiu do facto de, apesar de já se ter estudado correntes aniónicas em protoplastos de células vegetais, nomeadamente do meristema da folha, dos estomas e da raiz apical, os protocolos existentes eram desadequados, quer por não produzirem protoplastos de qualidade, quer por impedirem a aplicação da técnica de *patch clamp*. No protocolo para a produção e isolamento de protoplastos foi necessário ajustar os tempos de incubação na solução enzimática e a velocidade e tempo de centrifugação. Para o isolamento das correntes aniónicas foi necessário ajustar a osmolaridade das soluções de banho e de pipeta, ajustar as concentrações dos iões em solução.

As correntes aniónicas presentes na membrana plasmática dos protoplastos de grãos de pólen de *Arabidopsis thaliana* e *Lilium longiflorum* foram caracterizadas na configuração de *célula inteira* (Whole-Cell, WC) da técnica de *retalho controlado* (patch clamp), sob condições simétricas de concentração aniónica, sendo o Cl^-, o ião permeável presente em maior quantidade. Nestas condições experimentais foram identificadas nos protoplastos de *Arabidopsis thaliana* três populações diferentes de correntes aniónicas, todas com rectificação positiva: I_{Cl1} (corrente perdida por *rundown* depois da entrada em WC – diluição de factores intracelulares para a pipeta por difusão), I_{Cl2} (corrente insensível a NPPB), e I_{Cl3} (corrente inibida por 100 µM de NPPB). I_{Cl2} e I_{Cl3} foram medidas depois do *rundown*. Apesar da forte rectificação *outward*, os possíveis canais responsáveis pelas correntes aniónicas detectadas permitem a passagem de corrente em ambas as direcções (*inward* e *outward*), já que quer as correntes positivas, quer as negativas sofrem perda de intensidade por rundown e são inibidas por NPPB.

As correntes apresentam também uma activação dependente do tempo para os potenciais de membrana (V_m) mais positivos, isto é, induzida por potenciais de membrana (V_m) depolarizantes, podendo esta ser descrita com três componentes, uma instantânea - I_{inst} (sub milissegundos) e duas dependentes do tempo - I_1 e I_2, caracterizadas pelas constantes τ_1 (centenas de milissegundos) e τ_2 (dezenas de milissegundos),

respectivamente. Utilizando um protocolo de cauda, foi possível observar que estas correntes sofrem também uma desactivação dependente do tempo, desta vez induzida por V_m hiperpolarizantes.

A variação da condutância corda (G) destas correntes com V_m também foi estudada. Aos resultados obtidos foi ajustada uma equação de Boltzmann, cujos parâmetros demonstraram uma sensibilidade diferente de I_{Cl1} a variações no V_m. Diminuindo a concentração de Cl^- na solução de banho ($[Cl^-]_{out}$), depois de o *rundown* terminar, permitiu descobrir que as populações I_{Cl2} e I_{Cl3} são reguladas por $[Cl^-]_{out}$. A selectividade iónica das populações I_{Cl2} e I_{Cl3} foi estudada através da substituição de parte da $[Cl^-]$ na solução de banho por NO_3^-, chegando-se à conclusão que a permeabilidade ao NO_3^- era duas vezes maior que a permeabilidade ao Cl^- ($P_{NO_3^-}/P_{Cl^-}$).

Foi também averiguado o efeito de três concentrações intracelulares de cálcio diferentes ($[Ca^{2+}]_{in}$, na gama de nM, µM e mM), mostrando que as três diferentes populações de correntes viram a sua intensidade aumentar com o aumento de $[Ca^{2+}]_{in}$, enquanto a sensibilidade ao NPPB diminuía. A sensibilidade da condutância corda a variações do V_m não se modificou.

Três populações de correntes aniónicas - I_{Cl1}, I_{Cl2} e I_{Cl3} - com características semelhantes foram medidas em protoplastos de grãos de pólen de *Lilium longiflorum*. Estas diferiram não só na resposta ao $[Ca^{2+}]_{in}$ mas também na sensibilidade ao NPPB, que era inferior, já que a concentração mínima de NPPB necessária foi de 500 µM. Outras diferenças prenderam-se com $P_{NO_3^-}/P_{Cl^-}$, que no caso destas populações de correntes foi de 1.2, e com o facto de estas não serem reguladas por $[Cl^-]_{out}$.

A partir dos valores das correntes foi possível calcular os fluxos aniónicos que estas poderiam originar. Fazendo variar o V_m e a $[Ca^{2+}]_{in}$ foi possível fazer oscilar os valores dos fluxos calculados de forma compatível com os fluxos de Cl^- descritos em tubos polínicos em crescimento de *Lilium longiflorum*. Não foi possível realizar a mesma comparação para a *Arabidopsis thaliana*, uma vez que os fluxos de Cl^- ainda não foram descritos para esta espécie. Apesar disso é possível afirmar com alguma segurança que as correntes aniónicas aqui descritas podem ser responsáveis pelos fluxos observados.

Durante o meu doutoramento também foi realizada uma tentativa de identificar o canal ou canais responsáveis pelas correntes observadas. Através da análise transcriptómica dos

grãos de pólen de Arabidopsis foi possível isolar numa primeira fase os seguintes candidatos: CLC-c, CLC-d, MSL10, ALMT12, SLAH2, SLAH3 e CaCC. Os dois primeiros candidatos, CLC-c e CLC-d, foram eliminados numa segunda fase, não só por terem sido localizados em membranas intracelulares, nomeadamente no tonoplasto e nas vesículas trans-Golgianas, mas também porque até à data os CLC caracterizados revelaram-se cotransportadores anião:H^+. O MSL10 foi eliminado uma vez que estes canais não são regulados pelo Ca^{2+} citosólico ou pela voltagem. O ALMT12 foi eliminado como candidato pois, ao se adicionar 5mM de malato às correntes aniónicas encontradas nos protoplastos de grãos de pólen de *Arabidopsis thaliana*, estas sofreram uma diminuição na sua intensidade, indicando que estes canais são menos permeáveis ao malato, ao contrário dos ALMT12. Os possíveis canais SLAH2 e SLAH3, homólogos ao canal SLAC1, acabaram por não ser escolhidos uma vez que os respectivos canais ainda não foram caracterizados. O candidato que se revelou ser o melhor foi o CaCC, uma vez que as correntes dos homólogos em animais já foram caracterizadas, tendo-se revelado muito semelhantes às descritas nesta tese. Infelizmente foi impossível confirmar esta identificação devido à falta de um verdadeiro mutante KO para o gene em questão.

Palavras-chave: Canais aniónicos, Regulação por cálcio, Pólen, *Arabidopsis thaliana*, *Lilium longiflorum*, patch clamp

Anionic Currents in Pollen Grain Protoplasts from *Arabidopsis thaliana* and *Lilium longiflorum*

Abstract: Upon hydration in a simple medium, pollen grains germinate and develop a cytoplasmic extension designated as the pollen tube, the growth rate of which can reach up to 4 μm s^{-1}, making it one of the fastest polarized cellular growths in nature. This apical growth is oscillatory and its control has been systematically shown to be underlined by ion dynamics, namely ion fluxes across the membrane and cytoplasmatic ionic gradients. These phenomena were identified and characterized by means of imaging techniques and by Self Referencing Vibrating Probes. Thus far the ions known to be involved are Chloride (Cl^-), Calcium (Ca^{2+}), Proton (H^+) and Potassium (K^+), which apical fluxes oscillate with the same frequency as that of the apical growth.

Zonia *et al.* (2002) identified and characterized the Cl^- fluxes in growing pollen tubes from two species, *Lilium longiflorum* and *Nicotiana tabacum*, showing that this ion leaves the pollen tube through an oscillating efflux at the tip and enters through a non-oscillating influx at the shank of the tube, starting at approximately 15 μm from the tip. These authors also associated the efflux of Cl^- to the Ins(3,4,5,6)P4 (Inositol 3,4,5,6 tetra-*kis*-phosphate) signaling pathway. This compound, known for inhibiting receptor mediated Ca^{2+} dependent Cl^- currents, inhibited the pollen tube growth, induced the increase of the cellular volume and compromised the normal efflux of Cl^-. Other inhibitors were also tested: DIDS (4,4'-di-iso-tiocianate-stilbeno-2,2'-disulfonic acid), o NPPB (5-nitro-2-(3-fenil-propil-amino)benzoic acid) and niflumic acid completely inhibited the pollen tube growth, the cytoplasmic streaming and caused the increase of the cellular volume. Nevertheless, only DIDS completely abolished the oscillatory effluxes of Cl^-.

Zonia *et al.* (2002) showed that the Cl^- fluxes are essential to the pollen tube growth due to its role in the maintenance of the cellular volume. This observation let to the hypothesis that the fluxes of water through the plasma membrane follow the fluxes of Cl^-.

The work developed in this thesis lay with the isolation and characterization of the anionic currents present in the pollen grain protoplasts of two species, *Arabidopsis thaliana* and *Lilium longiflorum*. The first species was chosen due to the fact that it is the biological model for plants, endowing it with the necessary molecular tools for the latter identification of the channel or channels responsible for the Cl^- fluxes reported in Zonia *et al.* (2002). The

second species was chosen not only because it has been recurrently used as a model in the study of development of pollen tubes, but also because it would allow for a comparison between the same type of currents in two very different species.

The necessity of developing specific protocols for the isolation of the anionic currents in this system stemmed from the fact that, although there was already published reports on anionic currents in plant cell protoplasts, namely from leaf meristem, from stomata and from apical root cells, the existing protocols were inadequate, for producing quality protoplasts and for not allowing the patch clamp technique to be applied. It was necessary to adjust the time of incubation in the enzyme solution, and the time and speed of the centrifugation steps in the protocol for the production and isolation of protoplasts. For the isolation of the anionic currents it was necessary to adjust the osmolarity of the bath and pipette solutions, their ionic content.

The anionic currents found in the plasma membrane of pollen grain protoplasts from *Arabidopsis thaliana* and *Lilium longiflorum* were characterized by means of the Whole Cell (WC) configuration of the patch clamp technique, under symmetrical anionic concentrations, in which Cl^- was the permeable anion in greater concentration. Under these experimental conditions, it was possible to identify, in the protoplasts of *Arabidopsis thaliana*, three different anionic current populations, all with a strong outward rectification. These were I_{Cl1} (current lost during rundown, after the establishment of the WC configuration), I_{Cl2} (current insensitive to the inhibitor NPPB), and I_{Cl3} (current inhibited by 100 µM of NPPB). I_{Cl2} and I_{Cl3} were measured after rundown. Despite the strong outward rectification, the putative channels responsible for the detected anionic currents allow the passage of current in both directions (inwardly and outwardly), since both negative and positive currents suffered rundown and were inhibited by NPPB.

The currents presented a time dependent activation for the more positive membrane potentials (V_m), that is, an activation induced by depolarizing Vm. This can be described by three current components, one which is instantaneous - I_{inst} (sub millisec) and two which are time dependent - I_1 e I_2, characterized by the time constants τ_1 (hundreds of millisec) and τ_2 (tens of millisec), respectively. Using a tail protocol it was possible to observe that these currents are also characterized by a hyperpolarizing time dependent deactivation.

The variation of the cord conductance (G) with V_m was also studied, by fitting a Boltzmann equation to the values of G when plotted against V_m. This analysis revealed that I_{Cl1} has a different sensitivity to variation in V_m. By diminishing the Cl^- concentration in the bath solution ($[Cl^-]_{out}$) after the rundown, it was possible, not only to confirm the anionic nature of the currents but also to determine that I_{Cl1} and I_{Cl3} are regulated by $[Cl^-]_{out}$. The ionic selectivity of the two populations of currents was studied by replacing part of the $[Cl^-]_{out}$ by NO_3^-. It was possible to conclude that the permeability to NO_3^- was two times higher than to Cl^- ($P_{NO_3^-}/P_{Cl^-}$).

The effect of three different intracellular calcium concentrations ($[Ca^{2+}]_{in}$, in the nM, µM and mM range), was studied showing that all three currents increased in intensity with increasing $[Ca^{2+}]_{in}$, while their sensitivity to NPPB decreased. The sensitivity of G to variations in V_m was not changed.

The populations of anionic currents - I_{Cl1}, I_{Cl2} and I_{Cl3} – with very similar characteristics were also found in pollen grain protoplasts from *Lilium longiflorum*. These differed, not only in the response to $[Ca^{2+}]_{in}$, but also in the sensitivity to NPPB, which was inferior, since the minimal NPPB concentration needed was 500 µM. Other differences laid with the $P_{NO_3^-}/P_{Cl^-}$, which in these currents was 1.2, and with the fact that these were not regulated by $[Cl^-]_{out}$.

From the values of the currents it was possible to calculate the anionic fluxes that these could originate. By varying the V_m and $[Ca^{2+}]_{in}$ is was possible to oscillate the values of the calculated fluxes in a manner compatible with the observed Cl^- fluxes reported by Zonia *et al.* (2002) in growing pollen tubes from *Lilium longiflorum*. It was not possible to perform the same comparison for *Arabidopsis thaliana*, since the Cl^- fluxes in growing pollen tubes haven't been characterized in this species yet. Nevertheless it is possible to claim with some level of confidence that the anionic currents here described can be responsible for the observed fluxes.

The identification of the channel or channels responsible for the observed anionic currents was also attempted. Through the analysis of the pollen grain transcriptomic it was possible to isolate the following gene candidates: CLC-c, CLC-d, MSL10, ALMT12, SLAH2, SLAH3 and CaCC. The first two genes, CLC-c and CLC-d, were eliminated in a second selection phase, not only because they were both localized in intracellular membranes, namely the tonoplast and the trans-Golgi network, but also because all the CLC channels so far

characterized revealed themselves as anion:H^+ cotransporters. MSL10 was also eliminated because these channels aren't regulated by cytoplasmic Ca^{2+} or by V_m. ALMT12 was eliminated because, unlike the currents elicited by this channel, the anionic currents described here suffered a decrease in intensity when 5 mM of malate was added to the bath solution, indicating a smaller permeability to this anion. The candidates SLAH2 and SLAH3, homologues of SLAC1, were not selected because they have yet to be electrophysiologically characterized. The best candidate was CaCC, since the currents in the animal homologues have been characterized, revealing themselves very similar to the ones described in this thesis. Unfortunately it was impossible to confirm this identification due to a lack of a true KO mutant for this gene.

Keywords: Anionic channels, calcium regulation, pollen, *Arabidopsis thaliana*, *Lilium longiflorum*, patch clamp

Special thanks to:

Prof. Doutor José Feijó and Doutora Ana Bicho
for their support and supervision,

my patch clamp buddies Pedro Dias and Patrícia Gonçalves
because they know,

Filipe Borges, Leonor Boavida, Catarina Silva, Cláudia Campos,
Nuno Geraldo and Mr. Cardia
for their help,

Prof. Doutora Teresa Moura
for the opportunity,

Doutora Graça Soveral and Paula Martins
for their patience,

my family and friends
for their encouragement.

This work was supported by FCT fellowship SFRH/BD/27399/2006

“Good news everyone!”

Dr Hubert J. Farnsworth, b. 9th April 2841

Table of Contents

Figure Index

Table Index

Abbreviations

ABA → Abscisic acid

ATP → Adenosine triphosphate

$[Ca^{2+}]_{in}$ → Intracellular Calcium concentration

Compound 48/80 → Condensation product of formaldehyde with N-methyl-p-methoxy-phenethylamine

COS → Cell line derived from CV-1 cells, transformed with the SV40 virus

CV-1 → Cell line derived from the kidney of the African green monkey

DEPC → Di-ethyl-pyrocarbonate

Di-4-ANEPPS → 3-(4-(2-(6-(dibutylamino) -2-naphthyl) -trans-ethenyl) pyridinium) propane sulfonate

$DiBAC_4(3)$ → bis-(1,3-dibutyl-barbituric acid)-trimethine oxonol

DMSO → Dimethyl Sulfoxide

EDTA → Ethylenediamine tetraacetic acid

EGTA → Ethyleneglycol tetra-acetic acid

FM4-64 → N-(3-tri-ethyl ammonium propyl)-4-(6-(4-(di-ethyl amino) phenyl) hexa-tri-enyl) pyridinium dibromide

HEPES → 4-(2-hydroxyethyl)-1-piperazineethanesulfonic acid

$Ins(3,4,5,6)P_4$ → Inositol-3,4,5,6-tetra*kis*phosphate

MEQ → 6-methoxy-N-ethylquinolinium iodide

MES → 2-(*N*-morpholino) ethane-sulfonic acid

min → minutes

NAO → 10-n-Nonyl Acridine orange

NMG-OH → N-methyl-D-glucamine

ROS → Reactive Oxygen Species

SDS → Sodium Dodecyl Sulfate

sec → seconds

TAE buffer → Tris-acetate-EDTA

TEA^+ → Tetraethylamonium

Tris → Tris-(hydroxymethyl)-aminomethane

Tris-Cl → Tris base titrated with HCl

WC → Whole Cell

WT → Wild Type

Known Anion Channel Inhibitors:

A-9-C → Anthracene-9-carboxylic Acid

Bumetanide → inhibitor of the Na^+:K^+:$2Cl^-$ symporter

CFTRinh-172 → fibrosis transmembrane conductance regulator inhibitor–172

$DiBAC_4(5)$ → Bis-(1,3-dibutyl-barbituric acid)-pentamethine oxonol

DIDS → 4,4'-diisothiocyanatostilbene-2,2'-disulfonic acid

DPC → diphenylamine-2-carboxylic acid

EA → Ethacrynic Acid

Furosemide → inhibitor of the Na^+:K^+:$2Cl^-$ symporter

IAA-94 → (6,7-dichloro-2-cyclopentyl-2,3-dihydro-2-methy-1-oxo-1H-inden-5-yl) oxyacetic acid

NA → Niflumic Acid

NPPB → 5-nitro-2-(3-phenylpropylamino) benzoic acid

Probenecid → inhibitor of organic acid transporters

SITS → 4-acetamido-4′-isothiocyanatostilbene-2,2′-disulfonic acid

1. Introduction

1.1. The Pollen Tube

In order to sexually reproduce, higher plants must face a great challenge, the transport and delivery of non-motile male sperm, for great distances in dry and aggressive environments, while remaining sessile organisms. To do so, higher plants evolved an extraordinarily specialized structure which enabled them to colonize a startling range of habitats. This structure is the pollen grain (Feijo, 2010).

The pollen grain is the higher plants gametophyte. It is produced in copious quantities and transported either by air currents or by a variety of animal pollinators. Its success relies upon its remarkably tough external wall and its dehydrated state upon release. When the pollen grain lands on a compatible female sexual organ, it re-hydrates and germinates, originating the pollen tube.

The pollen tube is a highly specialised structure resulting from the growth of the vegetative cell after pollination. Its main function is the transport of the sperm cells, contained within, through the female reproductive tissues, and deliver them into the ovule, in order for the double fertilization to occur. While growing, the pollen tube never divides nor ramify, and yet its growth rate is one of the fastest in nature, reaching rates up to 4 μm s^{-1} (in Tradescantia or Hemerocallis) and lengths up to 50 cm (in maize), which may imply an increase in its volume of several orders of magnitude within a few hours (reviewed in Boavida *et al.*, 2005a; Boavida *et al.*, 2005b; Michard *et al.*, 2009). This intense growth, together with the almost complete description of the Arabidopsis pollen Transcriptome, makes this system an ideal model for the study of polarized growth in plant cells.

1.1.1. Ionic Fluxes, Intracellular Gradients and Oscillations

The association between pollen tube growth and ionic fluxes was established by Lionel Jaffe's group during the 1970s. They used what was, at the time, a newly developed method – the vibrating probe - which consisted in a platinum-black electrode that measured differences in voltage between two points, thus inferring the total electrical current flowing between them (Weisenseel and Jaffe, 1976; Weisenseel *et al.*, 1975). The introduction of ionic selectivity (though the use of selective ionophores) and further improvements to this

basic method allowed a deeper understanding of the ionic fluxes and the respective intervening ions. Advances in imaging techniques and in the development of fluorescent dyes permitted the discovery of intracellular ionic gradients that resulted from the ionic fluxes across the membrane. Both phenomena were found to oscillate with a similar period as that of growth, though with distinct phase delays, and of being essential for pollen tube growth (Feijo *et al.*, 2001; Holdaway-Clarke *et al.*, 1997; Holdaway-Clarke and Hepler, 2003; Messerli *et al.*, 1999; Zonia *et al.*, 2002). A more detailed description of the fluxes, gradients, and the intervening ions follows suite.

1.1.1.1. Calcium (Ca^{2+})

It has long been established the existence of an intracellular Ca^{2+} gradient, appressed to the plasma membrane, tip focussed, and intimately associated with an influx of Ca^{2+} at the tip, both closely tied with pollen tube growth and orientation (Holdaway-Clarke *et al.*, 1997; Malho *et al.*, 1995; Messerli *et al.*, 2000; Miller *et al.*, 1992; Pierson *et al.*, 1994; Pierson *et al.*, 1996; Rathore *et al.*, 1991; Reiss and Herth, 1985; reviewed in Holdaway-Clarke and Hepler, 2003). All three phenomenon, the tip focused intracellular Ca^{2+} gradient, the tip based Ca^{2+} influx, and the pollen tube growth rate, were latter discovered to be oscillating with the same period.

The tip focused intracellular Ca^{2+} gradient was firstly examined with fura-2-dextran in *Lilium longiflorum* growing pollen tubes, with values estimated to range from 3 μM (at the tip) to 200 nM (basal $[Ca^{2+}]_{in}$ level reached 20 μm from the tip). In 2000, Messerli *et al.* used aequorin, a bioluminescent $[Ca^{2+}]_{in}$ indicator with a better range, and estimated that the magnitude of the $[Ca^{2+}]_{in}$ at the tip oscillated between 10 and 3 μM, and that its peak was 4 sec delayed in relation to the growth oscillation peak (Messerli *et al.*, 2000). The influx of Ca^{2+} at the tip, observed in Lilium pollen tubes, oscillated from 1.4 to 14 pmol cm^{-2} s^{-1} (Miller *et al.*, 1992; Pierson *et al.*, 1994), and presented an 11 sec delay in relation to the tube growth (Holdaway-Clarke *et al.*, 1997; Michard *et al.*, 2009; Pierson *et al.*, 1996).

Michard *et al.* (2008) studied the Ca^{2+} apical gradient in *Nicotiana tabacum* pollen tubes, by means of the fluorescent genetic probe YC3.1 yellow CaMeleon, coupled to confocal microscopy. The authors found a V-shaped gradient extending from the tip to 40 μm into the tube. The $[Ca^{2+}]_{in}$ at the tip varied from 0.2 to 1 μM with a period of 1 to 4 min. A strong Ca^{2+} influx at the tip, which oscillated between 2 and 50 pmol cm^{-2} s^{-1}, and a small non-oscillatory efflux, approximately 100 μm down the shank of the tube, were also observed.

Using continuous wavelet analysis, one major oscillatory component was found in the intracellular Ca^{2+} gradient, while the tip Ca^{2+} influx presented up to two. Arabidopsis was recently found to show the same organization of events, with part of the Ca^{2+} influx at the tip being carried by glutamate receptor like channels (GLR) (Michard *et al.*, submitted in 17th February 2011).

1.1.1.2. Proton (H^+)

H^+ fluxes and its intracellular distribution were observed for the first time in pollen tubes from *Lilium longiflorum*, by means of H^+ - selective vibrating electrode and ratiometric wide-field fluorescence microscopy, respectively. The pollen tubes presented a constitutive alkaline band at the base of the clear zone and an acidic area at the tip. The distribution of the H^+ fluxes agreed with the intracellular H^+ gradient, with an oscillating H^+ influx at the tip, that varied between 0 and 4 pmol cm^{-2} s^{-1}, and a non-oscillating efflux in the region that corresponds to the alkaline band (Feijo *et al.*, 1999). This intracellular gradient of $[H^+]$ was also intimately associated with growth and with the spatial organization of the organelles in the cytoplasm, namely in the correlation of the alkaline band with the apical clear zone (Feijo *et al.*, 1999). In the same year, it was reported a far greater oscillating H^+ influx (0 to 490 pmol cm^{-2} s^{-1}) at the tip of pollen tubes from Lilium, but no efflux at the shank (Messerli *et al.*, 1999). The reason for this divergence is not known, but it may be related to differences in the buffering capacity of the medium (Messerli *et al.* (1999) used 5 mM MES while Feijó *et al.* (1999) used 0.05 mM), since the introduction of mM quantity of buffer in this kind of measurements is known to mask small fluxes and amplify large ones (Kunkel *et al.*, 2001).

Recently, Michard *et al.* (2008) studied the H^+ fluxes and the respective intracellular concentration ($[H^+]_{in}$) gradients in pollen tubes from *Nicotiana tabacum*, the latter by means of the fluorescent genetic probe pHluorin. This intracellular H^+ gradient displayed an acidic tip and manifested itself up to 40 µm along the tube shank. The pH gradient oscillated between 6.6 and 7.2 (at the tip) and between 7.2 and 7.7 (at 35 µm from the tip). The gradient was connected to growth, decreasing in the slow growing phase of the growth oscillations, but never dissipating and always showing a magnitude higher than 0.3 pH units. Some of the pollen tubes observed presented a narrow alkaline region appressed to the plasma membrane of the tube's shank, most likely representing a ring-shaped area close to the membrane. As described for Lilium, an oscillating H^+ influx occurred at the tip

of the tube, with values varying between 10 and 40 pmol cm^{-2} s^{-1}, while a non-oscillatory efflux occurred along the tube shank. The oscillations of the intracellular pH gradient and extracellular H^+ fluxes were analysed by Fourier decomposition and continuous wavelet methods. Both tests rendered one major frequency peak for both oscillations in the majority of the pollen tubes tested. The periods varied significantly, from 1.19 to 4.16 min, for the intracellular pH gradient oscillation, and from 1.15 to 4 min, for the tip H^+ influx (Michard *et al.*, 2008).

1.1.1.3. Potassium (K^+)

In 1999, Messerli *et al.* reported the presence of a strong oscillating K^+ influx at the tip of pollen tubes from Lilium detected with a K^+ - selective vibrating electrode, its values varying between 0 and 690 pmol cm^{-2} s^{-1}. The authors suggested that the transport of K^+ could be facilitated by a H^+:K^+ cotransporter, since both cations shared equally high oscillating influxes (H^+ influx of 0 to 490 pmol cm^{-2} s^{-1}) (Messerli *et al.*, 1999). However, these results have become controversial, as they seem to imply various biophysical incongruences, and so the reality of the K^+ transport is still to be determined. In our group the opposite phenomenon was observed (oscillatory efflux of K^+ at the tip and a non-oscillatory influx at the tube shank) in growing pollen tubes from several species (Cordeiro S, Dias P, Portes MT, and Feijó JA, personal communication).

1.1.1.4. Chloride (Cl^-)

In 2002, Zonia *et al.* characterized the chloride fluxes in growing pollen tubes from *Lilium longiflorum* and *Nicotiana tabacum*, by means of the ion-specific vibrating probe. They presented a strong oscillatory Cl^- efflux at the tip (50 – 8000 pmol cm^{-2} s^{-1} in Lilium and 400 – 1200 pmol cm^{-2} s^{-1} in Nicotiana) with a period of 13.2 and of 105 sec for Lilium and Nicotiana, respectively, and a non-oscillatory influx at approximately 12 µm from the tip, reaching a maximum at approximately 26 µm from the tip (4000 pmol.cm^{-2} s^{-1} in Zonia *et al.*, 2002). These Cl^- fluxes were further confirmed by the use of known Cl^- channel blockers DIDS, NA and NPPB. These compounds, not only completely inhibited the tobacco pollen tube growth, but also induced an increase in apical volume. Cytoplasmic streaming was stopped by NPPB and NA. DIDS did not affect the cytoplasmic streaming, but completely disrupted the Cl^- efflux. Ins(3,4,5,6)P_4, a known Ca^{2+}-activated Cl^- conductance blocker (Carew *et al.*, 2000), inhibited pollen tube growth, induced cell volume increase, and interrupted Cl^- efflux. These effects were specific for Ins(3,4,5,6)P_4. The Cl^-

efflux oscillation was coupled to, and temporally in phase with the growth oscillations. All these data indicated a role for Cl^- fluxes in the osmotic homeostasis and apical growth in pollen tubes (Zonia *et al.*, 2002).

Further evidence supporting the existence of Cl^- fluxes in growing pollen tubes was provided by several reports from different research groups. Matveyeva *et al.* (2003) studied the effect of several blockers of Cl^- channels and transporters in the germination and Cl^- efflux on pollen grains from *Nicotiana tabacum*. They observed that NPPB and NA completely inhibited pollen germination and significantly reduced Cl^- efflux from the grain. Furosemide, bumetanide, and $DiBAC_4(5)$, known inhibitors of chloride co-transporters, only suppressed the germination by less than 50%, while DIDS prevented pollen germination but had no effect on Cl^- efflux, unlike what was reported in Zonia *et al.* (2002). Matveyeva *et al.* (2003) suggested that this discrepancy could be explained by the involvement of distinct Cl^- channels in the activation of pollen grain germination and in the control of pollen tube growth. These authors believed that NPPB-sensitive anion channels were involved in the activation of pollen grains during germination (Matveyeva *et al.*, 2003). In 2009, Breygina *et al.* studied variations on membrane potential during pollen germination and pollen tube growth, by means of quantitative fluorescent microscopy, using the dyes $DiBAC_4(3)$ and Di-4-ANEPPS, and found that the plasma membranes of *Nicotiana tabacum* and *Lilium longiflorum* become hyperpolarized during pollen germination, and that they present an uneven potential distribution on pollen grain and tubes. These authors also showed the involvement of the plasma membrane H^+-ATPase and anion channels in membrane potential regulation, by means of the inhibitors orthovanadate and NPPB and the activator fusicoccin. This group also studied indirectly the exit of anions from pollen grains and pollen tubes from *Nicotiana tabacum*, during germination and growth, by means of the fluorescent dye MEQ (Breygina *et al.*, 2009b). By applying the inhibitor NPPB (40 μM) and by increasing the extracellular $[Cl^-]$ ($[Cl^-]_{ext}$) to 200 mM (during pollen germination) or 100 mM (during pollen tube growth), this group succeeded in completely block the efflux of anions and consequently stopped pollen grain germination and pollen tube growth. Additional analysis performed via the fluorescent dyes $DiBAC_4(3)$, FM4-64 and NAO, revealed that NPPB not only prevented the efflux of Cl^- and other anions, but also induced depolarization of the plasma membrane and the disruption of the pollen tube apical organization. Blocking selective Cl^- efflux in pollen tubes with 100 mM $[Cl^-]_{ext}$ caused a

significant hyperpolarisation of the plasma membrane. The authors concluded that the selective block of Cl^- release induced the efflux of other anions, namely organic anions, which caused the observed arrest of pollen germination and tube growth. This report showed the importance of Cl^- efflux through NPPB-sensitive channels for the normal germination of pollen grains and pollen tube growth (Breygina *et al.*, 2009a).

In 2010 Breygina *et al.* reported the effect that the anion channel blockers NPPB and DIDS had on *Nicotiana tabacum* pollen tube growth and its mitochondrial state, via fluorescence microscopy and flow cytometry. The authors found that 40 μM NPPB completely blocked pollen tube growth but caused no increase in its diameter, while 20 to 80 μM of DIDS induced pollen tube swelling and bursting. Isolated pollen mitochondria treated with DIDS showed hyperpolarized membranes and a variation on ROS content and excretion. This study suggested that pollen tube growth is dependent on the activity of different anion channels, namely in localization and function (Breygina *et al.*, 2010).

Overall there is a substantial amount of evidence pointing to the importance of Cl^- efflux in the germination of pollen grains and in the growth of pollen tubes, specifically in the regulation of cytoplasm compartmentalization, membrane potential regulation, and to a smaller extent mitochondrial regulation. But the main role that has been associated with Cl^- movements across the plasma membrane was that of maintaining the osmotic pressure and driving the water movement across the cell. There is abundant evidence of the importance of the regulation of osmotic pressure during the apical growth of pollen tubes, and it has been established that variations on cell volume osmotically induced, elicit rapid variations of phospholipid membrane composition and signalling (Zonia and Munnik, 2004). Even though the link between the Cl^- movements and the water movements in the growing pollen tube system has not been thoroughly recognized, the connection between these two phenomena in another important regulatory plant system – the Guard Cell – has been well established. The movement of guard cells is associated to variations in its turgor pressure, which are regulated by the flow of K^+, Cl^- and organic anions in and out of the cells.

In plants, anions may thus play a vital role not only in the maintenance of the membrane potential, by keeping the electroneutrality, and cell osmotic potential but also by directly controlling important cellular events. The cellular processes stated above have been proposed as the physiological effectors of the Ca^{2+} gradient (Becker *et al.*, 2004; Helling *et al.*, 2006; Hwang *et al.*, 2005; Parton *et al.*, 2003; Roy *et al.*, 1999). Thus one can

speculate that anions may also be responsible for the fine-tuning of the Ca^{2+} gradient, which would account for a feedback system (since Ca^{2+} also regulates anionic fluxes; e.g. Chen *et al.*, 2010) during pollen tube growth and development. The signalling cascades downstream Ca^{2+} are multiple (reviewed in Malho *et al.*, 2006), and may imply phosphorylation through Ca^{2+}-dependent protein kinases (Yoon *et al.*, 2006), small GTPases (Gu *et al.*, 2005) or calmodulin (Rato *et al.*, 2004), which could regulate anionic currents.

Regardless of the overwhelming evidence supporting the existence of Cl^- fluxes, these have been involved in controversy since their discovery. This debate began long before the Cl^- fluxes in pollen tubes were described, with the report of Weisenseel and Jaffe (1976) that stated that pollen tubes don't need anions in solution to grow. The authors were unaware, at the time, that growing pollen tubes extrude Cl^- into the germination medium, a phenomenon that was only latter investigated.

This disagreement was further enhanced by Messerli *et al.* (2004), in their report on the characterization of the Cl^- selective microelectrodes used in the experiments described in Zonia *et al.* (2002). They stated that the electrodes were poorly selective for Cl^- over other anions and claimed that it could indirectly detect H^+ gradients (Messerli *et al.*, 2004). However, they failed to reproduce the exact parameters of Zonia *et al.* (2002) experiments, namely the MES concentration and the pH. Since both will affect the activity of the anionic form of MES, their claim that the microelectrode was indirectly detecting variations on pH falls short of the mark. Furthermore Messerli *et al.* (2004) were unable to dismiss the pharmacological evidence presented by Zonia *et al.* (2002).
So far cell-attached patch clamp studies have failed to demonstrate the presence of Cl-channels in the plasma membrane of pollen protoplasts from Lilium longiflorum (Dutta and Robinson, 2004).

Figure 1 presents a schematic summary of the ionic fluxes and their respective intracellular gradients, as described for pollen tubes from *Lilium longiflorum* and *Nicotiana tabacum*.

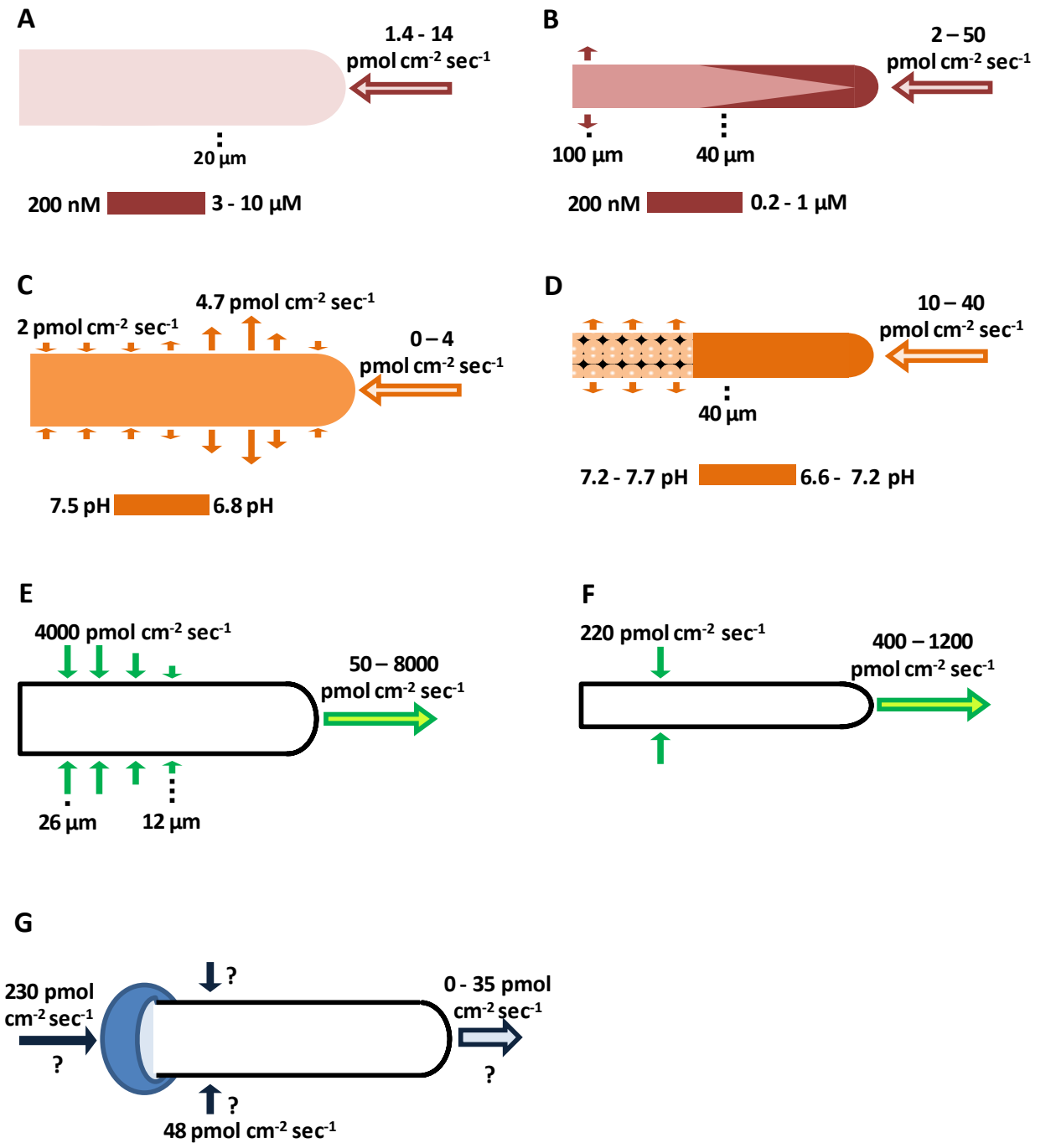

Figure 1. Schematic summary of the ionic fluxes and the intracellular ion concentration gradients. **A:** Ca^{2+} dynamics in *Lilium longiflorum*; **B:** Ca^{2+} dynamics in *Nicotiana tabacum*; **C:** H^{+} dynamics in *L. longiflorum*; **D:** H^{+} dynamics in *N. tabacum*; **E:** Cl^{-} extracellular fluxes in *L. longiflorum*; **F:** Cl^{-} extracellular fluxes in *N. tabacum*; **G:** Hypothetical K^{+} extracellular fluxes in *L. longiflorum* (Cordeiro S, Dias P, Portes MT, Feijó JA, personal communication). **Open arrows** indicate oscillatory fluxes, **closed arrows** indicate non-oscillatory fluxes.

1.1.2. Ionic Channels and Transporters in Pollen

Plasma membrane ionic transporters and channels have long since been associated with the regulation of intracellular ion gradients, with the ion fluxes across the membrane, with

the maintenance of turgor pressure and with the furnishing of materials necessary for pollen tube growth (revised in Feijo *et al.*, 2001; Holdaway-Clarke and Hepler, 2003; Song *et al.*, 2009). Transcriptome analysis in *Arabidopsis thaliana* has shown that there are 459 possible transporter genes expressed during the pollen germination and the tube growth. Of these 459 genes at least 8 were found to be pollen specific (Pina *et al.*, 2005; Wang *et al.*, 2008).

1.1.2.1. Calcium (Ca^{2+})

The first indication of the existence of Ca^{2+} channels in the plasma membrane from pollen tubes was reported by Reiss and Herth in 1985, by use of nifedipine, a well known Ca^{2+} channel blocker, on germinating pollen and on pollen tubes from *Lilium longiflorum* (Reiss and Herth, 1985). Studies with Lanthanum (La^{3+}), vanadate and compound 48/80 have suggested the existence of calmodulin-dependent Ca^{2+}-ATPases in pollen tube tips (Obermeyer and Weisenseel, 1991). Based on the observation that both the gradient and fluxes of Ca^{2+} were abolished under hypertonic conditions, Pierson *et al.* (1994) suggested the involvement of stretch activated Ca^{2+}-channels present at the tip. Additionally, intracellular microelectrode studies by Malhó *et al.* (1995) reported that a voltage-gated Ca^{2+}-channel might be involved in pollen tube reorientation in *Agapanthus umbellatus* (Malho *et al.*, 1995; Pierson *et al.*, 1994).

Two gene families of putative nonspecific cation channels, CNGC (Cyclic Nucleotide Gated ion Channel) and GLR (Glutamate Receptor) were found in the Arabidopsis genome. CNG18, one element of the CNGC family, was found to be specifically expressed in pollen of *Arabidopsis thaliana* and localized in the plasma membrane of growing pollen tube tips. The same study also showed that CNGC18 was permeable to Ca^{2+}, and that the loss of function of this protein caused male sterility by disrupting pollen tube growth (Frietsch *et al.*, 2007). Other CNGCs (CNGC7, 8, 9, 10 and 16) and a GLR2.1 were also found to be expressed in pollen, but their cellular localization and function has yet to be established (as revised in Song *et al.*, 2009).

Dutta and Robinson (2004) reported two stretch-activated Ca^{2+} channels in plasma membranes from pollen grain and pollen tube tip protoplasts from *Lilium longiflorum*. The channels were inward rectifiers (entrance of Ca^{2+}) and were sensitive to Gd^{3+} and unpurified spider venom. The main difference between the two was the greater permeability displayed by the channel in the protoplasts from pollen tube tips as compared

to whole-grain protoplasts. These authors claimed the nonexistence of other type of Ca^{2+} channels, namely hyperpolarisation-activated Ca^{2+} channels (Dutta and Robinson, 2004).

The existence of a hyperpolarisation-activated Ca^{2+} channel was first reported in the plasma membrane of pollen protoplasts from *Lilium davidii* D. The channel was inhibited by trivalent cations, verapamil, nifedipine and diltiazem, and its activity was associated with extracellular Calmodulin (CaM) and with cytosolic [Ca^{2+}] (Shang *et al.*, 2005). A similar channel was also found in pollen from *Arabidopsis thaliana* and from *Pyrus pyrifolia*. In Arabidopsis, the hyperpolarisation-activated Ca^{2+} channel was inhibited by trivalent cations but insensitive to organic blockers, and was regulated by a G-protein α subunit (G-alpha). In *Pyrus pyrifolia* the channel was inhibited by La^{3+} and Gadolinium (Gd^{3+}), and was regulated by extracellular pH. In both cases, the channels presented a high selectivity to divalent cations and the same permeability sequence (Qu *et al.*, 2007; Wu *et al.*, 2007). The genetic identities of these hyperpolarisation-activated Ca^{2+} permeable channels have yet to be determined.

The inconsistency of the above mentioned reports, regarding the existence of hyperpolarisation-activated Ca^{2+} channels, might be due to the use of different patch clamp configurations for, while Dutta and Robinson (2004) measured single channel currents, the other three groups worked under whole cell conditions.

Ten genes for auto-inhibited Ca^{2+}-ATPases (ACA) were found in the Arabidopsis genome. One element of this family, ACA9, was shown to be expressed only in pollen and was localized to the plasma membrane. The loss of function in ACA9 caused partial male sterility due to the reduced growth probability and a high frequency of aborted fertilization (Schiott *et al.*, 2004).

1.1.2.2. Proton (H^+)

H^+ fluxes have a well characterized and defined behaviour. It is widely believed that protons are actively pumped out of the tube at the sides (corresponding with the alkaline band found in Lilium) and passively permeated everywhere else (Feijo *et al.*, 1999).

Of the 11 P-type H^+-pump genes (AtAHAs) found in the *Arabidopsis thaliana* genome, 7 were detected, by Transcriptome analysis, during pollen germination and pollen tube growth (Song *et al.*, 2009). Of these, only AHA3 was proven to be essential for pollen development (Robertson *et al.*, 2004). Working with *Nicotiana tabacum*, Certal *et al.* (2008)

showed that cell polarity in pollen was associated with the exclusion of NtAHA (a pollen-specific H^+-ATPase) from the apex. NtAHA-GFP was co-localized with extracellular H^+ effluxes and was absent in areas of H^+ influx. It was found that NtAHA moves toward the apex of growing pollen tubes, by fluorescence recovery after photo-bleaching, but is excluded from the tip. NtAHA mRNA was also found to be excluded from the tip. It was also found that the cytosolic acidification, by means of localized additions of gramicidin A (a cation ionophore), was only possible where NtAHA was absent, and induced the reorientation of the pollen tube. Further evidence for the involvement of the NtAHA in pollen tube growth was given by the over-expression of NtAHA-GFP, which caused abnormal H^+ fluxes and the formation of abnormal callose plugs. It was also observed that there are no net H^+ fluxes in specific patches of membrane where callose plugs are to be formed (Certal *et al.*, 2008).

Cation-Hydrogen Exchangers (CHX) are believed to be involved in the regulation of the pH gradient immediately adjacent to the plasma membrane, in adjusting ion homeostasis, and in maintaining turgor and membrane potential (Holdaway-Clarke and Hepler, 2003). Eighteen CHX genes were found to be expressed during pollen germination and pollen tube growth in *Arabidopsis thaliana*. Of these, 9 were specifically or preferentially up-regulated during pollen tube growth (Song *et al.*, 2009; Sze *et al.*, 2004). Recently, two K^+:H^+ exchangers, CHX21 and CHX23 were found to be essential for pollen tube orientation towards the ovules. These transporters were localized to the endoplasmic reticulum and are believed to be involved in the signal reception and/or transduction that are critical to shifting the axis of polarity and directing pollen growth toward the ovule (Lu *et al.*, 2011).

1.1.2.3. Potassium (K^+)

K^+ fluxes across the plasma membrane of the pollen tubes have been associated with the control of the turgor pressure and the plasma membrane potential (Holdaway-Clarke and Hepler, 2003). Obermeyer and Kolb (1993) reported the first K^+ permeable channel activity in the plasma membrane of pollen protoplasts from *Lilium longiflorum*. This channel is characterized by a conductivity of 19 pS. Two other current components were later found in the plasma membrane of ungerminated pollen grains. These were an outward K^+ current ($I_{k,out}$) and an inward K^+ current ($I_{k,in}$). The outward K^+ currents were regulated by $[K^+]_{out}$ and were inhibited by TEA^+ and Barium (Ba^{2+}). By contrast, the activation of $I_{k,in}$ was less

affected by $[K^+]_{out}$. The authors believed that the detected K^+ current components might be involved in driving the water influx necessary for germination by allowing a K^+ influx after the membrane voltage had been driven more negative than E_K by an electrogenic pump (Obermeyer and Blatt, 1995; Obermeyer and Kolb, 1993).

Fan et al. (1999) applied the whole cell configuration of the patch clamp technique to protoplasts isolated from mature pollen from *Brassica chinensis* var. chinensis, and found a hyperpolarisation-activated inward rectifying K^+ channel. This channel was highly selective for K^+, it was inhibited by Ba^{2+}, and regulated by external $[Ca^{2+}]$. The authors considered that this channel could promote the entrance of K^+ into the growing pollen tube (Fan *et al.*, 1999). In 2001 the same group studied the regulatory role of K^+ influx in *Arabidopsis* pollen germination and pollen tube growth. They reported that low external $[K^+]$ inhibited pollen germination and tube growth, while an increase in the external $[K^+]$ stimulated pollen tube growth and inhibited pollen germination. Using the same method, the authors also found the activity of hyperpolarisation-activated inward rectifying K^+ channels. These were inhibited by high external $[Ca^{2+}]$, Ba^{2+} and TEA^+, and strongly regulated by external pH. The authors successfully showed that K^+ influx and regulation (by inward channels) are essential for Arabidopsis' pollen germination and tube growth (Fan *et al.*, 2001).

The inward K^+ current found in Arabidopsis was latter linked to a K^+ channel of the Shaker family (SPIK), which was found to be specifically expressed in pollen and was characterized as a hyperpolarisation-activated K^+ channel (from the heterologous expression in COS cells) by Mouline *et al.* (2002). SPIK is believed to contribute to the K^+ uptake in pollen tubes and in their competitive ability. Disruption of the SPIK coding sequence interfered with the inwardly rectifying K^+-channel activity in the plasma membrane of pollen grain protoplasts, strongly impairing pollen tube growth and their probability of fertilization (Mouline *et al.*, 2002).

Griessner and Obermeyer (2003), using the whole cell configuration of the patch clamp technique, characterized the outward and inward K^+ currents across the plasma membrane of pollen grain and pollen tube protoplasts from *Lilium longiflorum*. The outward currents were similar in the pollen grain protoplasts and in the pollen tube protoplasts. In both cases, the opening and closing kinetics, and the current density were similar. It was also observed that conductance did not depend on extracellular $[K^+]$, whereas the activation voltage did. The currents were reversibly inhibited by Ba^{2+} and TEA^+. Unlike the outward K^+

current, the inward K^+ current from pollen grain protoplasts differed in all measured parameters from the one obtained in pollen tube protoplasts. This last one was characterized by a higher current density, less negative activation potential, faster activation kinetics and slower closure kinetics. In both protoplast types, the inward K^+ current could be attributed to either two different channels or to a channel with two open states. The authors believed that the outward and inward currents could explain the endogenous K^+ fluxes found in a growing pollen tube (Griessner and Obermeyer, 2003). In the same year, another outward K^+ channel was found, this one in pollen protoplasts from *Brassica chinensis*. This channel was reported to be regulated by both internal and external pH. The conductance of the channel was inhibited by low extracellular pH, while its response to positive membrane potentials decreased. More acidic intracellular pH not only increased the channel conductance but also its response to positive membrane potentials, and caused the acceleration of the activation of the channel (Fan *et al.*, 2003).

Becker *et al.* (2004) reported the existence of AtTPK4, a tandem-pore K^+ (TPK) channel that localizes to the plasma membrane and was mainly expressed in pollen. By heterologous expression in Xenopus oocytes, the channel was observed to be voltage-independent (allowing the passage of K^+ for both positive and negative membrane potentials), blocked by extracellular Ca^{2+} and intracellular low pH. The authors believed that AtTPK4 had a role in K^+ homeostasis and membrane voltage control of the growing pollen tube.

Dutta and Robinson (2004) found two different K^+ channels in pollen protoplasts from *Lilium longiflorum*, by means of the cell attached configuration of the patch clamp technique. The first channel was voltage-independent, showed no reaction to membrane deformation and to Gd^{3+}. The second one was stretched-activated, voltage-independent and sensitive to Gd^{3+} (Dutta and Robinson, 2004).

1.1.2.4. Chloride (Cl^-)

Among the possible transporters found in pollen Transcriptome, several were putative anion channels. These genes included two CLC transporters (AtCLC-c, which was pollen enriched, and AtCLC-d), two SLAC1 homologues (SLAH2 and SLAH3), an Al^{3+}-activated Malate Transporter, known to be responsible for the R-type currents found in guard cells (ALMT12), an anion:cation symporter (CCC), an anion exchanger, and a divalent anion:Na^+ symporter. Transporters of the ABC family have also been found, 5 of which

were pollen enriched and 3 were pollen specific (Becker and Feijo, 2007; Pina *et al.*, 2005; Song *et al.*, 2009). Even though the functions of these putative transporters are still unknown, one must keep in mind that one of the main Cl^- transporters in mammals – CFTR - is an ABC transporter. The cation:Cl^- cotransporter (CCC) showed a preferential expression in the root and shoot vasculature at the xylem-symplast boundary, root tips, trichomes, leaf hydathodes, leaf stipules, anthers and pollen grains. Plants mutated for the AtCCC transporter presented shorter organs, inflorescence necrosis, reduced seed production, and defective Cl^- homeostasis under high salinity conditions. In *Xenopus laevis* oocytes, AtCCC proved to be a $1K^+$:$1Na^+$:$2Cl^-$ symporter and its activity was inhibited by bumetanide (Colmenero-Flores *et al.*, 2007). This protein could be responsible for the influx of Cl^- in the pollen tube, although its localization in this organ has yet to be determined. Since the efflux of anions from the guard cells has been associated with the SLAC1 and the ALMT12 channels, it is possible that the efflux of Cl^- observed at the tip of growing pollen tubes could be due to the activity of the SLAC1 homologues and the ALMT12 channel.

Figure 2 presents a hypothetical schematic summary of the ionic channels and transporters and their hypothetical position in the pollen tube.

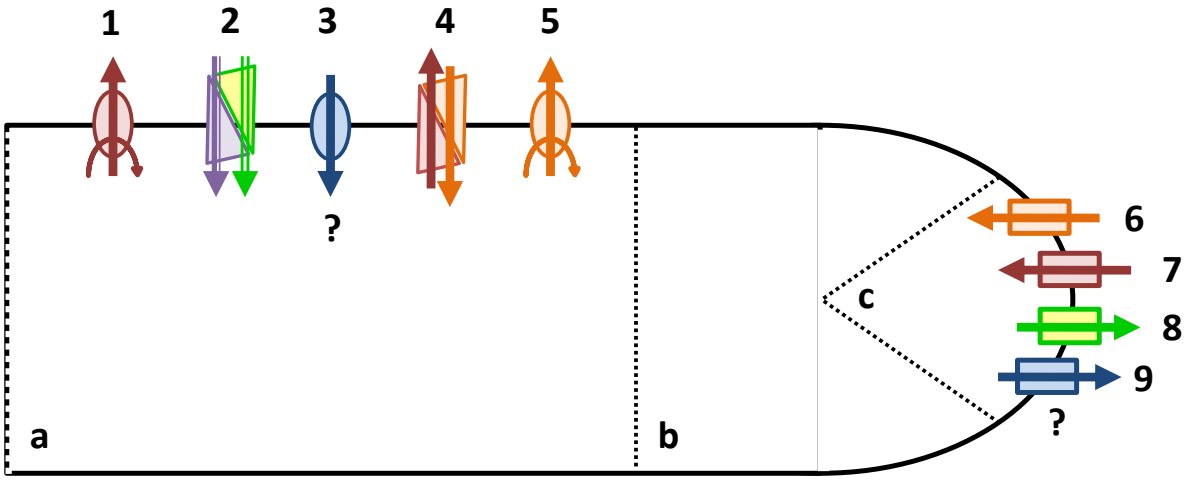

Figure 2. Hypothetic schematic summary of the ionic channels and transporters in growing pollen tubes. **1:** Auto-inhibited Ca^{2+}-ATPase ACA9 from *Arabidopsis thaliana*. **2:** Cation-chloride co-transporter ($1Na^+$:$1K^+$:$2Cl^-$ symporter) from *A. thaliana*. **3:** SPIK K^+ channel in *A. thaliana*? **4:** Cation-proton exchanger (CHX) from *A. thaliana*. **5:** P-type H^+-ATPase (AHA3 in *A. thaliana*, and NtAHA in *Nicotiana tabacum*). **6:** H^+ channel or the CHX. **7:** Ca^{2+} channel (stretch activated?, Voltage gated?) or/and a CNGC18 (cyclic nucleotide gated channel) or/and GLR (glutamate receptor). **8:** Putative Cl^- or anion channel. **9:** AtTPK4 K^+ channel in *A. thaliana* (stretched-activated?)? **a:** tube shank; **b:** clear zone; **c:** inverted cone.

1.2. Anion Transporters and Channels in Plants

1.2.1. Anionic current characteristics in Plants

Most of the known anionic transport in plant cells was discovered and studied by means of electrophysiological techniques. The result is well characterized anion currents that result from the activity of genetically unknown transporters and/or channels. The major exceptions to this trend are the R-type channel activity (AtALMT12) and the S-type channel activity (SLAC1) in guard cells from *Arabidopsis thaliana*. The general characteristics of these channels are summarized in Table 1.

1.2.1.1. Depolarization-activated anion channels

Rapidly activating anion efflux channels or *R-type* channels have been found and thoroughly studied in the plasma membrane of *Vicia faba* guard cells, *Arabidopsis thaliana* hypocotyl epidermal cells and guard cells, and *Nicotiana tabacum* suspension cultured cells. Their main characteristics are summarized in Table 1 (reviewed in Roberts, 2006; Tavares *et al.*, 2011b).

The molecular identity of the *R-type* channel activity in the plasma membrane of guard cells from *Arabidopsis thaliana* was recently revealed to be a member of the ALMT family. AtALMT12 was found to be highly expressed in guard cells and allocated to the plasma membrane. Expression of this protein in Xenopus oocytes rendered voltage-dependent anion currents, which voltage activation threshold is shifted towards more hyperpolarized potentials in the presence of extracellular malate. Plants deficient in this gene are impaired in the stomata closure induced by dark, CO_2 and abscisic acid (ABA), and their guard cell protoplasts display reduced *R-type* currents (Meyer *et al.*, 2010).

Slowly activating anion efflux channels or *S-type* channels have been described in the guard cells of several species such as *Vicia faba*, *Arabidopsis thaliana*, *Nicotiana benthamiana* and *Xanthium strumarium*, in the epidermal cells of *Arabidopsis thaliana* hypocotyls, and in *Coffea arabica* suspension cultured cells. Their main characteristics are summarized in Table 1 (reviewed in Roberts, 2006; Tavares *et al.*, 2011b).

The molecular identity of the *S-type* channel activity in the plasma membrane of the guard cells from *Arabidopsis thaliana* has been recently attributed to a distant homologue of fungal and bacterial organic acid transport proteins. The channel was designated as SLAC1 (Slow anion channel-associated 1) and was found to be preferentially expressed in

guard cells, and to be permeable to malate. This protein is fundamental for stomata closure in response to CO_2, ABA, ozone, light/dark transitions, humidity variations, elevation of $[Ca^{2+}]_{cyt}$, H_2O_2 and NO. Mutation in this protein results in an ozone sensitive plant, with impaired *S-type* current activity, but with no change in *R-type* currents or Ca^{2+} channel activities (Vahisalu *et al.*, 2008).

Outwardly rectifying anion channels or ORACs

Under physiological conditions, the electrochemical gradient for anions in plant cells favours anion efflux (Hedrich and Becker, 1994), and yet outwardly rectifying depolarization-activated anion channels, which may mediate anion influx, have been reported in *Zea mays* and *Arabidopsis thaliana* suspension cultured cells, root cells of *Lupinus albus*, and in *Zostea muelleri* leaf cells. The physiological role in these last cells is believed to be the stabilization of the plasma membrane voltage and turgor pressure in the estuarine environment of this specie, which is known to contains high levels of Cl^- (Garrill *et al.*, 1994). An outward rectifying anion channel was also reported in root cells from *Triticum aestivum*, and is believed to allow the entrance of either Cl^- or NO_3^- into the cell when the extracellular concentrations of these ions are high (Skerrett and Tyerman, 1994). The main characteristics of these channels are summarized in Table 1 (reviewed in Roberts, 2006; Tavares *et al.*, 2011b).

1.2.1.2. Hyperpolarisation-activated anion channels or HAACs

Inward rectifying hyperpolarization activated anion channels have been detected in various species of plants and algae, such as in *Amaranthus tricolor* cotyledons, in the mesophyll and epidermal leaf cells of *Pisum sativum*, in the seed coats of *Phaseolus vulgaris*, in suspension cultured cells from *Daucus carota*, in *Arabidopsis thaliana*, in *Hordeum vulgare* and *Asclepias tuberose*, in *Chara inflata*, in the marine phytoplankton *Coccolithus pelagicus*, and the marine alga *Valonia utricularis*. The only feature that these channels have in common is a voltage-dependent inward rectification, which might indicate different natures for these channels. The remaining features are summarized in Table 1 (reviewed in Roberts, 2006; Tavares *et al.*, 2011b).

1.2.1.3. Mechanosensitive Anion-selective Channels or MS

Stretch-activated anion-selective channels were found in the plasma membrane of cultured stem cells from *Nicotiana tabacum*, guard cells from *Vicia faba*, and mesophyll cells from

Arabidopsis thaliana leaves by means of the patch clamp technique (Cosgrove and Hedrich, 1991; Falke *et al.*, 1988; Qi *et al.*, 2004). All these channels are believed to be involved in osmoregulation during osmotic stress and cell expansion, but the differences in their biophysical properties suggest that they have distinct roles in this process. The first channel is believed to be involved in mediating large (turgor resetting) anion fluxes, while the second could have a role in osmosensing (reviewed in Roberts, 2006; Tavares *et al.*, 2011b). The main characteristics of these channels are summarized in Table 1.

More recently the molecular identities of two MSL (Mechanosensitive channel of small conductance – MscS-like channel) were reported in the plasma membrane of root cells from *Arabidopsis thaliana*. These were designated as MSL9 and MSL10 and had unitary conductances of 45 ± 2 pS and 137 ± 5 pS, respectively (in 100 mM $[Cl^-]_{out}$: 150 mM $[Cl^-]_{in}$). They were activated with positive pressure and were suggested to rapidly depolarize the membrane or to alter the turgor pressure of plant cells in response to mechanical force (Haswell *et al.*, 2008; Peyronnet *et al.*, 2008).

1.2.1.4. Light-activated anion channels

Cho and Spalding (1996) reported a blue light activated anion channel in the plasma membrane from *Arabidopsis thaliana* hypocotyl cells, by means of the patch clamp technique, in which activity is believed to cause the transient depolarization of the plasma membrane induced in hypocotyl cells by blue light. Elzenga and Van Volkenburgh (1997a) reported a light-activated anion channel, in the plasma membrane of mesophyll cells from *Pisum sativum* leaves. The authors asserted that this channel was responsible for the light induced transient depolarization in present in these cells (reviewed in Roberts, 2006; Tavares *et al.*, 2011b). The main characteristics of these channels are summarized in Table 1.

Table 1 (Part I). Summary of the plant anion channels electrophysiologically characterized. Malate (mal^{2-}), Acetate ($acet^{-}$); Propionate ($prop^{-}$); Extracellular anion concentration ($[anion]_{out}$); cyt (cytosolic); GCAC1; ORAC (outward rectifying anion channel); HAAC (hyperpolarization activated anion channel).

Designation	Channel type and gating	Kinetics	Unitary conductance	Selectivity	Regulation	Inhibition	Cell type	References
R-type or GCAC1	Depolarization-activated; Hyperpolarization deactivated U-shaped I/V curve; Activation current peaks at V_m more negative than the E_{A-}; Inward rectifying;	Rapid (ms), time dependent activation and deactivation; Slow inactivation	Small, 30–40 pS (154 mM $[Cl^-]_{in}$: 40 $[Cl^-]_{out}$); dependent on $[anion]_{out}$	$SCN^- > NO_3^- > I^- > Br^- > Cl^- > mal^{2-} >> acet^- > pro^-$	$[Ca^{2+}]_{cyt}$, $[ATP]_{cyt}$, pH_{cyt}. Auxin, mal^{2-}, $acet^-$, pro^-, Cl^- and SCN^-.	NA = IAA-94 = NPPB > DIDS >> EA > A-9-C > probenecid	*V. faba* guard cells	Dietrich and Hedrich, 1998; Hedrich *et al.*, 1990; Hedrich and Marten, 1993; Hedrich *et al.*, 1994; Keller *et al.*, 1989; Marten *et al.*, 1991; Schmidt *et al.*, 1995; Schmidt and Schroeder, 1994; Schroeder and Keller, 1992; Schulz-Lessdorf *et al.*, 1996
R-type			Small, 21 pS (150 mM $[Cl^-]_{in}$: 100 $[Cl^-]_{out}$)	$NO_3^- > SO_4^{2-} > Cl^- > HCO_3^- >> mal^{2-}$	$[ATP]_{cyt}$, $SO_4^{2-}{}_{cyt}$, $[anion]_{out}$.	NA >> NPPB > IAA-94	*A. thaliana* hypocotyl epidermal cells	Diatloff *et al.*, 2004; Frachisse *et al.*, 1999; Thomine *et al.*, 1997; Thomine *et al.*, 1995
R-type or TSAC			Small, 15 pS (150 mM $[Cl^-]_{in}$: 100 $[Cl^-]_{out}$)	-	$[ATP]_{cyt}$, phosphorylation	NPPB > DIDS > A-9-C	*N. tabacum* suspension cultured cells	Zimmermann *et al.*, 1998; Zimmermann *et al.*, 1994
S-type	Depolarization-activated; Voltage independent; Inward rectifying; Less pronounced U-shaped I/V curve; Activation current peaks at V_m more negatives than the E_{A-}	Slow (≤1 min) activation and deactivation; Never inactivate	Moderate, 33–35 pS; Long open and closed durations; Non dependent on $[anion]_{out}$	High NO_3^-. Impermeable to SO_4^{2-}	Phosphorylation, $[Ca^{2+}]_{cyt}$, ABA	NA >> NPPB > A-9-C > IAA-94	*V. faba* guard cells	Schroeder and Keller, 1992
						A-9-C = NA	*N. benthamiana* guard cells,	Grabov *et al.*, 1997
						DPC = glibenclamide >> A-9-C	*A. thaliana* guard cells,	Forestier *et al.*, 1998
						DIDS	*A. thaliana* hypocotyl epidermal cells	Frachisse *et al.*, 2000
							X. strumarium guard cells, and *C. arabica* suspension cultured cells	Dieudonne *et al.*, 1997; Linder and Raschke, 1992

Table 1 (Part II)

Designation	Channel type and gating	Kinetics	Unitary conductance	Selectivity	Regulation	Inhibition	Cell type	References
ORAC	Depolarization-activated, outward rectifying.				Induced by high $[Cl^-]_{out}$		*Z. mays* and *A. thaliana* suspension cultured cells, and *Z. muelleri* leaf cells	Cerana and Colombo, 1992; Fairley *et al.*, 1991; Garrill *et al.*, 1994
		Rapid activation (ms)	Very small, 4 pS	$NO_3^- = Cl^- > I^-$	Unaffected by $[Na^+]_{out}$ or $[K^+]_{out}$; $[Ca^{2+}]_{cyt}$	DIDS > ClO_4^-	*T. aestivum* root cells	Skerrett and Tyerman, 1994
				$Cl^- >$ citrate		A-9-C	*L. albus* root cells	Zhang *et al.*, 2004a
HAAC	Strong voltage-dependence, inward rectification	Time dependent activation (100 to 400 ms), slow inactivation (1-10 s)	Large, 300 pS	$F^- > I^- > Cl^- > Br^- > malate^{2-}$	$[Ca^{2+}]_{cyt}$, $[ATP]_{cyt}$	SITS	*P. sativum* mesophyll leaf cells	Elzenga and Van Volkenburgh, 1997a; Elzenga and Van volkenburgh, 1997b
		Rapid activation (20 ms), rapid inactivation (300 ms)	Large, 100 pS		Slight negative pressure		*D. carota* culture cells	Barbara *et al.*, 1994
		Rapid activation (<200 ms)		Cl^- >> other anions		Zn^{2+}> EA	*C. pelagicus*	Taylor and Brownlee, 2003
		Rapid activation (<200 ms)					*V. utricularis*	Binder *et al.*, 2003; Heidecker *et al.*, 1999
		Slow activation (1.5 s)					*A. tuberosa*	Schauf and Wilson, 1987
			Large, 200 pS				*A. tricolor* cotiledones	Terry *et al.*, 1991
	Weak voltage-dependence, inward rectification		Large, 150 pS		$[Ca^{2+}]_{cyt}$, $[ATP]_{cyt}$		*H. vulgare suspension cultured cells*	Amtmann *et al.*, 1997
							A. thaliana callus cells	Lew, 1991
			Small, 7 – 44 pS		$[Ca^{2+}]_{cyt}$	La^{3+}	*C. inflata*	Kourie, 1994
			Small, 18 pS				*coats of developing seeds of P. vulgaris*	Zhang *et al.*, 2004b

Table 1 (Part III)

Designation	Channel type and gating	Kinetics	Unitary conductance	Selectivity	Regulation	Inhibition	Cell type	References
Anion selective MS		long open periods	Large, 97 pS (220 mM $[Cl^-]_{out}$: 25 mM $[Cl^-]_{in}$)				*N. tabacum* cultured stem cells	Falke *et al.*, 1988
		rapid flickering between the open and closed states	Small, 27 pS - outward current, 13 pS - inward current (154 mM $[Cl^-]_{out}$: 85 mM $[Cl^-]_{in}$)				*V. faba* guard cells	Cosgrove and Hedrich, 1991
			Small		Positive pressure		*A. thaliana* mesophyll lea cells	Qi *et al.*, 2004
Light-activated anion channels	Voltage dependent	remains open after the stimulus is removed	Small, ranging from 23 pS to 46 pS depending on V_m		Blue light	NPPB (20 μM)	*Arabidopsis thaliana* hypocotyl cells	Cho and Spalding, 1996
			Small, 32 pS (symmetrical 100 mM KCl solutions)		Blue light; $[Ca^{2+}]_{cyt}$;		*Pisum sativum mesophyll leaf cells*	Elzenga and Van Volkenburgh, 1997a

1.2.2. CLC channel family

Chloride channel (CLC) proteins constitute anionic channels/transports ubiquitously found in eukaryotes and prokaryotes (Mindell and Maduke, 2001). The fist member of this vast family to be characterized was the ClC-0, a voltage-gated chloride channel, found in the electric organ of *Torpedo californica* (White and Miller, 1979). Mammalian CLCs are the best known elements of this family, and they encompass both Cl^- channels, in the plasma membrane, and $Cl^-:H^+$ antiporters in intracellular compartments (Jentsch, 2008; Zifarelli and Pusch, 2007).

In *Arabidopsis thaliana* seven homologues, AtCLC-a to g, have been identified (Hechenberger *et al.*, 1996; Lv *et al.*, 2009). The expression of the AtCLC family was studied and it was found to be ubiquitous both temporally and spatially, but with distinct expression patterns. Lv *et al.* (2009) found that all members of the AtCLC family were predominantly expressed in the vascular tissues, both in roots and in shoots, implying a possible role for this family in long-distance ion transport within the plant. A strong expression of all AtCLCs, particularly AtCLCc, was also found in guard cells (Lv *et al.*, 2009). The cellular localization of these proteins placed them all in intracellular membrane systems. The main characteristics of these channels are summarized in Table 2. Two CLCs, CLC-c and d were found to be transcribed in pollen, the first being overexpressed (Pina *et al.*, 2005).

1.2.3. ALMT channel family

Aluminium-activated malate transporters were found to promote Aluminium (Al^{3+}) tolerance in several cultivars, by excreting into the root system Al^{3+}-chelating organic anions, such as malate and citrate, in response to Al^{3+} exposure. Al^{3+} was shown, by means of electrophysiological essays, to activate these channels in cortical cells in the root apex (Kollmeier *et al.*, 2001; Pineros and Kochian, 2001; reviewed in Ward *et al.*, 2009). Further evidence for the regulation of these channels by Al^{3+} was provided by the expression of ALMTs in Xenopus oocytes. This was enough to mediate Al^{3+}-induced malate currents, suggesting a direct Al^{3+} sensor role for ALMT transporters (Hoekenga *et al.*, 2006).

There are 14 predicted members of the ALMT channel family in the genome of *Arabidopsis thaliana*. Of these only three, AtALMT1, AtALMT9 and AtALMT12, had their physiological

role unravelled. AtALMT1 was found to be a plasma membrane Al^{3+}-activated malate transporter, expressed in the roots and was associated with Al^{3+} tolerance in *Arabidopsis* (Hoekenga *et al.*, 2006). AtALMT9 is targeted to the tonoplast and mediates malate uptake into the vacuole (Kovermann *et al.*, 2007). AtALMT12 was recently associated with the R-type anion currents found in guard cell's plasma membrane (Meyer *et al.*, 2010). This gene is transcribed in pollen (Pina *et al.*, 2005).

Table 2. Summary of the characteristics of the *Arabidopsis thaliana* CLC family. u.n. stands for unknown.

	AtCLCa	**AtCLCb**	**AtCLCc**	**AtCLCd**	**AtCLCe**	**AtCLCf**	**AtCLCg**
Localization	Tonoplast	Tonoplast	Tonoplast	TGN; co-localized with the VHA-a1 subunit of the V-type ATPase	Chloroplast	TGN	Tonoplast
Expression Pattern	Ubiquitous; Vascular tissues	Roots, stems and siliques; Vascular tissues	Ubiquitous; Vascular tissues; Guard cells	Ubiquitous; Vascular tissues	Leaves, flowers and siliques; Vascular tissues	Roots, leaves and stems; Vascular tissues	Ubiquitous; Vascular tissues
Transporter type	$2NO_3^-/1H^+$ exchanger	NO_3^-/H^+ exchanger	u.n.	Anion channel (Cl^- or NO_3^-)	Anion channel (Cl^- or NO_2^-)	u.n.	u.n.
Function	accumulation of NO_3^- in the vacuole	u.n.	Anion transport and accumulation	To counter the pumping of H^+ by the V-ATPase acidification of TGN vesicles	NO_3^- assimilation through cytosolic NO_2^-	acidification of TGN vesicles	u.n.
Voltage dependence	Slight outward rectification	Strong outward rectification	u.n.	u.n.	u.n.	u.n.	u.n.
Selectivity	$NO_3^- = I^- > Br^- > Cl^- > SO_4^{2-} >$ glutamate	$NO_3^- > Br^- > Cl^- >$ malate$^{2-} = I^-$	u.n.	u.n.	u.n.	u.n.	u.n.
References	De Angeli *et al.*, 2006	Lv *et al.*, 2009; von der Fecht-Bartenbach *et al.*, 2010	Harada *et al.*, 2004; Lv *et al.*, 2009	Lv *et al.*, 2009; von der Fecht-Bartenbach *et al.*, 2007	Lv *et al.*, 2009; Marmagne *et al.*, 2007; Monachello *et al.*, 2009	Lv *et al.*, 2009; Marmagne *et al.*, 2007	Lv *et al.*, 2009

1.2.4. ABC transporter family

ATP-binding cassette transporters received their name from their possession of one or two ATP-binding cassettes or Nucleotide Binding Folds (NBFs). Thus far, as many as 130 genes from the ABC transporter family were found in *Arabidopsis thaliana* genome (Pina *et*

al., 2005). They are known to be involved in a wide range of processes, such as polar auxin transport, lipid catabolism, xenobiotic detoxification, disease resistance, and stomata function (reviewed in Rea, 2007; Sanchez-Fernandez *et al.*, 2001; Verrier *et al.*, 2008). To date only two genes, *AtMRP1* and *AtMRP2*, were associated with anionic transport in plants. AtMRP1 promotes the accumulation of folates in the vacuole (Raichaudhuri *et al.*, 2009), while AtMRP2 was found to contribute to cell detoxification and to chlorophyll degradation, and to transport organic anions into the vacuole (Frelet-Barrand *et al.*, 2008). The transcript of both genes is absent in pollen (Pina *et al.*, 2005).

1.3. Regulation of Anion Channels and Transporters

Higher plant cells are equipped with a variety of anion channels, controlled by various signalling pathways and their messengers, including Ca^{2+}, pH, nucleotides, and protein kinases and phosphatases. Unfortunately a characterization of the regulation of plant anion channels is only available for the anion channels involved in the stomata movements and in the elongation of hypocotyl cells. For other anionic channels, such as the CLCs or the Ca^{2+} activated Cl^- Channels (CaCCs), one can only infer their regulation in plant cells from what is known of their regulation in the animal model.

Because of their importance in closing the stomata, the regulation of the anion channels SLAC1 and ALMT12 has been extensively studied (reviewed in Ward *et al.*, 2009). Both these channels are activated by membrane depolarization (Keller *et al.*, 1989; Schroeder and Keller, 1992), and by ABA (e.g. Roelfsema *et al.*, 2004).

SLAC1 is activated by ABA by means of two pathways, a Ca^{2+}-dependent one and a Ca^{2+}-independent one (reviewed in De Angeli *et al.*, 2007; Sirichandra *et al.*, 2009). In the first pathway, the fastest acting one, the increase in the $[Ca^{2+}]_{in}$ activates Ca^{2+}-dependent protein kinases CPK3, CPK6, and CPK21, which then activate SLAC1 by phosphorylation (Geiger *et al.*, 2010; Mori *et al.*, 2006; Siegel *et al.*, 2009). In the second pathway, an active OST1 protein kinase (Open Stomata 1) activates SLAC1 by phosphorylation of the N-terminus (Lee *et al.*, 2009; Vahisalu *et al.*, 2010). Both these pathways are regulated by ABA by means of the ABI1 protein phosphatase (ABA Insensitive 1), which in the absence of the hormone, maintains SLAC1 inactive either by direct interaction or by inactivating

OST1 or CPK21 (Geiger *et al.*, 2010; Geiger *et al.*, 2009; Lee *et al.*, 2009; Vahisalu *et al.*, 2010, see detail in Figure 3A, page 44).

ALMT12 or R-type channel is regulated by $[mal^{2-}]_{ext}$, which shifts the threshold for voltage activation towards more hyperpolarized membrane potentials. The channel is activated by intracellular SO_4^{2-}, and by an increase in $[Cl^-]_{in}$. The channel is also modulated by intracellular ATP, by means of a binding site for nucleotides, and not by phosphorylation, although the mechanism by which this regulation is achieved is still unknown (Hedrich *et al.*, 1990; Meyer *et al.*, 2010).

The mammalian CLC family can be divided into two functional groups: the voltage-gated Cl^- channels and $Cl^-:H^+$ exchangers. It is known, from comprehensive studies, that the first group is regulated not only by the membrane potential, but also by the extracellular and intracellular $[Cl^-]$ and pH (Niemeyer *et al.*, 2009, reviewed in Duran *et al.*, 2010). The $Cl^-:H^+$ exchangers have proved to be localized mainly in endomembranes and to have a $2Cl^-:1H^+$ estequiometry. They have a varied regulation; for example, ClC-3, an endosomal exchanger, is regulated by phosphorylation and by $Ins(3,4,5,6)P_4$ (Alekov and Fahlke, 2008; Mitchell *et al.*, 2008, reviewed in Duran *et al.*, 2010). So far, all the plant CLCs were localized to the intracellular membranar system, and the few that were characterized proved to be $NO_3^-:H^+$ cotransporters. These may share common regulatory features with the animal $Cl^-:H^+$ exchangers.

The recently discovered mammalian chloride cannel family TMEM16 or Anoctamin, is regulated by $[Ca^{2+}]_{in}$ and is believed to encode for the CaCCs. These proteins have a putative Ca^{2+} binding site in the first intracellular loop (Duran *et al.*, 2010), and are regulated by the plasma membrane potential (Caputo *et al.*, 2008; Schroeder *et al.*, 2008; Yang *et al.*, 2008, reviewed in Duran *et al.*, 2010). Anoctamins are found in all eukaryotic kingdoms (Duran *et al.*, 2010), and in *Arabidopsis thaliana* at least one gene was found to share homology with the human TMEM16A, and to have an ubiquitous expression (Pina *et al.*, 2005), but its physiological role is still unknown.

1.4. Chloride and Osmotic Regulation – the Guard Cell Model

The results presented in this thesis were gathered under the scope of the hypothesis that the movement of water in the growing pollen tube follows that of the ions Cl^- and K^+. *In*

planta, the best known system in which this phenomenon is known to happen is the regulation of the stomata's aperture. The following paragraphs summarize the ionic and water movements found in guard cells.

Guard cells regulate the aperture of stomata pores, and consequently the availability of water and CO_2 to the plant, in response to many environmental (light, CO_2 concentration, ozone, and humidity) and physiological (hormones such as ABA and auxin, $[Ca^{2+}]$, and [ROS]) cues (e.g. Ward *et al.*, 2009). By means of a non-invasive pressure probe, it has recently been established that changes of the turgor pressure at the leaf are directly correlated with the degree of plant transpiration and therefore guard cell regulation. Furthermore, experiments with open stomata mutants indicated that the hydraulic conductance of leaf stomata is higher than that of the root-shoot continuum (Ache *et al.*, 2010).

It has been well established that stomata movements require net cellular fluxes of solutes, mainly K^+, Cl^- and malate (mal^{2-}) (e.g. Ward *et al.*, 2009), in and out of the cell, in order to drive the corresponding water movements, thus varying the guard cell volume and consequently the stomata aperture. It is now believed that the closure of the stomata is driven by the efflux of Cl^- and mal^{2-} into the apoplast carried by SLAC1 and ALMT12 anion channels (S-type and R-type channels respectively). This efflux causes the depolarization of the membrane, which then activates the outward rectifying depolarization-activated K^+ channel GORK (Ache *et al.*, 2000; Hosy *et al.*, 2003). This further increases the osmotic pressure that will lead to the exit of water from the cell. Since the majority of the volume of the guard cell is occupied by the vacuole, the channels involved in the exit of the solutes into the cytoplasm also play an essential role. The extrusion of K^+ is carried out by the vacuole inward rectifying Ca^{2+}-activated K^+ channel TPK1 (Gobert *et al.*, 2007; Ward and Schroeder, 1994), while the anion extrusion could be performed by a anion:H^+ exchanger, such as a CLC transporter. The regulation of this mechanism can be performed by the modulation of the $[Ca^{2+}]_{in}$ since SLAC1, ALMT12, GORK, and TPK1 channels are activated by Ca^{2+}. The elevation of $[Ca^{2+}]_{in}$ is triggered by a hyperpolarisation-activated, ROS modulated Ca^{2+} channel I_{Ca} at the plasma membrane (Hamilton *et al.*, 2000; Pei *et al.*, 2000). This process will also activate the inward rectifying Ca^{2+}-activated Ca^{2+} channel TPC1 present in the tonoplast which will contribute to the increase of the $[Ca^{2+}]_{in}$ (Peiter *et al.*, 2005; Ward and Schroeder, 1994). The increase of the [ROS] in the cytoplasm is

performed by two NADPH oxidases, AtrbohD and AtrbohF, (Kwak *et al.*, 2003), which are indirectly activated by ABA or ozone (Vahisalu *et al.*, 2010) (see Figure 3A).

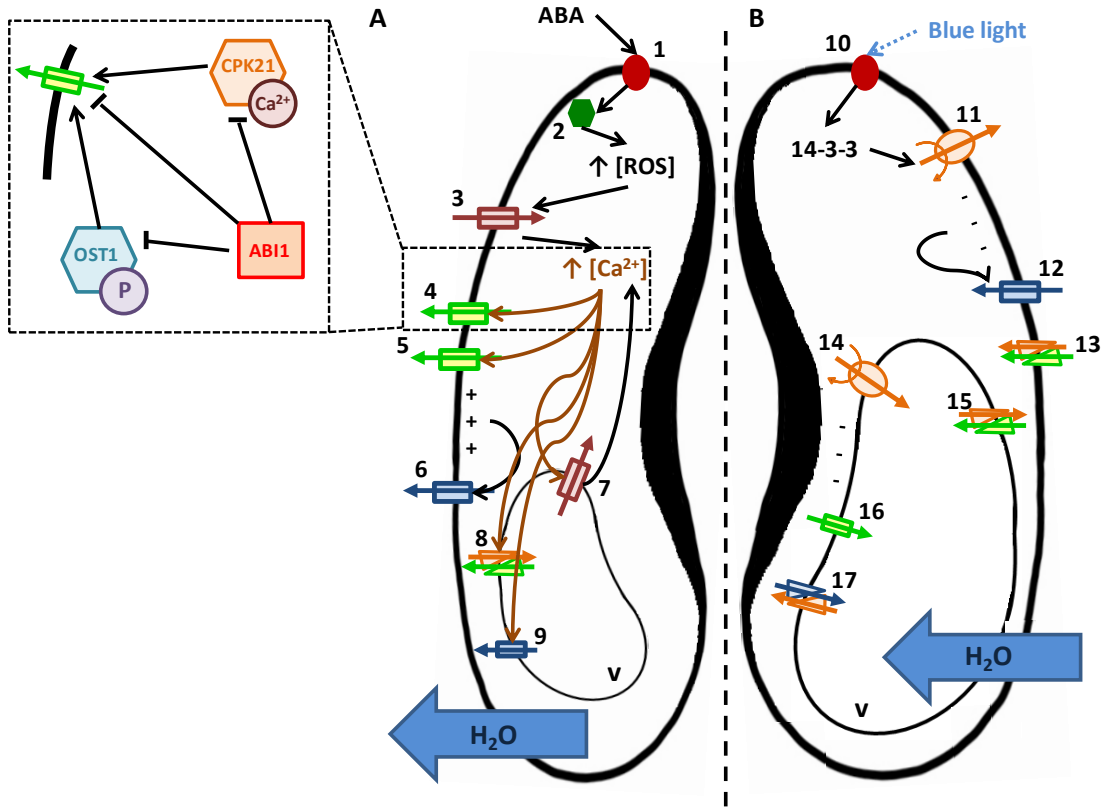

Figure 3. Schematic representation of some of the events leading to the closing (**A**) and opening (**B**) of the stomata (adapted from Ward *et al.*, 2009). **1** - ABA receptor; **2** – NADPH oxidase; **3** – Inward rectifying ROS-activated Ca^{2+} channel I_{Ca}; **4** – SLAC1 channel; **5** – ALMT12 channel; **6** – Outward rectifying K^+ channel GORK; **7** – Inward rectifying Ca^{2+}-activated Ca^{2+} channel; **8** – Cl^-:H^+ exchanger; **9** – Inward rectifying Ca^{2+}-activated K^+ channel TPK1; **10** – Blue-light receptor; **11** – H^+ ATPase; **12** – Inward rectifying hyperpolarisation-activated K^+ channel KAT1; **13** – Cl^-:H^+ cotransporter; **14** – vacuole H^+ ATPase; **15** – anion:H^+ antiporter; **16** – Anion channel; **17** – K^+:H^+ antiporter CHX20. **v** – vacuole.

The opening of the stomata is driven by the influx of K^+ from the apoplast into the cytoplasm and from this to the vacuole. The process is triggered by blue light (Roelfsema *et al.*, 2001), which leads to the activation of plasma membrane H^+ ATPases, by means of 14-3-3 proteins (Roelfsema *et al.*, 1998; Sottocornola *et al.*, 2006). The activity of the ATPase causes the membrane to become hyperpolarised, activating the plasma membrane inward rectifying K^+ channel KAT1 (Kwak *et al.*, 2001; Sottocornola *et al.*, 2006). The necessary charge balancing anions (Cl^- and mal^{2-}) could enter the cell by means of a plasma membrane anion:H^+ cotransporter. At the vacuole level, the accumulation of K^+ is carried out by the K^+:H^+ antiporter CHX20 (Padmanaban *et al.*,

2007), which is driven by the H^+ gradient generated by the vacuole H^+ ATPase. Anion uptake into vacuoles may occur through a combination of low-affinity anion transporters (Kovermann *et al.*, 2007; Pei *et al.*, 1996) and an active anion:H^+ exchange mechanism (De Angeli *et al.*, 2006) (see Figure 3B).

Figure 3 shows a schematic representation of some of the events that lead to the closing (Figure 3A) and opening (Figure 3B) of the stomata. The detail present in Figure 3A summarizes the Ca^{2+}-dependent and the Ca^{2+}-independent regulation of SLAC1 activity by ABA.

1.5. Electrophysiology

1.5.1. The electrical properties of a living cell

The electrical properties of a cell derive mainly from the electrical properties of its plasma membrane. These are due to the lipids and proteins, such as ion channels, transporters and pumps, from which it is constituted. The lipid bilayer behaves as an insulator, while the ion channels, transporters and pumps behave as conductors. In order to study such a complex system, these properties can be represented by an equivalent electronic circuit and the Laws of Electronics can be applied to it (Axon Instruments, 1993; Halliwell *et al.*, 1987). Figure 4 represents the electronic analogue for the cell membrane. The lipid bilayer is represented by the capacitor *C*, while the membranar transporters are represented by the resistance *R* (Halliwell *et al.*, 1987).

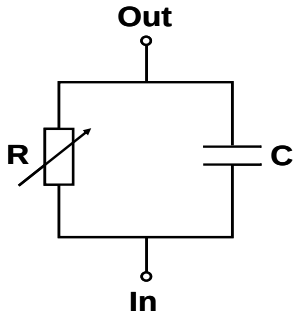

Figure 4. Simple electronic analogue of a cellular membrane. ***C*** stands for capacitor and ***R*** for resistance. This image was taken from Halliwell *et al.*, 1987.

1.5.1.1. Potential, Current and Ohm's Law

Because of the insulating characteristics of the lipid bilayer, living cells possess an *electrical potential difference* between its interior and the extracellular medium, which by convention is zero. This difference or ΔV is designated by Membrane Potential (V_m) and is

measured in *Volts*. In animal cells V_m varies between -30 and -90 mV and in plant cells V_m can reach up to -150 or -200 mV. Even though the salt rich cytoplasm and extracellular solutions are good current conductors, there is very little difference in potential, between two points within the cytoplasm or within the extracellular solution. The V_m is limited to the immediate vicinity of the plasma membrane, and its value depends on the type, quantity and permeability of the ionic channels, transporters, and pumps present in the cell membrane and on the composition of the intra and extracellular solutions (Axon Instruments, 1993).

In live systems, the current (*I*) is also defined as the flow of electrical charge passing a point per unit of time and is measured in amperes (*A*). But, unlike in electronic circuits, the current that crosses the plasma membrane is conducted by ions, such as Na^+, K^+, H^+, Ca^{2+}, and Cl^-, which permeate through the membrane channels, transporters and pumps. Since these proteins constitute parallel conductors, the total conductance of a membrane patch is simply the sum of the conductances of the individual channels that constitute it (Axon Instruments, 1993). The current that crosses the plasma membrane and its difference of potential are linked by means of the Ohm's Law.

1.5.1.2. Capacitance

The capacitance of a membrane (*C*, measured in farads, F) consists in the ability of storing a charge *Q* when a difference of potential ΔV is applied between its two sides. This relation can be expressed as:

$$\boldsymbol{Q = C \times \Delta V}$$

A capacitor is usually constituted by two conducting sheets separated by a thin insulating layer. Its capacitance *C* will be proportional to the area of the capacitor and inversely proportional to the thickness of the insulating layer. When several capacitors are connected side by side or in parallel, as is the case of the phospholipids in the lipid bilayers, the resulting capacitance is the sum of all the individual capacitances (Axon Instruments, 1993). When a ΔV is applied to a capacitor, the current that will result from the accumulated charge will be proportional to the change of voltage with time (Δt):

$$\boldsymbol{I = C \times \frac{\Delta V}{\Delta t}}$$

A biologic membrane is usually 10 nm thick and because it is also a good insulator, with a transmembrane resting potential, it not only behaves as a capacitor, but also generates a

considerable electric field. The membrane capacitance increases with cell size and can be represented as a value per unit of area. The majority of cellular membranes have a capacitance of 1 μF cm^{-2}. As a consequence, when a pulse of current is applied to a cellular membrane, the current first charges up the capacitor and only then changes the transmembrane voltage (Axon Instruments, 1993).

1.5.2. The patch clamp technique

The patch clamp technique is a versatile method for studying the electrophysiological properties of biological membranes (Penner, 1995). It was first developed by Erwin Neher and Bert Sakmann in 1976, in order to demonstrate the existence of single channels in biological membranes, a concept first suggested by Bernard Katz and Ricardo Miledi in 1970-1972 (Katz and Miledi, 1970, 1971). Neher and Sakman were able to measure the size and duration of ionic currents trough a single channel, an acetylcholine receptor, in the plasma membrane of muscular fibbers (Neher and Sakmann, 1976; Penner, 1995). Since 1976 several key improvements, such as the development of “Giga-seals”, which greatly improved the signal to noise ratio, and the establishment of the various patch clamp configurations, have refined this technique to a level that allows it to be applied to completely different biological preparations such as animal and plant cells, yeast, bacteria and cellular organelles (Penner, 1995).

The main difficulties associated with patch clamping plant cells are the presence of a rigid cell wall that prevents the microelectrode from reaching the plasma membrane, and the fact that the thin layer of cytoplasm (2 to 5 μm) around the periphery, is separated from a large central vacuole by an additional membrane. It is possible to produce protoplasts (wall-less plant cells) from most plant cells, by either treatment with enzymes that digest the cell wall or by UV laser microsurgery, but these techniques may create additional problems, since in order to prevent the protoplast from bursting, the cells must be kept in a medium with a high osmotic potential, which could have unknown effects on the membrane properties (Brownlee, 1987; Hedrich, 1995).

A more serious difficulty lies with the thinness of the cytoplasm associated with the large vacuole and its membrane. This configuration of the plant cells may result in the measurement of events occurring in a system of two membranes in series, if the patch clamp technique isn’t carefully applied (Brownlee, 1987).

There are also difficulties when establishing a Giga-seal with a protoplast. These can be due to a variety factors, which have to be addressed independently for each type of protoplast preparation, but the main issue is the *de novo* formation of the cell wall (Hedrich, 1995).

1.5.2.1. Voltage Clamp

In a voltage clamp experiment, the membrane voltage is held under control by means of a *feedback amplifier*, while the transmembrane ionic currents are measured. The method was first developed by Cole and Hodgkin (1949 – 1952) for use with the squid giant axon. Although this process is completely artificial, its value as an experimental technique lies with the fact that clamping the voltage at constant values eliminates most of the capacitive currents (Figure 5), so that the current that flows is proportional only to the membrane conductance. Additionally, it also allows for a better control when studying the voltage gating of the channels involved (Axon Instruments, 1993; Halliwell *et al.*, 1987).

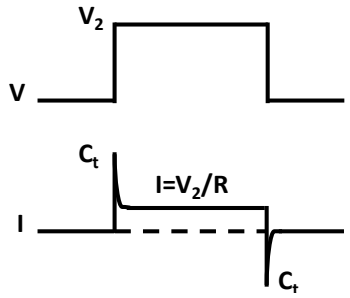

Figure 5. Typical voltage clamp record of a cellular membrane. C_t stands for Capacitance transient.

The *patch clamp* technique is a special type of voltage clamp that allows the study of currents flowing through a single ion channel, or the currents flowing through the membrane of a whole cell (Axon Instruments, 1993; Halliwell *et al.*, 1987).

1.5.2.2. Patch clamp configurations

After a Giga-seal has been established and the capacitive transient currents have been compensated it is possible to initiate the experimental measurements in the *Cell-attached* configuration, which allows the study of the current flowing through an individual channel (Axon Instruments, 1993; Penner, 1995).

If the objective of the experiments is the study of the currents flowing across the membrane's entirety, then a new configuration must be attained. This is designated by *Whole-cell* (Figure 6) and is achieved by rupturing the membrane sequestered by the tip of the pipette, by applying negative pressure. In this configuration, the ionic content of the

cytoplasm is replaced by the contents of the pipette, allowing for the control not only of the extracellular solution but also the intracellular. From these two configurations other can be produced, such as the *inside-out*, and the *outside-out* (Figure 6).

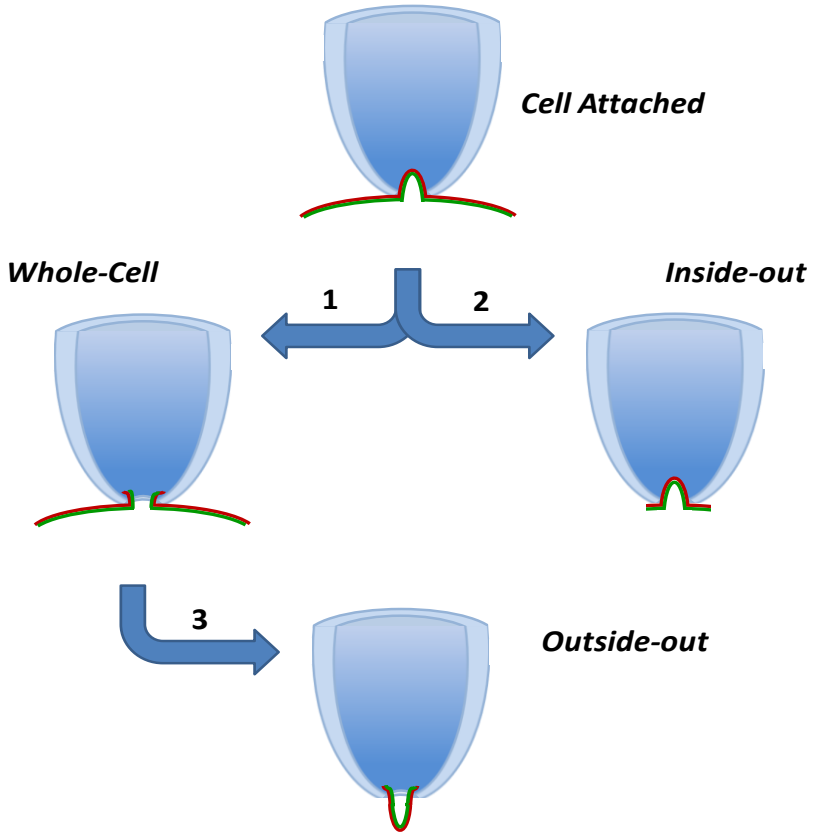

Figure 6. Representation of the basic configurations used in patch clamp. **1** – Suction, **2** – Pulling in low Ca^{2+} medium, and **3** – Pulling.

1.5.3. The patch clamp amplifier

All the patch clamp results presented in this thesis were obtained using a continuous single-electrode amplifier. In this method, the same electrode is used simultaneously for voltage recording and for current passing, which originate a loss of voltage across the pipette. This series resistance (R_s) of the electrode that connects to the cell can be corrected by *positive feedback* circuits present in the patch clamp amplifier (Axon Instruments, 1993). This correction gains even more relevance if the whole cell currents are large (nA), or if R_s has a high value, which will slow the charging of the membrane capacitance when a voltage step is applied to the pipette electrode:

$$\tau = R_s \times C_m$$

When measuring currents with this technique, the best way to avoid introducing errors in the membrane potential is to choose cells with a small surface area, and with low access resistance.

This simultaneous voltage recording and current injection can be achieved with the *Resistor feedback technology* (Axon Instruments, 1993; Halliwell *et al.*, 1987). Figure 7 represents a simplified continuous single electrode voltage-clamp circuit. A sensitive current-to-voltage converter is built with a high Mega-Ohm resistor (R_f) and an operational amplifier (A_1). The pipette is connected to the negative input of A_1 and the command potential (V_{COMM}) is connected to the positive input. Due to its high gain, all current flowing through the pipette also flows through R_f. This current is proportional to the voltage across R_f, which is measured at the output of the differential amplifier (A_2). A_2 subtracts V_{COMM} from the output of A_1 in order to generate a voltage proportional to the voltage across R_f, and therefore the *feedback* current (I_f), which is injected back into the microelectrode, thus maintaining constant the transmembrane voltage (Axon Instruments, 1993).

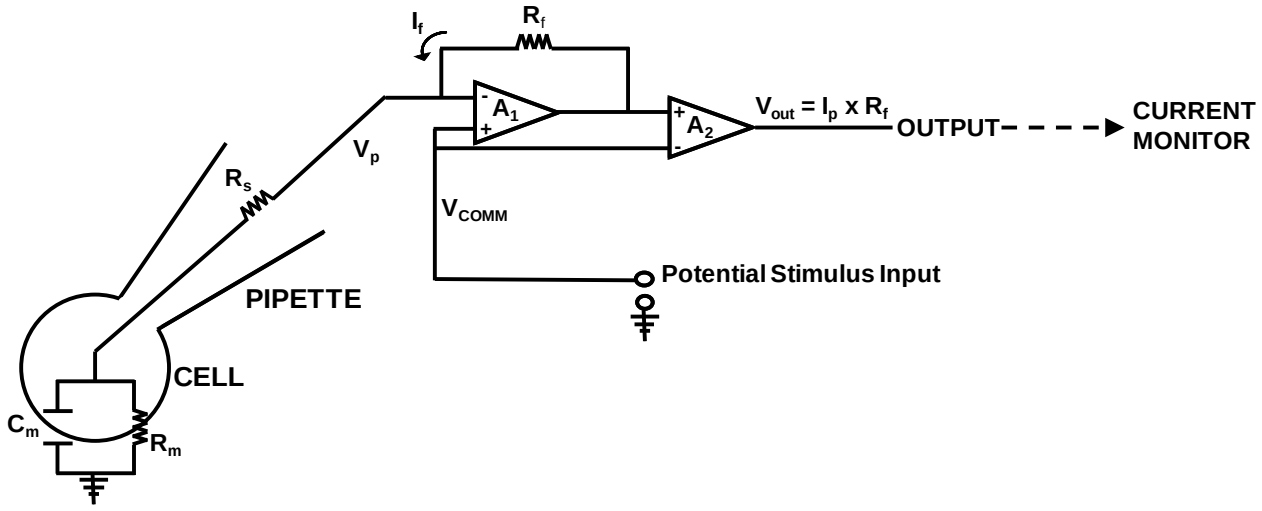

Figure 7. Simplified continuous single electrode voltage clamp circuit for Whole-cell records. $\mathbf{R_s}$ – Series resistance, $\mathbf{V_p}$ – Pipette potential (in this case it is equal to V_m), $\mathbf{V_{COMM}}$ – Command potential (in this case it corresponds to the applied potential), $\mathbf{I_f}$ – *Feedback* current, $\mathbf{R_f}$ – *Feedback* resistance, $\mathbf{A_1}$ – Operational amplifier is a current-to-voltage converter, $\mathbf{A_2}$ – Differential amplifier, $\mathbf{C_m}$ – Membrane capacitance, $\mathbf{R_m}$ – Membrane resistance.

2. Hypothesis and Thesis

The extraordinarily fast and tightly regulated growth of the pollen tube, namely in its ionic homeostasis, is expected also to have a tight control over the entrance and exit of water. The hypothesis in which this thesis was based is that the fluxes of water in and out of the growing pollen tube follow the fluxes of Cl^-. This thesis aims to find and characterize, for the first time, anionic currents in the pollen grain protoplasts of two species, *Arabidopsis thaliana* and *Lilium longiflorum*, by means of the Whole Cell configuration of the patch clamp technique. This thesis also proposes to identify the channel or channels responsible for the anionic currents.

3. Objectives

In order to fulfil the general objectives of this thesis, the following aims were pursued:

1. The optimisation of a protocol for the routine production of pollen grain protoplasts;
2. The optimisation of a protocol for the routine formation of a tight seal or “Giga-seal” with pollen grain protoplasts;
3. The development of adequate internal and external solutions for the isolation of the anionic currents;
4. The development of adequate voltage protocols for the characterization of the anionic currents found in a novel system;
5. The characterization of the anionic currents present in the pollen grain protoplasts from *Arabidopsis thaliana*, by means of the whole-cell configuration of the patch clamp technique;
6. The characterization of the anionic currents present in the pollen grain protoplasts from *Lilium longiflorum*, by means of the whole-cell configuration of the patch clamp technique;
7. The identification of the channel or channels responsible for the anionic currents present in the pollen grain protoplasts from *Arabidopsis thaliana.*

4. Experimental Procedures

4.1. Plants, Culture Conditions and Pollen Grain Collection

i. *Arabidopsis thaliana* wild type seeds (WT), ecotype Columbia, were obtained from the Nottingham Arabidopsis Stock Centre (NASC).

ii. The mutant line FLAG_526A10 - *Arabidopsis thaliana* plants, ecotype Wassilewskija (Ws), with a T-DNA insertion in the fourth exon of the *At1g73020* gene, coding for a putative TMEM16A protein homologue - was obtained from the Versailles Genetics and Plant Breeding Laboratory - *Arabidopsis thaliana* Resource Centre.

iii. Pots with 300 mL capacity (Desch Plantpak) were used to grow *Arabidopsis thaliana* plants. These were filled with a 3:1 mixture of soil and vermiculite. The soil mixture was soaked with water and left to drain. The non-systemic insecticide DESTROYER 5G (5% (w/w) chlorpyrifos) from AGRIPHAR was then added in a concentration of 0.1 g per pot.

iv. All seeds were incubated at 4 ºC for 3 to 4 days – stratification process. The WT seeds were then transferred to pre-prepared pots (5 seeds per pot) and left to germinate in a growth chamber. The FLAG_526A10 seeds were transferred to 10 cm Ø Petri dishes containing 50 mL of Germination Medium complemented with kanamycin (50 µg mL^{-1}). They were left to germinate in a growth chamber for 2 weeks and then were transferred to pre-prepared pots (3 seedlings per pot).

Germination Medium: Murashige and Skoog Basal Medium supplemented with 1% (w/v) Sucrose, 0.05% (w/v) MES, 1x Gamberg's B5 vitamins, 8% (w/v) Agarose, pH 5.7.

v. All *A. thaliana* plants were germinated and grown in a growth chamber with a short day light regime (8h day/16h night) for 4 to 6 weeks and then transferred to a long day light regime (16h day/8h night) to promote flowering. The light was supplied by fluorescent lamps and its intensity varied between 60 and 80 µmol m^{-2} s^{-1} (µE m^{-2} s^{-1}). The temperature in the chamber ranged from 22 ºC during the day to 18 ºC during the night. The humidity levels ranged between 60 and 65%. For the patch clamp experiments the pollen grains were collected from freshly blossomed flowers and used in the same day.

vi. *Lilium longiflorum* plants were purchased from local suppliers. The pollen grains were taken from mature anthers, aliquoted in individual doses and kept frozen in -20 ºC until later use.

4.2. Molecular Biology

4.2.1. Genome analysis of the mutant line FLAG_526A10

4.2.1.1. Isolation of Genomic DNA:

i. The plant material was collected from seedlings. A sample of the WT plants was also collected for control purposes. These were stored in a 1.5 mL centrifuge tube and frozen in liquid nitrogen.

ii. To each sample 300 µL of DNA Extraction Buffer were added. The tissue was ground, and 150 µL of Sodium Acetate (3 M; pH 5.2) was added. The mixture was then vortexed and left to incubate at -20 ºC for 10 min.

DNA Extraction Buffer: 200 mM Tris-Cl, 250 mM NaCl, 25 mM EDTA, 0.5% (w/v) SDS, pH 8

iii. The mixture was centrifuged for 5 min at 14250 g and the supernatant was transferred to a new 1.5 mL centrifuge tube.

iv. 400 µL of isopropanol was added to the supernatant. The mixture was then vortexed and left to incubate for 5 min at room temperature.

v. The mixture was centrifuged for 5 min at 14250 g and the pellet was washed with 200 µL of 70% ethanol. This centrifugation step was repeated.

vi. The pellet was dried at room temperature and resuspended in 50 µL of TE buffer (Tris-EDTA, pH 8). The concentration of the DNA in solution was determined in a NanoDrop 1000 Spectrophotometer (Thermo Fisher Scientific, USA). The DNA sock solutions were stored at -20 ºC until further use.

This experimental protocol was modified from Cenis, (1992) and Edwards *et al.*, (1991).

4.2.1.2. PCR analysis:

i. A DNA solution with approximately 30 ng μL^{-1} was prepared by diluting a portion of the corresponding DNA stock solution. This was used in the Polymerase Chain Reaction (PCR). A genomic DNA sample was used in each PCR mix as a positive

control for the primers and the reaction mix. A negative control (sample without DNA) was also used.

ii. The PCR was conducted in a Programmable Thermal Controller PTC-100 (MJ Research, Inc., USA) according to the protocol described in Table 3.

Table 3. Details of the Polymerase Chain Reaction used in the Genome analyses of the mutant line FLAG_526A10.

Reaction mix (per sample)		**PCR protocol**		
Genomic DNA	1 µL	**step**	**Temperature (ºC)**	**time**
Forward primer	0.5 µL	1	95	1’
Reverse primer	0.5 µL	2	95	30’’
dNTPs mix	0.4 µL	3	56	45’’
DNA Polymerase Paq5000 buffer	2 µL	4	72	1’
DNA Polymerase Paq5000	0.2 µL	5	Repeat steps 2-4 30 times	
Water	15.4	6	72	7’
		7	4	
Total volume	20 µL			

iii. The primers used were,

Mutant Line	**Primer name**	**Direction**	**Sequence 5’ to 3’**
FLAG_526A10	FLAG_526A10_F	Forward	CGGCAACCTGATGGGTTATTA
	FLAG_526A10_R	Reverse	GTCTACCTTTGCACCAAAGT
	LB4	Reverse	CGTGTGCCAGGTGCCCACGGAATAGT

in the following combinations,

Mutant line	**Primer combination**	**Band size**	**T-DNA**
FLAG_526A10	FLAG_526A10_F + FLAG_526A10_R	500 bp	absent
	FLAG_526A10_F + LB4	300 bp	present

The primers locations on the gene are represented in Figure 8.

iv. In order to separate and analyze the products of the PCR, the technique of agarose gel electrophoresis was used. The agarose gel was constituted by a TAE buffer supplemented with 1% agarose and 1 µM of Ethidium Bromide (Bio Rad Laboratories, USA). The bands in the gel were visualised in a Molecular Imager Gel Doc XR (Bio Rad Laboratories, USA), by means of the Quantity One 4.6.7 software (Bio Rad Laboratories, USA).

4.2.2. mRNA analysis of the mutant line FLAG_526A10

The plants chosen for this analysis were all homozygous for the T-DNA insertion in the *At1g73020* gene. A control was performed with a WT plant.

4.2.2.1. Total mRNA isolation:

i. The plant material was collected from seedlings. These were stored in a 1.5 mL centrifuge tube and frozen in liquid nitrogen.

ii. The samples were processed with a mortar and pestle, while the liquid nitrogen evaporated. The mortar and pestle were previously cooled with liquid nitrogen.

iii. 750 µL of TRI Reagent LS (Sigma) were added to each sample. Using the pestle, this compost was incorporated into the pulverized sample until its colour changed from pink to light brown. The blending was continuous until the mixture defrosted.

iv. The mixture was pipetted into a 1.5 mL centrifuge tube, vortexed for a few sec in order to separate the RNA from the associated proteins, and left to incubate at room temperature for 5 min.

v. 200 µL of chloroform were added to the mixture. It was vortexed and left to incubate at room temperature for approximately 15 min. The mixture was then centrifuged for 15 min at 10500 g.

vi. The aqueous fraction was transferred to a new 1.5 mL centrifuge tube and 400 µL of isopropanol were added. The mixture was left to incubate at room temperature for 20 min and then was centrifuged for 15 min at 10500 g.

vii. The pellet was then washed with 200 µL of 70% ethanol and was centrifuged for 15 min at 10500 g. This washing step was repeated.

viii. The pellet was resuspended in 50 µL DEPC treated water and was incubated at 55 ºC for 5 min. The concentration of the RNA in solution was determined in a NanoDrop 1000 Spectrophotometer (Thermo Fisher Scientific, USA). The RNA stock solutions were stored at -80 ºC until further use.

4.2.2.2. Preparation of the cDNA:

For the preparation of the cDNA, 1.2 µg of total RNA was used in each sample. The first step consisted in the removal of any contamination of the samples with genomic DNA, followed by the Reverse Transcription reaction. The protocol was as follows:

Reagent	Quantity per sample	Reaction
Total RNA	1.2 µg	Removal of DNA contamination
10x RQ1 RNase-Free DNase Reaction buffer	1 µL	
RQ1 RNase-Free DNase	1.2 µL	
DEPC-treated water	to a final volume of 10 µL	
1. Incubation at 37 ºC for 37 min		
RQ1 DNase Stop Solution	1 µL	
2. Incubation at 65 ºC for 10 min		
$Oligo(dT)_{18}$	1 µL	Reverse Transcription
dNTPs mix	1 µL	
3. Incubation at 65 ºC for 5 min 4. Incubation on ice for 1 min		
5x First-Strand buffer	4 µL	
0.1 M DTT	1 µL	
SuperScript III RT	1 µL	
RNaseOUT Recombinant RNase Inhibitor	1 µL	
5. Incubation at 50 ºC for 60 min 6. Incubation at 70 ºC for 15 min		
RNase H	1 µL	
7. Incubation at 37 ºC for 20 min		

The incubation steps 1 to 3 were performed in a Stirred Thermostatic bath GD120S12 (Grant Instruments, Great Britain). The last three incubation steps (steps 5 to 7) were performed in a Programmable Thermal Controller PTC-100 (MJ Research, Inc., USA).

4.2.2.3. PCR analysis of the cDNA:

Immediately after the Reverse Transcription reaction, the resulting cDNA was used in a PCR, with the following primers:

Gene	Primer name	Direction	Sequence 5' to 3'	Band size
At1g73020	AT1G73020_F	Forward	TGATCCAACGGTTAATAATCTCACAG	800 bp*
	AT1G73020_R	Reverse	GTGCATATGGACATAACTACTAGAAA	416 bp
At1g73020	AT1G73020_2_F	Forward	GGGAGTAATGGGGAGGAGCGAGTT	967 bp*
	AT1G73020_2_R	Reverse	GACGCCCTCTGATTCCAACCTTCG	453 bp
Actin	Actin_F	Forward	GTTAGCAACTGGGATGATATGG	610 bp*
	Actin_R	Reverse	CAGCACCAATCGTGATGACTTGCCC	532 bp

***** Band size obtained with Genomic DNA.

Figure 8 shows the location of the primers. AT1G73020_F and AT1G73020_R were designed downstream of the T-DNA insert, while the pair AT1G73020_2_F and AT1G73020_2_R were designed flanking the region of the T-DNA insert. The Actin primers were used as a control for the quality of the cDNA samples.

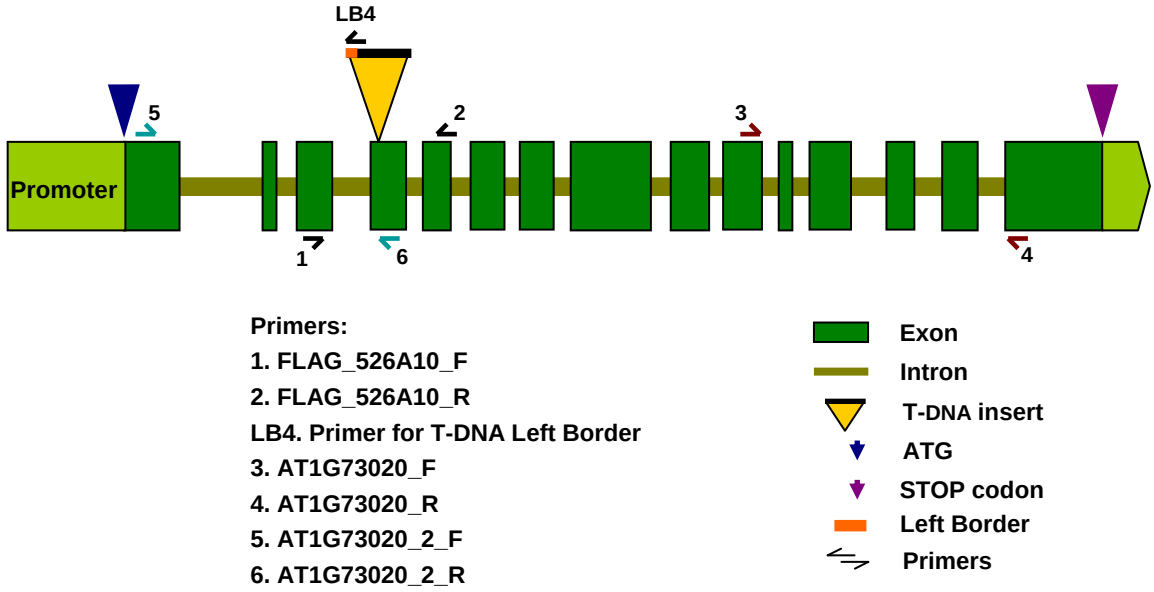

Figure 8. Map of the *At1g73020* gene, in which are pinpointed the Exons, the Introns, the start and stop codons, the T-DNA insert and the primers used. The primers 1, 2 and LB4 were used in the Genome analysis. And the pair of primers 3 + 4 and 5 + 6 were used in the mRNA analysis.

The PCR details are described in Table 4. A genomic DNA sample was used in each PCR mix as a positive control for the primers and the reaction mix. A negative control (sample without DNA) was also used.

Table 4. Details of the Polymerase Chain Reaction used in the mRNA analyses of the mutant line FLAG_526A10.

Reaction mix (per sample)		**PCR protocol**		
DNA sample	1.5 µL	**step**	**Temperature (ºC)**	**time**
Forward primer	1.3 µL	1	95	1’
Reverse primer	1.3 µL	2	95	30’’
dNTPs mix	1 µL	3	56	45’’
DNA Polymerase Paq5000 buffer	5 µL	4	72	1’
DNA Polymerase Paq5000	0.2 µL	5	Repeat steps 2-4 40 times	
water	39.6 µL	6	72	7’
		7	4	
Total volume	50 µL			

The products of the PCR were analysed by agarose gel electrophoresis, and the resulting fragments were sequenced.

4.2.2.4. DNA fragment sequencing:

The DNA resulting from the PCR was cleaned by means of the NucleoSpin Extract II kit (Macherey-Nagel, Germany) and then used in the Cycle Sequencing depicted in Table 5.

Table 5. Details of the Cycle Sequencing used in the sequencing of the DNA fragments obtained in the RT-PCRs.

Reaction mix (per sample)		**CS protocol**		
dsDNA template	200 ng	**step**	**temperature (ºC)**	**time**
primer	3.2 pM	1	96	1’
Buffer	2 µL	2	96	10’’
Terminator Ready Reaction mix	2 µL	3	50	5’’
		4	60	4’
Total volume	10 µL	5	Repeat steps 2-4 25 times	
		6	4	

The resulting DNA fragments were precipitated with the following protocol:

Reagents (per sample):		**DNA Precipitation Protocol**			
Sodium Acetate 3M, pH 4.6	2 µL	**step**	**time**	**temperature (ºC)**	**speed**
Ethanol 95%	50 µL	Incubation	60’	-20	
Water	10 µL	Centrifugation	30’	4	10500 g
		Aspiration of the supernatant and discard			
		Addition of 250 µL ethanol 70%			
		Centrifugation	15’	4	10500 g
		Aspiration of the supernatant and discard			
		Desiccation of pellet at room temperature			

The samples were sequenced in the 3130xl Genetic Analyzer (Applied Biosystems, USA) and were analyzed with the software Sequencing Analysis 5.2 (Applied Biosystems, USA).

4.3. Pollen Protoplast Production

4.3.1. This experimental protocol was adapted from Tanaka *et al.*, (1987), Fan *et al.*, (2001), and Mouline *et al.*, (2002) during the course of this project.

i. 2 mL of standard solution (Table 6) was added to the *Lilium longiflorum* pollen grains. These were then shaken for approximately 90 sec, and left to incubate for 10 min at 20 ºC.

ii. 2 mL of standard solution was added to Arabidopsis flowers freshly collected. These were then shaken for 2 min in order to separate the pollen grains from the anthers. The pollen in solution was separated from the flowers using a 29 µm mesh filter and left to incubate for 10 min at 20 ºC.

iii. The pollen of the two species was centrifuged for 5 min at 160g or at 63g for *A. thaliana* and *L. longiflorum* respectively. The standard solution was subsequently removed and the enzyme solution added (Table 6). The pollen was incubated in this solution at 30 ºC with mild agitation (~100 rpm) for 80 min or 90 min for *L. longiflorum* and *A. thaliana* respectively.

Table 6. Composition of the solutions used to prepare the protoplasts. The osmolar adjustment was made with sorbitol. The pH was rectified with Tris and NMG-OH in Standard and Washing Solutions respectively. In the Enzyme Solution concentrations are in % (w/v).

Standard Solution		**Enzyme Solution**	
KNO_3	1mM	**Cellulase**	1%
KH_2PO_4	0.2 mM	**Macerozyme**	0.5%
$MgSO_4$	1 mM	**BSA**	0.2%
KI	1 mM		
$CuSO_4$	0.1 mM	in standard solution	
$CaCl_2$	5 mM		
MES	5 mM	kept at -80º C until use.	
Glucose	500 mM		
Sorbitol	1000 mM		
pH 5.8 (Tris)			
1500 mOsmol			

iv. The resulting mixture of protoplasts and pollen grains was centrifuged 63g for 5 min, the enzyme solution was removed (supernatant) and 2 mL of the washing solution (bath solution with 1500 mOsmol) was added.

v. The protoplasts suspension was then centrifuged at 63g for 5 min and the supernatant was discarded. This step was repeated once, after which 1 mL of the bath solution (external solution) was added (Table 7).

vi. The protoplasts suspension was kept in ice and used for patch clamp studies up to 8 hours after isolation.

vii. Pollen grain protoplasts from *Arabidopsis thaliana* and *Lilium longiflorum* were routinely obtained with this protocol (Figure 9).

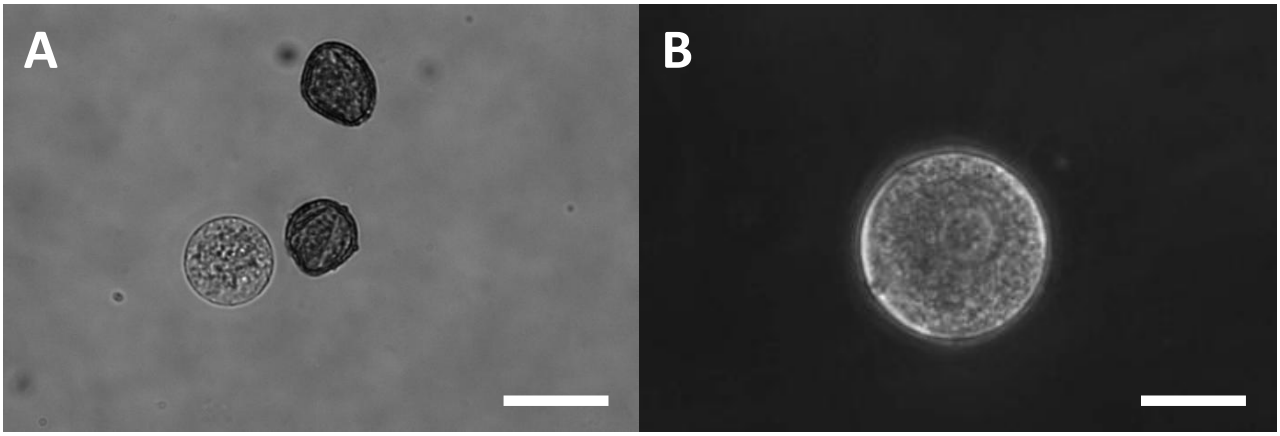

Figure 9. A: *Arabidopsis thaliana* pollen grain protoplast. **B:** *Lilium longiflorum* pollen grain protoplast. White bar represents 20 µm. Images taken in a BX51 Olympus Microscope, clear field (**A**) and phase contrast (**B**).

4.4. Electrophysiological essays

4.4.1. The micropipette, the microelectrode and the reference electrode

The micropipettes used were pulled from a GB150F-8P borosilicate glass capillary with 1.5 mm external diameter and 0.86 mm internal diameter (Science Products GmbH). The puller used was a PB-7 vertical puller from Narishige (Japan). The micropipette production method comprises two heating steps. In the first step the capillary is stretched and thinned, and in the second the diameter of the tip, and consequently the resistance of the microelectrode is defined.

The microelectrode is composed by a micropipette filled with the internal solution (Table 7) and with a reversible silver/silver chloride (Ag/AgCl) electrode electrically connected to the headstage. A microelectrode thus produced presented a resistance that ranged from 7 to 9 MΩ. The reference electrode was constituted by a Ag/AgCl electrode embedded in a 0.5 M KCl/agar bridge. The Ag/AgCl electrode permits a smooth transition between the electric current carried by electrons and the current carried by the ions in solution, reducing the contribution of possible junction potentials between the silver wire and the bath solution.

4.4.2. Recording solutions

The solutions used in the electrophysiological essays were designed in order to have as the main permeant ion either Cl^- (B1, B2, B5, B6, P1, P2 and P3) or NO_3^- (B3, B4 and P4). To achieve this, permeant cations such as K^+ and Na^+ were replaced by NMG^+, a non permeable ion, and the cation channel inhibitors TEA^+ and Gd^{3+} were used to block K^+ and Ca^{2+} channels, respectively (Dutta and Robinson, 2004; Fan *et al.*, 2001; Wang *et al.*, 2004).

Table 7 depicts the ionic composition of the external (B1 to B6) and internal (P1 to P4) solutions. The pH was adjusted to 7.2 (pipette) and 5.8 (bath) with NMG-OH and the osmolarity was adjusted with sorbitol to 700 mOsmol kg^{-1} (*Lilium longiflorum*) and to 800 mOsmol kg^{-1} (*Arabidopsis thaliana*). The internal solutions were complemented with EGTA as a Ca^{2+} e Mg^{2+} chelator, in order to maintain constant the free $[Ca^{2+}]_{in}$ in the pipette solutions. The values for the free $[Ca^{2+}]_{in}$ were estimated using the software WEBMAXCLITE v1.15, available online. These are 6.04 nM for P1 and P4, 8.50 μM for P2, and 0.54 mM for P3. ATP was added preventively to power any anionic transporters present in the membrane. The pH in these solutions was buffered by HEPES. In the external solutions the pH was buffered by MES. All chemicals were purchased from Sigma unless stated otherwise.

Table 7. Recording solutions: P1 to P4 are internal solutions (pipette) and B1 to B6 are external solutions (bath). The concentrations are in mM. The free $[Ca^{2+}]_{in}$ in the pipette solutions was estimated using the software WEBMAXCLITE v1.15, available online on http://www.stanford.edu/~cpatton/webmaxc/webmaxclite115.htm. The values are: 6.04 nM (P1, P4), 8.50 μM (P2) and 0.54 mM (P3).

	P1	P2	P3	P4	B1	B2	B3	B4	B5	B6
NMG-Cl	134.4	125	122	4.4	109	-	-	-	79	129
NMG-NO_3	5	5	5	135	5	1	110	114	31	5
$CaCl_2$	0.3	5	6.5	0.3	3	1	3	-	3	3
$Ca(NO_3)_2$	-	-	-	-	-	2	-	3	-	-
$MgCl_2$	-	-	-	-	1	1	1	1	1	1
MgATP	5	5	5	5	-	-	-	-	-	-
TEA-Cl	-	-	-	-	20	20	20	-	20	-
TEA-NO_3	-	-	-	-	-	-	-	20	-	-
$GdCl_3$	-	-	-	-	1	1	1	1	1	1
EGTA	5	5	5	5	-	-	-	-	-	-
MES	-	-	-	-	5	5	5	5	5	5
HEPES	5	5	5	5	-	-	-	-	-	-

The internal solutions P1, P2 and P3 were used in the study of the influence of the free $[Ca^{2+}]_{in}$ in the activity of the anionic channels. The external solution B2 was designed to confirm the presence of anionic currents and the solutions B3, B4 and B5 were used to study the relative permeability of the channels to Cl^- and NO_3^-.

Table 8 presents the equilibrium potentials (E) for the permeable ions in solution as predicted by the Nernst Equation.

Table 8. Equilibrium potentials for the permeable ions in solution, as predicted by the Nernst Equation. All values are in mVolts.

	E_{Cl^-}	$E_{NO_3^-}$	$E_{Ca^{2+}}$	$E_{Mg^{2+}}$	E_{H^+}
B1 x P1	-0.92	0.00	165.01	15.32	81.11
B1 x P2	-0.92	0.00	73.81	11.55	81.11
B1 x P3	-0.92	0.00	21.55	-0.88	81.11
B2 x P1	40.50	0.00	165.01	15.32	81.11
B3 x P1	37.02	-77.78	165.01	15.32	81.11
B4 x P4	0.00	-0.92	165.01	15.32	81.11
B5 x P4	-77.78	37.02	165.01	15.32	81.11
B6 x P1	-0.92	0.00	165.01	15.32	81.11

The inhibitory effect of NPPB, a known inhibitor of anionic currents (Gogelein, 1988), were tested on the currents. NPPB was first dissolved in DMSO, in a stock solution of 25 mM concentration and kept at 4ºC, previous to its utilization. Before it was used, the NPPB:DMSO solution was dissolved in bath solution. To determine the effect of the solvent DMSO in the anionic currents, an equivalent amount of this chemical was dissolved in bath solution and them added to the experimental preparation. The effect of TEA in the anionic currents was also studied (bath solution B6).

4.4.3. The voltage protocols

The voltage protocols used to study current activation and channel tail currents are shown in detail in Figure 10.

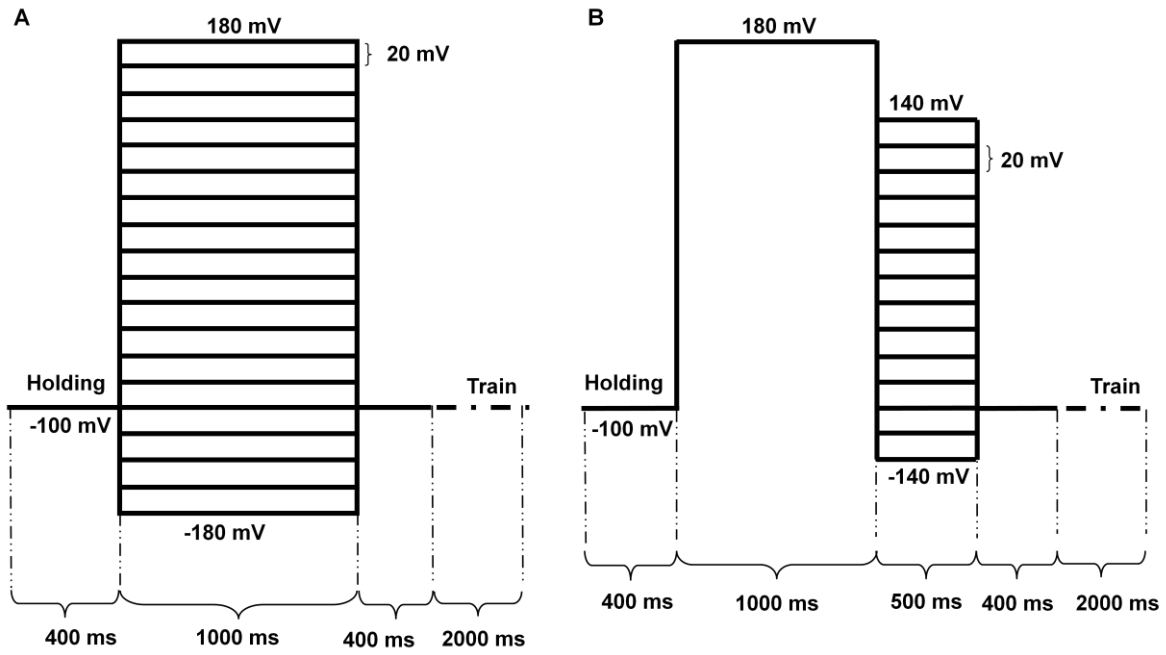

Figure 10. Voltage Protocols used. **A:** Voltage protocol used to study current activation. During experiments, the cell membrane was kept at a holding potential of -100 mV, which was followed by a series of 1 sec voltage jumps that ranged from -180 mV to +180 mV. The cell membrane was kept at -100 mV for 2 sec in between each voltage jump. **B:** Voltage Protocol used to study the channel tail currents. For these experiments the membrane potential was clamped at +180 mV for 1 sec in order to completely open all channels. This was followed by a series of 500 msec voltage jumps that range from -140 mV to +140 mV. In between each jump the cell membrane was clamped at -100 mV for 2 sec (train).

In both protocols, the cell membrane was kept at a holding potential of -100 mV. This potential was chosen because it maintains the seal stability between voltage jumps. Protocol A was designed to study current activation. This protocol has voltage jumps with duration of 1 sec, in order to guarantee that the currents generated had time to stabilise. Protocol B was designed to study channel deactivation. The membrane is initially clamped for 1 sec at +180 mV in order to guarantee that all the channels present in the membrane present their maximum conductivity state, then the membrane potential is changed into the test potential that ranged from -140 to + 140 mV.

4.4.4. Patch clamp protocol

i. For the electrophysiological essays, Petri dishes of 34 mm Ø with a 1 mL central chamber with glass bottom were used.

ii. The central chamber was filled with 400 µL of the external solution (Table 7) and 100 µL of the protoplasts suspension and then placed in the microscope stage.

iii. The protoplasts were allowed to set for 20 min. The reference electrode with the saline bridge was then mounted on the central chamber and connected to the ground slot of the headstage.

iv. The protoplast to be studied was chosen using an amplification of 300x (Table 9). It had to have a smooth plasma membrane and be preferably isolated from its shell.

v. A micropipette, filled with the appropriate internal solution (Table 7) and checked for air bubbles (that could interrupt the passage of current), was then introduced in the pipette holder, allowing the Ag/AgCl electrode to contact the pipette solution.

vi. With the aid of a syringe, connected through a tube to the pipette holder, a positive pressure is applied to the microelectrode, which is then dipped into the external solution, closing the electric circuit. It is now possible to measure the microelectrode resistance, by measuring the current elicited by a 5 mV square pulse.

vii. Using the macro and micromanipulators, the microelectrode is positioned immediately above the chosen protoplast, taking care to always keep the protoplast in the focal plane.

viii. The *pipette offset* command of the patch clamp amplifier is then used to correct the current generated by the difference of potential that is originated by the use of two different electrodes.

ix. To form a tight seal between the microelectrode tip and the plasma membrane, it is necessary to use the micromanipulator and to monitor the progressive loss of current in the oscilloscope. This loss is the consequence of the increase of resistance to the passage of ionic current between the external solution and the interior of the pipette, due to the approximation of the plasma membrane.

x. It is then necessary to remove the positive pressure in the microelectrode and apply negative pressure, in order to facilitate the seal formation. The seal resistance must be higher than 1 GΩ, since in its quality lies the best way of reducing the level of noise generated by the passage of current through the seal (Axon Instruments, 1993).

xi. Once the Giga-seal is established it is necessary to compensate for the capacitive transient currents generated not only by the pipette holder, but also by the patch

pipette, which when in contact with the extracellular solution behaves as a capacitor (Axon Instruments, 1993; Halliwell *et al.*, 1987). This compensation is performed by the *fast* and *slow pipette capacitance compensation* commands in the patch clamp amplifier.

xii. The *whole cell* (WC) configuration was obtained by applying negative pressure with the syringe, thus establishing an electrical continuity between the pipette solution and the cell's interior.

xiii. After the cell stabilizes, the cellular parameters of *access resistance* (R_a), *membrane resistance* (R_m) and *membrane capacitance* (C_m) are registered. R_a refers to the access to the cell's interior and dictates whether it is being completely clamped by the amplifier. Its value should always be kept low ($R_a \leq 10$ MΩ, Penner, 1995). R_m refers to the integrity and permeability of the membrane ($R_m \geq 1$ GΩ). C_m refers to the area of the membrane that is being clamped and its value is used to normalize the current values.

xiv. Using the *whole cell capacitance* and *series resistance* commands in the patch clamp amplifier it is possible to compensate for the capacitive currents due to the plasma membrane.

xv. It is then applied the voltage protocols represented in Figure 10. The first protocol to be used is protocol A, followed by protocol B (Figure 11, step 1). The anionic currents under study undergo a process of Rundown; this is monitored with the protocol A. When the currents stabilize, the protocols A and then B are applied (Figure 11, step 2). It is then either applied a known inhibitor of anionic channels or the bath solution is changed. Changes in the currents are monitored with the protocol A. When the currents stabilize, the protocols A and then B are applied (Figure 11, step 3). All the currents produced were acquired and recorded with a computer, using pCLAMP software (version 8.0, Axon Instruments).

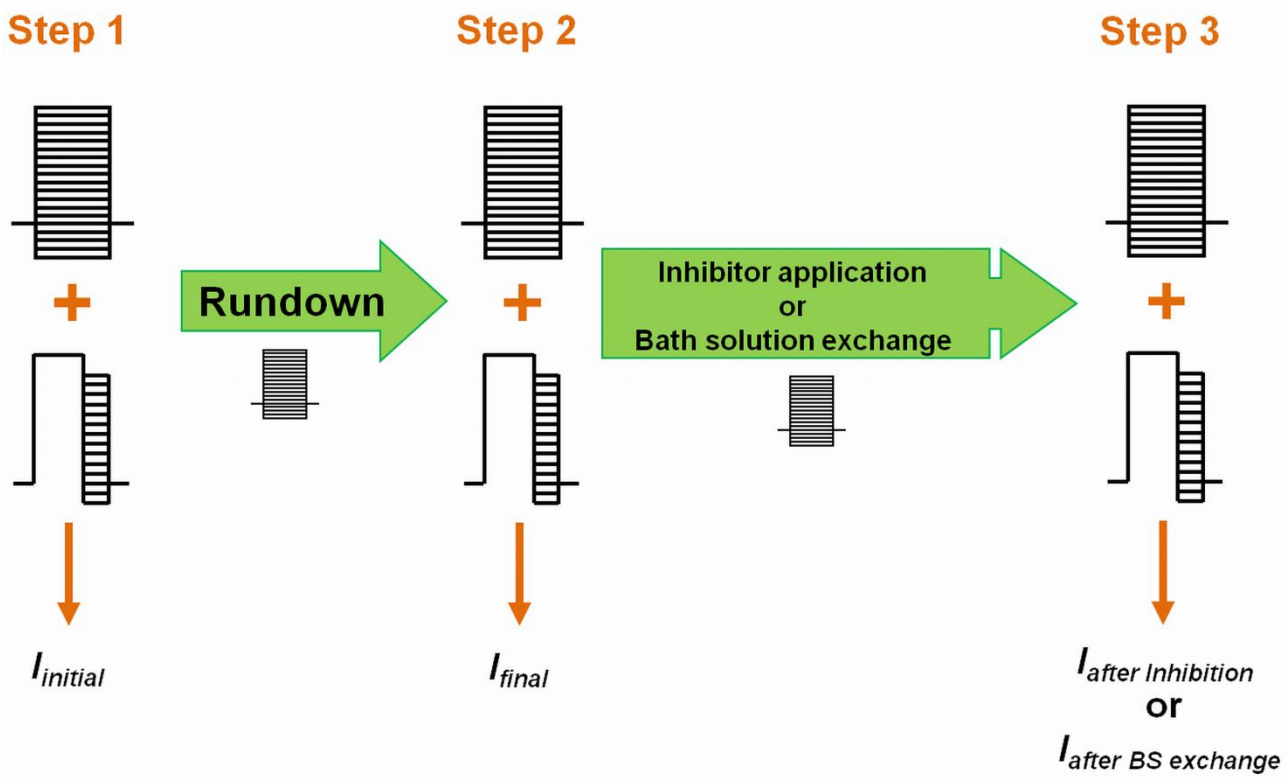

Figure 11. Layout of a typical experimental protocol.

xvi. Bath solutions were changed by injection of a continuous flow rate of approximately 20 $cm^2\ s^{-1}$, through a tube with 500 μm of internal diameter, placed at one end of the circular measuring chamber and removed at the same rate from the opposite side. This system was used because of the size of the protoplasts. In the case of the Lilium protoplasts, these were too big to be lifted without the seal being lost. Although the Arabidopsis' protoplasts were small enough to be lifted, when they were taken close to the tube, the flowing solution caused the destabilization of the seal, and in some cases, the protoplast was dragged away from the pipette.

xvii. Currents were measured using a patch clamp amplifier, and the electrical signal was sampled at 50 kHz and was filtered at 5 kHz.

xviii. The pCLAMP software (version 8.0, Axon Instruments) was used to generate command potentials, and to collect and analyze the data.

xix. The data obtained by these protocols were used to build Current-Voltage (I/V) curves and to gather information on the nature of the currents and the channels involved.

All experiments were performed at temperatures between 19º and 20 ºC.

4.4.5. The patch clamp setup

The patch clamp setup consists of a microscope mounted on top of an anti-vibrating table, inside a Faraday's Cage, a patch clamp amplifier, a pulse generator, a micromanipulator and data-recording devices (Penner, 1995). Figure 12 shows the patch clamp setup used to gather the results presented here.

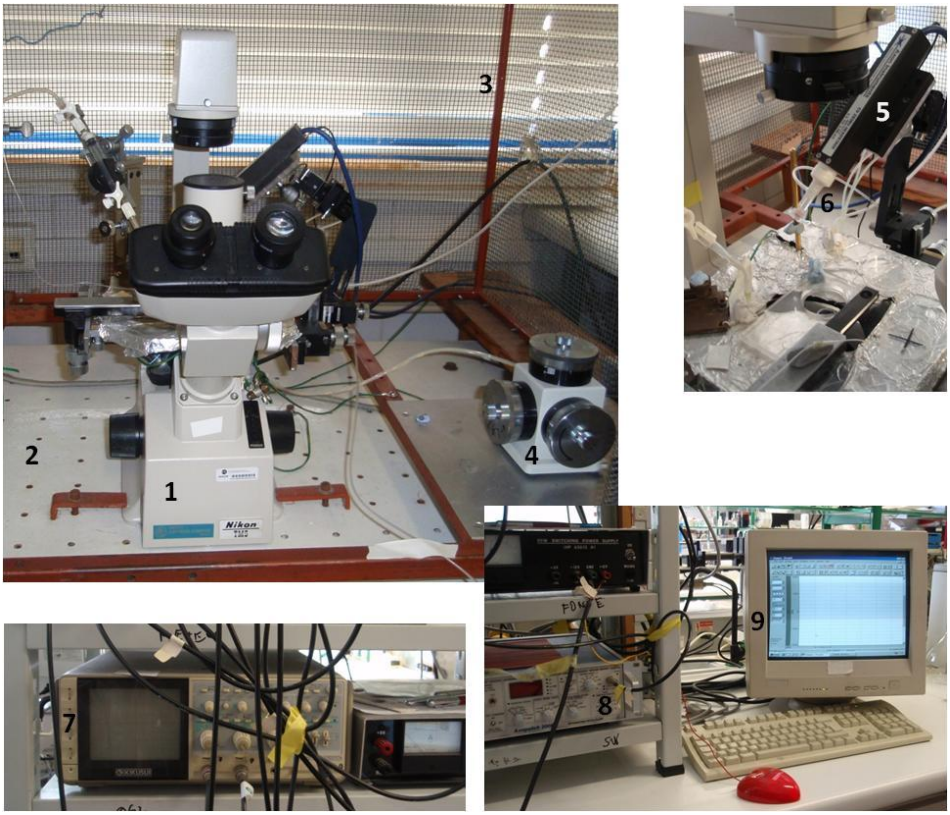

Figure 12. Patch clamp setup: 1 – Inverted Microscope; 2 – Vibration Isolation Table; 3 – Faraday's cage; 4 – Micromanipulator; 5 – Headstage; 6 – Pipette holder; 7 – Oscilloscope; 8 – Amplifier; 9 – Computer.

The setup can be divided in three parts:

I. Optic - means of visualizing the preparation, achieved by means of an inverted microscope, since this one grants greater stability to the preparation (Figure 12 - 1).
II. Mechanic – means of getting a stable and clear electrical signal:
    a. a Vibration Isolation Table, essential to attain stable recordings (Figure 12 - 2);
    b. a Micromanipulator to precisely control the movements of the patch pipette in a sub-µm range (Figure 12 - 4).
III. Electronic - means to amplify, visualise and record the electric signal:
    a. an amplifier to apply the electric stimulus and to amplify and record the received electric signal (Figure 12 - 8);

b. a Digital to Analogue (D/A) converter;
c. a Faraday's cage, which shields the sensitive headstage from electrical noise (Figure 12 - 3);
d. a computer to design and control the application of the electric protocols. It is also used to visualise and store the acquired data (Figure 12 - 9).
e. the appropriated software that performs the interface between the user and the electronic devices.

Because of the extreme sensitivity of the headstage, all elements that constitute the three parts of a patch clamp setup must be grounded (Penner, 1995). Table 9 presents a summary of the models and brands of the instruments that constitute the setup used.

Table 9. Summary of the models and brands of the instruments that constitute the setup used in the electrophysiological essays.

	Model	Brand	Country
Microscope	TMS	Nikon	Japan
Objective lenses	Plan 20/0.40 160/1.2 ELWD	Nikon	Japan
	Plan 40/0.55 160/0-2.5 ELWD	Nikon	Japan
Eyepiece lenses	CFWE 15x/14	Nikon	Japan
Micro-manipulator	MMO-203	Narishige	Japan
Macro-manipulator	MN-	Narishige	Japan
Headstage	CV203BU	Axon Instruments	U.S.A
Patch clamp amplifier	Axopatch 200B	Axon Instruments	U.S.A
DigiData	1320A - 16 Bit Data Acquisition System	Axon Instruments	U.S.A
Digital Oscilloscope	COR 5501U	KIKUSUI	Japan

4.4.6. Data analysis

i. The data analysis was performed with Clampfit 8.0 (Axon Instruments) on raw data from cells which presented stable seals with GΩ resistances.

ii. At the interface between two different salt solutions, a difference of potential sets in. This is designated by liquid junction or diffusion potential (V_j), and results from different anionic and cationic mobilities and from different solute concentrations (Halliwell *et al.*, 1987). The V_j will affect the actual potential that is being applied to the membrane during a patch clamp experiment and therefore must be accounted

for (Axon Instruments, 1993). Liquid junction potentials were calculated with the Clampex 8.0 software and corrected for all whole-cell recordings (Table 10).

Table 10. Liquid junction potentials (V_j) calculated with the Clampex 8.0 software for all experimental conditions. All values are in mV.

	B1 x P1	**B1 x P2**	**B1 x P3**	**B1 x P1 → B2**	**B1 x P1 → B3**	**B4 x P4**	**B4 x P4 → B5**
V_j (mV)	-0.1	-0.2	-0.3	-4.0	-0.5	-0.2	0.0

iii. All linear and non-linear data fitting was performed with Origin 6.1 software (OriginLab Corporation).

iv. Statistical significances were determined using the t-Test with Origin 6.1 software, unless stated otherwise, and differences were considered significant if $p < 0.05$. The Carl Pearson Coefficient of correlation was used to measure the linear relationship between two variables.

v. For the experiments with *Arabidopsis thaliana*, the intensity of the currents of each protoplast was normalized with the respective membrane capacitance (C_m), producing the current density values (pA/pF) used to build the Current – Potential (I/V) relationships.

vi. For each experimental condition data from different cells were averaged. The data shown are mean ± SE (n), where n is the number of cells obtained for a particular experiment.

vii. Asymptotic forward and backward conductances (g_F and g_B respectively) were estimated by means of a least-mean-square linear fit, using the values of the current density that were proportional to the variations of V_m.

viii. Relative permeability was determined by measuring the shift in reversal potential (V_{rev}) upon changing the bath or external solution from one containing a high [Cl^-] (B1) to another with high [NO_3^-] (B3) and vice-versa (B4 to B5). The permeability ratio was estimated using the Goldman-Hodgkin-Katz equation:

$$\frac{P_{NO_3}}{P_{Cl}} = e^{(\Delta V_{rev} * F)/RT}$$

Equation 1

where ΔV_{rev} is the difference between the V_{rev}s obtained with the bath solution with high [NO_3^-] and the bath solution with high [Cl^-], F is the Faraday's constant, R is the gas constant and T is the temperature in Kelvin degrees.

ix. The cord conductance (G) was derived from the I/V relationships according to:

$$\boldsymbol{G = \frac{I_{ss}}{V_m - V_{rev}}}$$

Equation 2

where I_{ss} is the steady-state current at the end of the test potential (averaged from the last 50 ms of the respective test potential), V_m refers to the membrane potential and V_{rev} is the reversal potential of the current. The cord conductance values were normalized for the maximum response, plotted against V_m and fitted with a Boltzmann type equation:

$$\boldsymbol{\frac{G}{G_{max}}(V_m) = A_2 + \frac{A_1 - A_2}{1 + e^{(V_m - V_h)/V_s}}}$$

Equation 3

where A_1 and A_2 are the values for the minimum and maximum conductance, respectively, when this no longer varies with V_m, V_h is the potential for the half-maximal chord conductance and indicates at which V_m the transition between the two states of conductance occurs, and V_S is the slope of the $G/G_{max}(V_m)$ curve and a measure of the sensitivity of the currents to variations in V_m.

x. The currents elicited $I_{(t)}$ could be fitted with the following equation:

$$\boldsymbol{I_{(t)} = \sum_{i=0}^{n} I_i * e^{-t/\tau_i} + I_{inst}\,, \qquad n \in \mathbb{N}_0, \qquad i = 0 \Rightarrow I_0 = 0}$$

Equation 4

where $I_{(t)}$ is the total current, I_{inst} is the instantaneous current component, I_i is the time dependent current component, τ_i is the time constant, and t stands for time. When i=0, there is no I_i.

xi. In order to calculate the corresponding anion fluxes that the elicited currents could produce the following formula was used:

$$\boldsymbol{Flux = \frac{I}{zF * C_m}}$$

Equation 5

where I is the current (in Amperes), z is the ion's valence, F is the Faraday's constant (96485.3415 s A mol^{-1}), and C_m is the membrane's capacitance (C_m = 1 µF cm^{-2}). Using this formula it is possible to convert *Current Density* (pA/pF) into *Ion Flux* (pmol cm^{-2} s^{-1}).

5. Results

5.1. Anionic currents in pollen grain protoplasts from **Arabidopsis thaliana**

5.1.1. Three different activities of outward-rectifying, depolarization-activated anionic currents were found

To investigate the presence of anionic currents in pollen grains protoplasts from *Arabidopsis thaliana*, the whole cell (WC) configuration of the patch clamp technique was used under symmetrical Chloride concentrations ($[Cl^-]$). These experimental conditions were accomplished by using the pipette or internal solution P1 combined with the bath or external solution B1 (Table 7 in Experimental Procedures, page 62), and can be referred to as the *Control*. The symmetrical $[Cl^-]$ were chosen in order to eliminate the chemical potential, while isolating the dependence of the currents on the variation of the membrane potential (V_m). Under *Control* conditions, the voltage protocol A (Figure 10 in Experimental Procedures, page 64), elicited anionic currents dominated by Cl^-, since this was the major permeable ion present. These were characterized by a time-dependent activation at positive membrane potentials (V_m). The currents were fitted with Equation 4 (Experimental Procedures, page 71), showing one instantaneous component I_{inst} (sub msec range) and two time dependent current components I_1 and I_2, characterized by τ_1 and τ_2 respectively, with τ_1 greater than τ_2 (Table 11). It was also possible to characterize these currents as outwardly rectifying, since the positive currents (Cl^- entering the cell) were larger than the negative currents (Cl^- exiting the cell), for symmetrical electrochemical gradients. These properties can be observed in the raw data and the Current – Potential (I/V) curves present in Figure 13.

It was observed in all protoplasts, a gradual decrease of the currents' intensity after breaking into the WC configuration. This behaviour, commonly referred to as rundown, is relatively frequent in currents elicited by channels with intracellular regulation, and is probably due to the dilution of the regulators during the equilibration of the cytoplasm with the pipette solution (Becq, 1996; Binder *et al.*, 2003; Marty and Neher, 1995). Under control conditions the percentage of anionic current lost during rundown (%Rundown) increased for negative V_m, in a statistically significant manner, and was constant for positive V_m, which might indicate that the effector that regulates these currents is sensitive

to changes in the electric field that surrounds the plasma membrane. Nevertheless, in order to simplify the comparative analysis of this factor in different experimental groups, only the %Rundown obtained for representative V_m (-160 mV and +160 mV) were considered. The values of this parameter for -160 and +160 mV are 43 ± 5 % and 56 ± 5 %, respectively (Table 11). After the stabilization of the rundown, the anion channel inhibitor NPPB was tested on the remaining current. A maximum inhibition of the chloride currents was obtained for a NPPB concentration ([NPPB]) of 100 µM. Unlike the %Rundown, the percentage of inhibited current (%Inhibition) increased with V_m for both positive and negative potentials. This increase was statistically significant, and could indicate a different sensitivity of the process of inhibition to changes in the electric field that surrounds the plasma membrane. Again, only the values obtained for the V_m -160 and +160 mV were considered for comparative purposes. These were 22 ± 4 % and 36 ± 4 %, respectively (Table 11).

Three different populations of outwardly rectifying anionic currents can therefore be inferred from these results: I_{Cl1}, is the current lost during rundown and can be calculated by the point-by-point subtraction of the raw data from the initial current ($I_{initial}$) and the current after rundown (I_{final}); I_{Cl2} is the current resistant to NPPB; and I_{Cl3} is the inhibited current ($I_{final} – I_{Cl2}$). From these WC currents it is not possible to determine whether I_{Cl1}, I_{Cl2} and I_{Cl3} are the result of three different conductance states of one channel or of three different channels. Therefore, from this point on, I_{Cl1}, I_{Cl2} and I_{Cl3} will be address as *current populations*, and will be the only currents considered for analysis.

Figure 13-A shows the raw data for the anionic currents thus far described, obtained from one protoplast under *Control* conditions. They represent, from A1 to A5, $I_{initial}$, I_{final}, I_{Cl2}, I_{Cl1} and I_{Cl3}, respectively. Figure 13B shows the Current - Voltage (I/V) curves obtained by plotting the elicited steady-state currents (average from the final 50 ms – orange line) against the corresponding V_m. These curves refer to $I_{initial}$ (black squares - ■), I_{final} (orange circles - ●), and I_{Cl2} (green triangles - ▲), and represent the final result of the three steps of the experimental protocol (Figure 10 in Experimental Procedures, page 64). In Figure 13B, it is possible not only to observe the decrease in the currents amplitude before and after rundown, but also the reduction caused by the inhibitor NPPB. Both reductions occurred for negative and positive V_m (better observed in Figure 14), which suggests that these channels allow the passage of current in both directions (inwardly and outwardly).

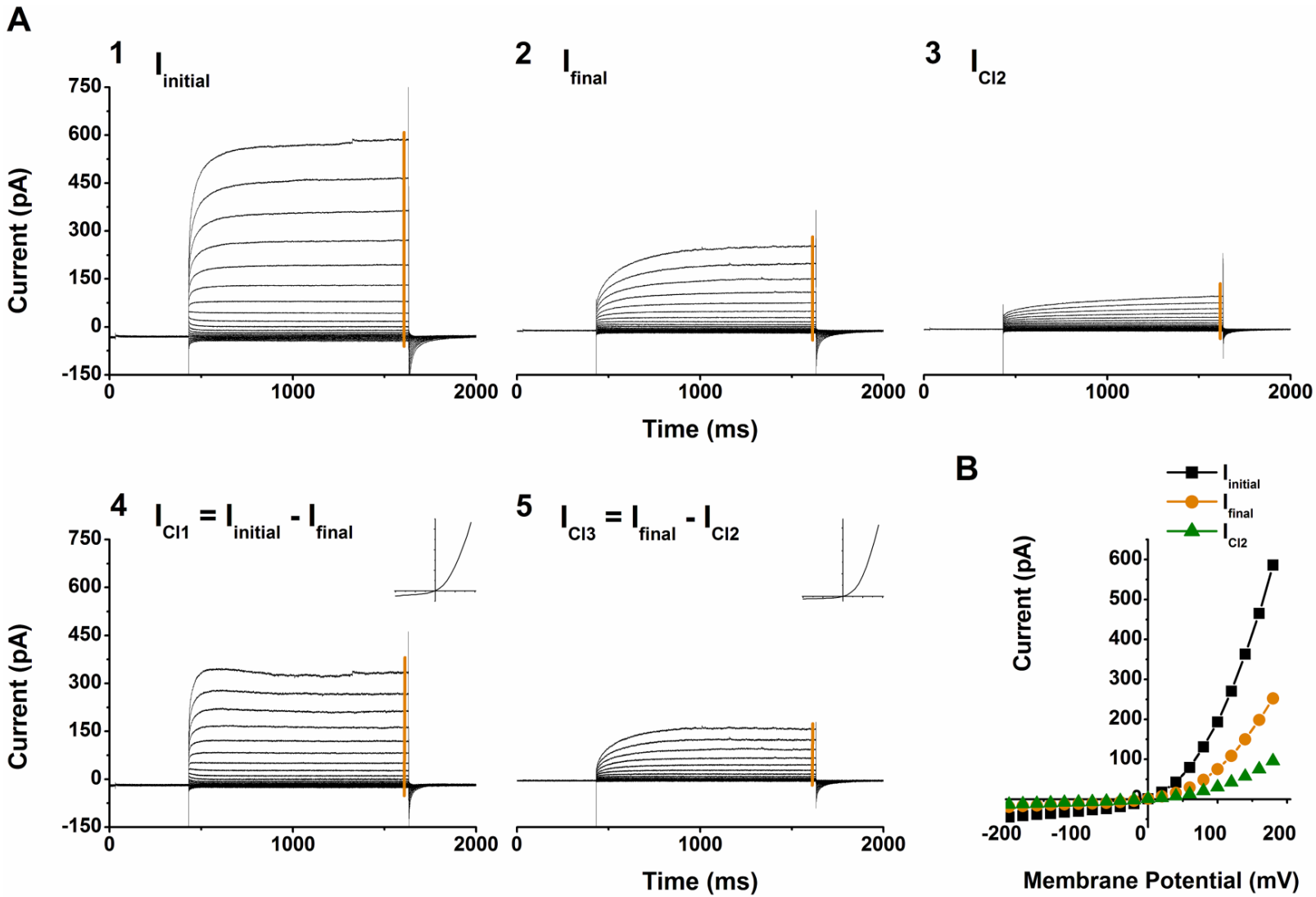

Figure 13. Typical chloride whole-cell currents from a pollen grain protoplast of *Arabidopsis thaliana*, measured with B1/P1 solutions (control group, nM $[Ca^{2+}]_{in}$). The currents were elicited from a holding potential of -100 mV with the voltage protocol depicted in Figure 10A. **A1 - 5** portray the raw data obtained for these currents: **A1** represents the Initial current recorded immediately after entering whole-cell configuration ($I_{initial}$); **A2**, the current recorded after Rundown (I_{final}); **A3**, the current recorded after inhibition by 100 µM NPPB (I_{Cl2}); **A4**, the current lost during rundown (I_{Cl1}) obtained by subtracting $I_{initial}$ and I_{final}; **A5**, the Inhibited Current (I_{Cl3}) obtained by subtracting I_{final} and I_{Cl2}. **B** represents the Current-Potential (I/V) relationships of $I_{initial}$ (■), I_{final} (●), and I_{Cl2} (▲). The data to construct this curve was averaged from the last 50 ms of the respective raw data (orange line). The inserts in **A4** and **A5** represent the respective I/V curves.

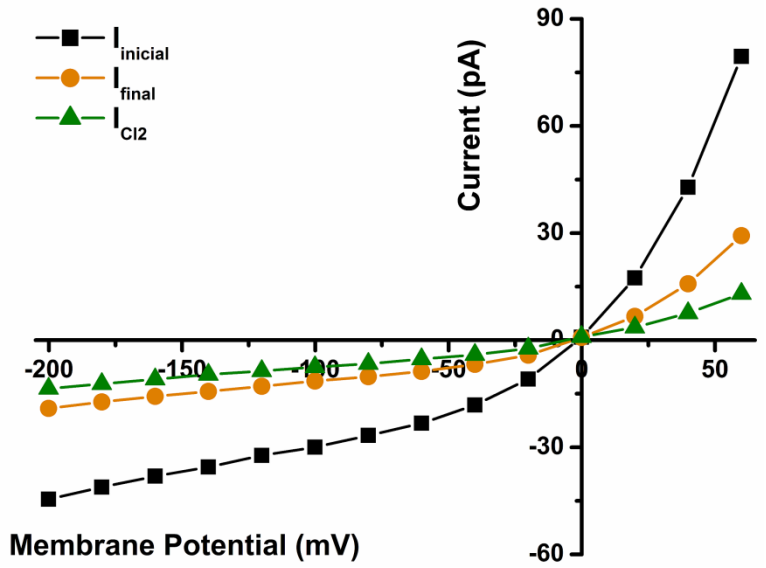

Figure 14. Detail from Figure 13-B, where the negative currents can be better observed. As in Figure 13-B, the symbols (■), (●) and (▲) stand for $I_{initial}$, I_{final}, and I_{Cl2}, respectively.

Before a more thorough analysis of these current populations was performed, the intensity of the currents of each protoplast was normalized with the respective membrane capacitance (C_m), producing the current density values (pA/pF) that were used to build the Current – Potential (I/V) curves. From these, other important data that can be obtain, such as the asymptotic forward and backward conductances (g_F and g_B respectively), estimated from the first and last four points or the curves (Experimental Procedures, page 70). Taken together with the values for the current density it is possible to confirm that all three populations of currents – I_{Cl1}, I_{Cl2} and I_{Cl3} – rectify outwardly (Table 11).

Table 11 presents a summary of the parameters that characterize the three current populations obtained under *Control* experimental conditions. As expected, the reversal potentials (V_{rev}) for I_{Cl1} and I_{Cl3} (-1.0 ± 0.7 and -1.1 ± 1.1 mV, respectively) were similar to the E_{Cl-} (-0.92 mV), which further confirms the nature of these currents. On the other hand, the V_{rev} for I_{Cl2} (-5.0 ± 0.8 mV) was significantly more negative than the other two. This discrepancy cannot be explained by the passage through the membrane of any of the other permeable ions in solution, for this would cause a shift of V_{rev} to more positive values (Table 8 in Experimental Procedures, page 63). The probability that it is due to the exit of endogenous K^+ from the cell is remote, since all experiments were performed in the presence of two cation channel inhibitors, TEA and Gd^{3+}, in the bath solution, and because the equilibration of the pipette solution with the cytoplasm had already occurred. This

divergence in the V_{rev} from I_{Cl2} could be an artefact, since it is not always present, but when it happens it is kept more or less constant throughout the whole experiment.

Table 11. Steady-state chloride currents' parameters obtained in *Control* experimental conditions (B1/P1 - nCa). $\mathbf{I_{(-160\ mV)}}$ and $\mathbf{I_{(+160\ mV)}}$ correspond to the current density (pA/pF) elicited by V_m of -160 mV and +160 mV respectively. $\mathbf{g_B}$, $\mathbf{g_F}$, and $\mathbf{g_F/g_B}$ refer to the backward conductance, the forward conductance and their ratio, respectively ($\mathbf{g_B}$ and $\mathbf{g_F}$ are in nSiemmens). $\mathbf{V_h}$ is the potential for the half-maximal chord conductance and indicates at which V_m the transition between the minimum and maximum states of conductance occurs, and $\mathbf{V_s}$ is the slope of the $G/G_{max}(V_m)$ curve and a measure of the sensitivity of the currents to variations in V_m. ($\mathbf{V_h}$ and $\mathbf{V_s}$ are in mVolts). $\mathbf{V_{rev}}$ refers to the reversal potential and is in mVolts. **Activation** refers to the currents elicited by voltage protocol A. $\boldsymbol{\tau_1}$ and $\boldsymbol{\tau_2}$ refer to the time constants that characterize the time dependent current components I_1 and I_2 respectively ($\boldsymbol{\tau_1}$ and $\boldsymbol{\tau_2}$ are in msec). $\mathbf{I_{Cl1}}$, $\mathbf{I_{Cl2}}$ and $\mathbf{I_{Cl3}}$ refer to the current lost during Rundown, the current after NPPB inhibition, and the inhibited current, respectively. **%Rundown** refers to the percentage of current lost during rundown for V_m = -160 and +160 mV. **%Inhibition** refers to the percentage of inhibited current for those same V_m. $\mathbf{[NPPB]_{mean}}$ and $\mathbf{[NPPB]_{max}}$ refer to the average [NPPB] and the maximal [NPPB] needed for maximal inhibition, respectively. Data are represented as mean ± SE. *, refer to significant differences ($p < 0.05$).

	Control Group (B1/P1 – nCa)			
	$\mathbf{I_{(-160\ mV)}}$ **(pA/pF)**	$\mathbf{I_{(+160\ mV)}}$ **(pA/pF)**	$\mathbf{V_{rev}}$ **(mV)**	**n**
$\mathbf{I_{Cl1}}$	-4.4 ± 1.0	60.8 ± 9.5*	-1.0 ± 0.7	17
$\mathbf{I_{Cl2}}$	-5.2 ± 0.7	26.6 ± 3.4*	-5.0 ± 0.8*	16
$\mathbf{I_{Cl3}}$	-0.8 ± 0.3*	16.0 ±2.8*	-1.1 ± 1.1	16
%Rundown	43 ± 5	56 ± 5		17
%Inhibition	22 ± 4	36 ± 4		16
$\mathbf{[NPPB]_{mean}}$		100 ± 0 µM		16
$\mathbf{[NPPB]_{max}}$		100 µM		
	$\mathbf{g_B}$ **(nS)**	$\mathbf{g_F}$ **(nS)**	$\mathbf{g_F/g_B}$	**n**
$\mathbf{I_{Cl1}}$	0.018 ± 0.005	0.600 ± 0.098*	47 ± 5	17
$\mathbf{I_{Cl2}}$	0.032 ± 0.004	0.315 ± 0.039*	12 ± 2*	16
$\mathbf{I_{Cl3}}$	0.007 ± 0.002*	0.202 ± 0.035*	53 ± 11	16
			Activation	
	$\mathbf{V_h}$ **(mV)**	$\mathbf{V_s}$ **(mV)**	$\boldsymbol{\tau_1}$ **(ms)**	$\boldsymbol{\tau_2}$ **(ms)**	**n**
$\mathbf{I_{Cl1}}$	88 ± 7*	55 ± 2	455 ± 34	67 ± 3*	17
$\mathbf{I_{Cl2}}$	142 ± 6	59 ± 3	488 ± 56	36 ± 1*	16
$\mathbf{I_{Cl3}}$	137 ± 11	64 ± 5	240 ± 5*	49 ± 1*	16

Another characteristic that distinguishes between the 3 populations of currents is the g_F/g_B ratio, which in the case of I_{Cl2} is significantly lower (12 ± 2), indicating a weaker rectification than in I_{Cl1} and I_{Cl3}.

It was previously explained that the currents elicited by voltage protocol A could be described by the sum of three components that can be expressed by the following form of Equation 4 (Experimental Procedures, page 71):

$$I_{(t)} = I_{inst} + I_1 * e^{-t/\tau_1} + I_2 * e^{-t/\tau_2}$$

Equation 6

Of the three components, one is instantaneous (I_{inst}), while I_1 and I_2 are time dependent, and characterized by τ_1 and τ_2. There was no statistical evidence pointing to the variation of τ_1 and τ_2 with V_m, with no significant patterns emerging when these two variables are plotted against each other (Figure 15). So, with the objective of facilitating their comparison, the values shown in Table 11 for τ_1 and τ_2 are averages of all values. τ_1 was significantly lower for I_{Cl3}, while τ_2 varied significantly between all three current populations, reaching the highest value for I_{Cl1} and the lowest for I_{Cl2}.

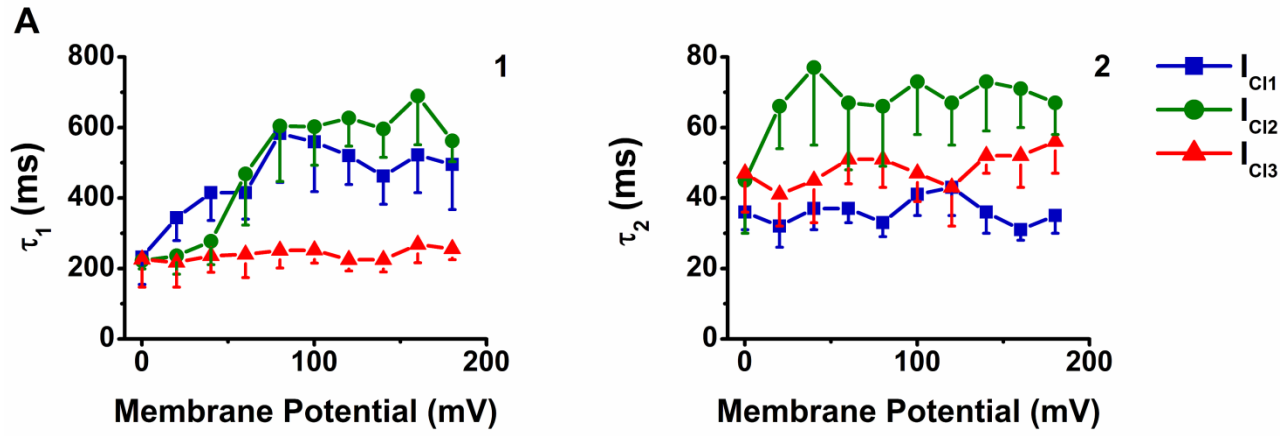

Figure 15. Variation of the activation τ_1 (**1**) and τ_2 (**2**) with V_m, in the Control Experimental Group (B1/P1). Blue squares refer to I_{Cl1} (■), dark green circles refer to I_{Cl2} (●), and red triangles refer to I_{Cl3} (▲).

In order to study the variation of the conductance with the applied V_m, the values for the current intensity were converted into their respective cord conductances (G) by applying Equation 2 (Experimental Procedures, page 71). They were then normalized and plotted against V_m. Figure 16 illustrates the voltage dependence of the averaged normalized cord conductances (G/G_{max}) for the three current populations. The data was fitted with Equation 3 (Experimental Procedures, page 71), and the characterizing parameters V_h – potential corresponding to the half-maximal chord conductance, indicating at which V_m the transition between the two states of conductance (minimum and maximum) occurs – and V_s –the slope of the $G/G_{max}(V_m)$ curve and a measure of the sensitivity of the currents to variations in V_m – are summarized in Table 11. According to this data, I_{Cl1} has a different sensitivity to variations in V_m, since the transition between the minimum and the maximum conductance states occurs at significantly lower V_m (V_h = 88 ± 7 mV). Experimentally it was not possible

to elevate V_m to values higher than +200 mV. Nevertheless, from Figure 16, it is possible to observe that at $V_m \approx$ +200 mV the maximum conductance had not been achieved and its variation was still dependent on the potential. Therefore, the values of V_s and V_h for these currents (especially I_{Cl2} and I_{Cl3}) are an approximation.

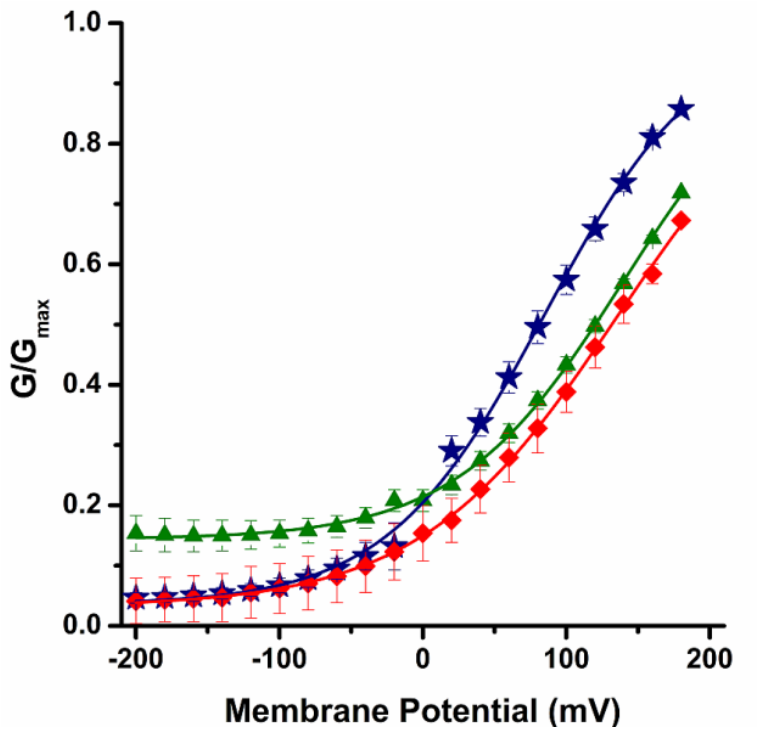

Figure 16. Voltage dependence of the averaged normalized chord conductances (G/G_{max}), obtained in *Control* experimental conditions (B1/P1 - nCa), for I_{Cl1} (*), I_{Cl2} (▲), and I_{Cl3} (♦).

In order to determine the effect of the inhibitor TEA^+ and the solvent DMSO on these anionic currents, controls with these substances were performed, and it was possible to conclude that both TEA^+ and DMSO, in the concentrations used, had no effect in the currents.

5.1.2. The three populations of currents are deactivated by hyperpolarization

The protocol B (Figure 10B in Experimental Procedures, page 63) was used to test whether the three current populations described, were deactivated by membrane hyperpolarization. In this protocol V_m was clamped at +180 mV in order to maximize the conductive state of the channels. This step was followed by a series of voltage jumps that ranged from -180 mV to +140 mV. Figure 17A shows the typical raw data for the WC deactivation current. It is possible to observe in the raw data that the channels responsible for these currents have a time-dependent, hyperpolarization induced deactivation, which

can also be fitted with Equation 6, even though it is, in this case, describing a phenomenon of decay.

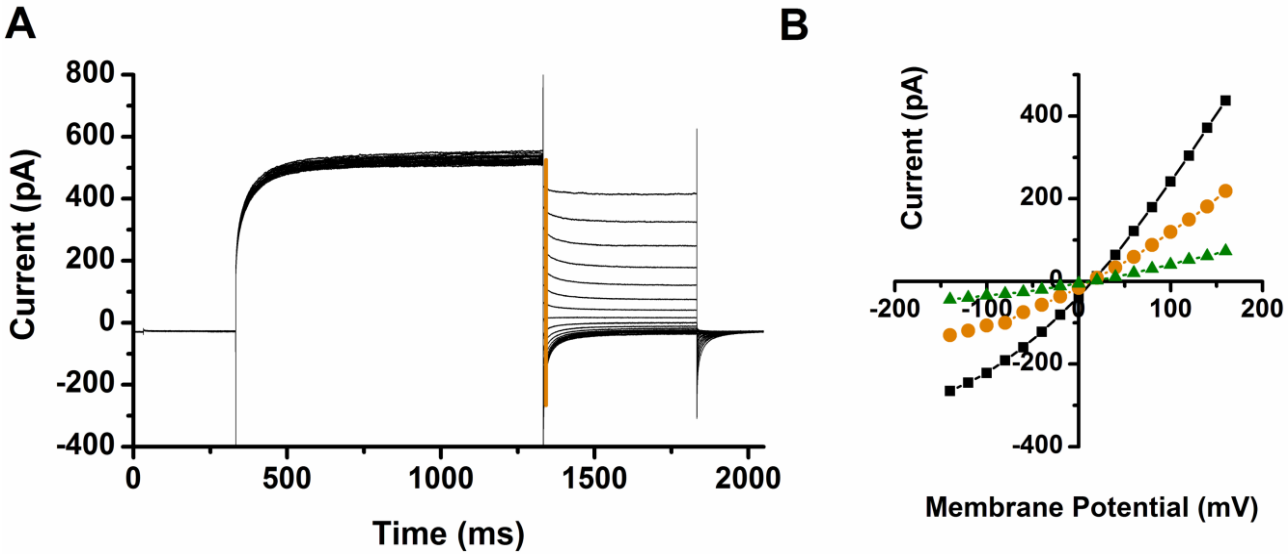

Figure 17. A: Typical raw data for the WC deactivation current ($I_{initial}$). **B:** I/V curve of $I_{initial}$ (■), I_{final} (●), and I_{Cl2} (▲), which was constructed from the current values obtained immediately after the test potential was applied (orange line). Currents were measured with protocol B (see Figure 10B in Experimental Procedures, page 64), in *Control* experimental conditions (B1/P1 - nCa).

Figure 17B contains the I/V curves constructed by plotting the current obtain immediately after the test potential is applied (Figure 17A, orange line) against the V_m. By using these current values it is possible to not only confirm the nature of the currents but also to isolate them from their characteristic rectification. The curves presented refer to one cell, and correspond to $I_{initial}$ (black squares - ■), I_{final} (orange circles - ●), and I_{Cl2} (green triangles - ▲). From this figure it is possible to observe that the instantaneous behaviour of the channels has an expected weak outward rectification, since for V_m = +180 mV, the channels had not reached their maximum conductivity state, and that the V_{rev} is more positive than E_{Cl^-} (= -0.92 mV). These observations are confirmed by the values of the parameters g_B, g_F, g_F/g_B, and V_{rev} present in Table 12. Of these only g_F varied significantly between the three current populations. The observed shift of the V_{rev} to more positive V_m could be explained by the leakage of cations, such as Ca^{2+}, Mg^{2+} or H^+, from the pipette into the bath solution, or by the passage of H^+ through transporters such as H^+ - anion antiporters. The first explanation, although more common, is less likely since the seals in these cells ranged between 2 and 10 GΩ.

Table 12. WC deactivation current parameters calculated for *Control* experimental group (B1/P1 - nCa). Parameters g_B, g_F, g_F/g_B, V_{rev}, τ_1, τ_2, I_{Cl1}, I_{Cl2}, and I_{Cl3} as described in Table 11. **Deactivation** refers to the currents elicited by voltage protocol B. Data are represented as mean ± SE. *, refer to significant differences ($p < 0.05$).

Control Group (B1/P1 – nCa)				
	g_B (nS)	g_F (nS)	g_F/g_B	n
I_{Cl1}	0.217 ± 0.079	0.467 ± 0.071*	4 ± 2	6
I_{Cl2}	0.083 ± 0.031	0.300 ± 0.045*	4 ± 1	6
I_{Cl3}	0.050 ± 0.034	0.100 ± 0.037*	2 ± 0	6
		Deactivation		
	V_{rev} (mV)	τ_1 (ms)	τ_2 (ms)	n
I_{Cl1}	11.8 ± 1.4	200 ± 15*	30 ± 3	17
I_{Cl2}	5.4 ± 1.8	133 ± 8	21 ± 2*	16
I_{Cl3}	17.4 ± 13.9	164 ± 14	33 ± 2	16

The time constants τ_1 and τ_2 that characterize the time dependence of the deactivation WC currents are also summarized in Table 12. Both τ_1 and τ_2 presented no evidence pointing to their variation with V_m, and no significant pattern when plotted (Figure 18A and B). Consequently the values presented in Table 12 are averages calculated from all the values obtained at different V_m. τ_1 and τ_2 were significantly lower for I_{Cl1} and I_{Cl2}, respectively.

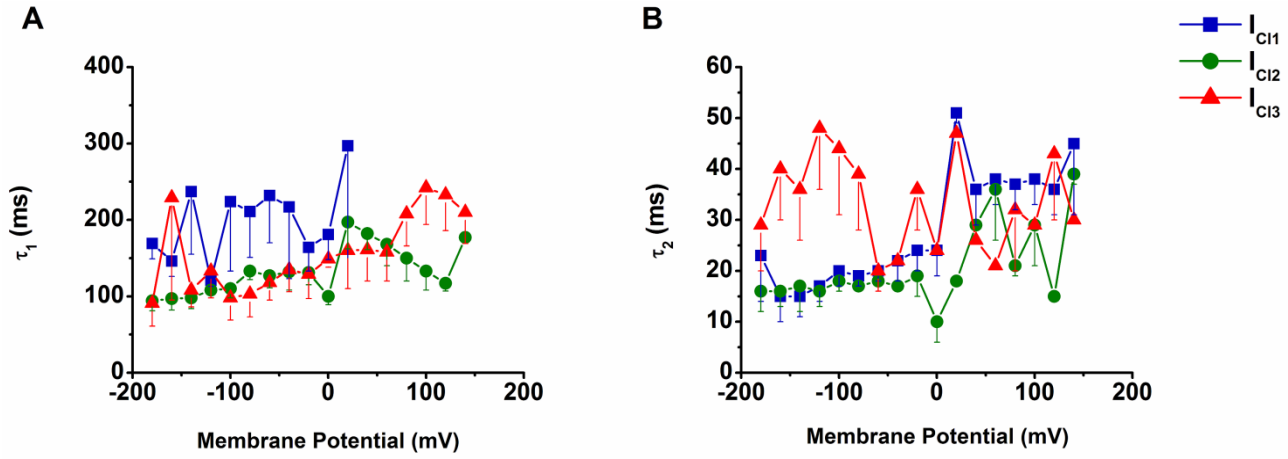

Figure 18. Variation of the deactivation τ_1 (**A**) and τ_2 (**B**) with V_m, for the Control Experimental Group (B1/P1). Blue squares refer to I_{Cl1} (■), dark green circles refer to I_{Cl2} (●), and red triangles refer to I_{Cl3} (▲).

5.1.3. The magnitudes of outward and inward currents are dependent on external [Cl^-]

The results so far described, were obtained under experimental conditions in which Cl^- was not only the major anion present in solution, but was also in symmetrical concentrations. To confirm the nature of the Cl^- currents a lower $[Cl^-]_{out}$ was tested, by exchanging the bath solution B1 ($[Cl^-]$ = 140 mM; $[NO_3^-]$ = 5 mM) for B2 ($[Cl^-]$ = 27 mM; $[NO_3^-]$ = 5 mM) (Table 7

in Experimental Procedures, page 62) after the stabilization of the Rundown (Figure 11 in Experimental Procedures, page 67).

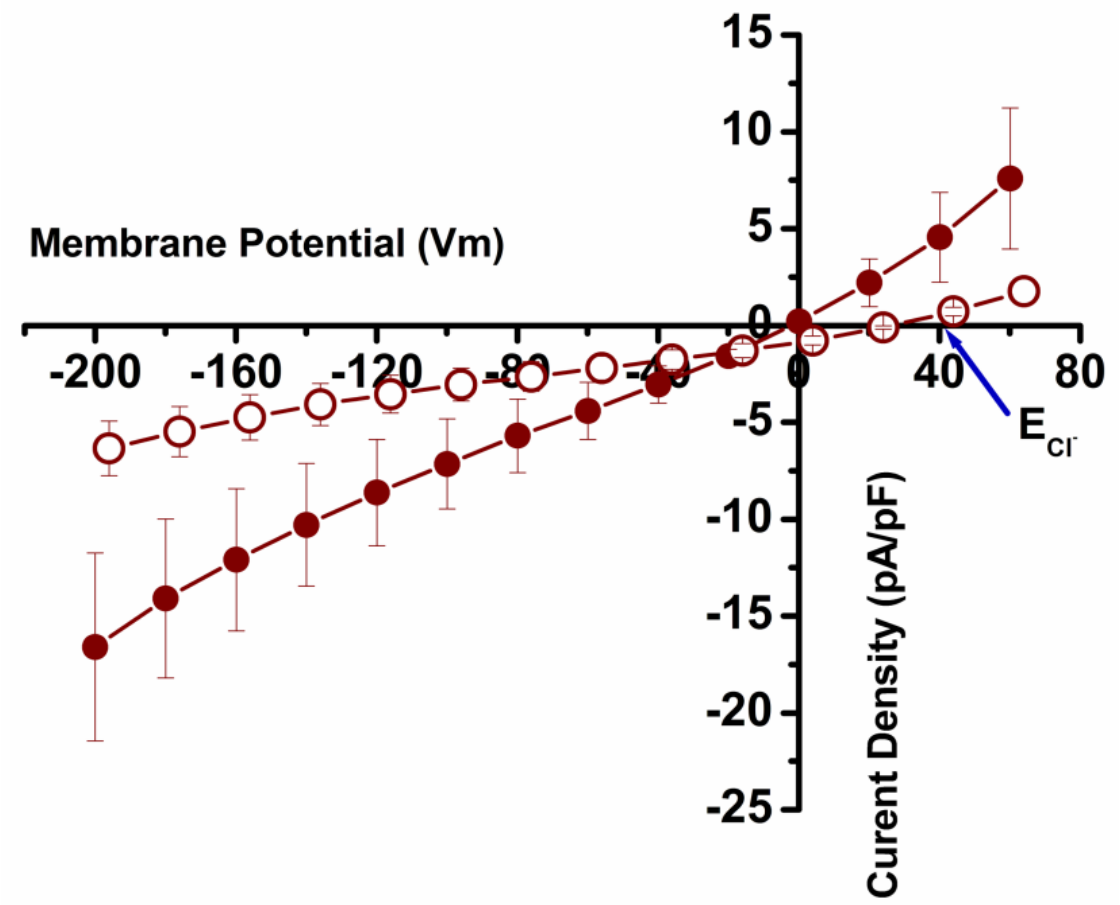

Figure 19. Average I/V curves obtain before (●, B1) and after the substitution of the external solution (○, B2) (n=5). The blue Arrow shows the E_{Cl^-} for the B2/P1 combination.

Figure 19 depicts the average I/V curve (n=5) obtained before (●, B1/P1) and after (○, B2/P1) bath solution exchange 1 (BSE1: B1/P1 → B2). As expected, there was a decrease in the positive currents intensity (59 ± 7 %) and a shift of the V_{rev} to a more positive value (+25.8 ± 2.2 mV). However this shift did not reached the expected E_{Cl^-} (+40.50 mV). This could be due to the presence of 5 mM NO_3^- ($E_{NO_3^-}$ = 0 mV) in the bath and pipette solutions (Table 7 in Experimental Procedures, page 62), which permeability gains relevance with the decrease of $[Cl^-]_{out}$. Unexpectedly the negative currents also suffered a reduction in intensity (51 ± 9 %), which may reveal a regulation mechanism of these channels by $[Cl^-]_{out}$. This can also be found in the R-type currents present in hypocotyl epidermal cells from *Arabidopsis thaliana*; and in the ORAC currents from *Zea mays* and *Arabidopsis*

thaliana suspension cultured cells, and *Z. muelleri* leaf cells (Table 1, in Introduction, page 36).

Table 13. Steady-state anion currents' parameters calculated before and after Bath Solution Exchange 1 (B1/P1 to B2). $I_{(-160\ mV)}$, $I_{(+160\ mV)}$, g_B, g_F, and g_F/g_B, V_h and V_s ,**Activation** and **Deactivation**, τ_1 and τ_2 as described in Table 11. $I_{140mM\ Cl^-}$, $I_{27mM\ Cl^-}$ refer to the currents before and after bath solution exchange, respectively. **%∆Subst** refers to the percentage of current amplitude variation before and after bath solution exchange. Data are represented as mean ± SE. *, refer to significant differences ($p < 0.05$).

	Bath Solution Exchange 1 (B1/P1 → B2)				
	$I_{(-160\ mV)}$ **(pA/pF)**	$I_{(+160\ mV)}$ **(pA/pF)**	V_{rev} **(mV)**		**n**
$I_{140mM\ Cl^-}$	-12.1 ± 3.7	40.0 ± 17.2	1.6 ± 2.5*		5
$I_{27mM\ Cl^-}$	-4.8 ± 1.2	14.7 ± 6.8	25.8 ± 2.2*		5
%∆Subst	51 ± 9	59 ± 7			
	g_B **(nS)**	g_F **(nS)**	g_F/g_B		**n**
$I_{140mM\ Cl^-}$	0.106 ± 0.035	0.540 ± 0.215	6 ± 2		5
$I_{27mM\ Cl^-}$	0.038 ± 0.007	0.224 ± 0.108	6 ± 2		5
	V_h **(mV)**		V_s **(mV)**		**n**
$I_{140mM\ Cl^-}$	163 ± 4		53 ± 7		5
$I_{27mM\ Cl^-}$	178 ± 3		57 ± 9		5
	Activation		**Deactivation**		
	τ_1 **(ms)**	τ_2 **(ms)**	τ_1 **(ms)**	τ_2 **(ms)**	**n**
$I_{140mM\ Cl^-}$	741 ± 141*	64 ± 5*	165 ± 10*	24 ± 3*	5
$I_{27mM\ Cl^-}$	409 ± 65*	38 ± 3*	117 ± 8*	13 ± 1*	5

Table 13 summarises the parameters of the currents obtained for this experimental group. It is possible to observe that the reduction in the current's intensity is accompanied by a corresponding reduction in g_B and g_F, without changing the g_F/g_B ratio, which is expected since a very similar decrease in current intensity occurred for both positive and negative currents. There was no significant change in the Boltzmann parameters V_h and V_s which indicates that the decrease in $[Cl^-]_{out}$ does not affect the channels' sensitivity to V_m. The parameters τ_1 and τ_2 for the activation and deactivation (tail) currents suffered a significant decrease, which confirms that the gating mechanism in these channels is modulated by $[Cl^-]_{out}$. In Figure 20 it is possible to observe both the reduction in current intensity and the change in the shape of the curves (the result of different τ_1 and τ_2 parameters).

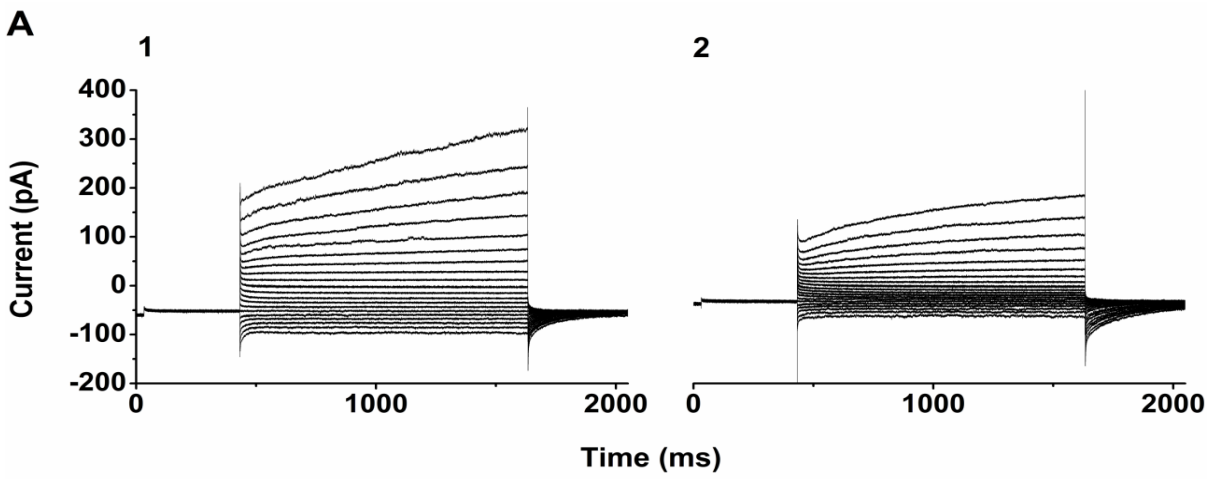

Figure 20. A: Typical raw data for the WC activation currents obtained in one cell before (**1**) and after (**2**) the Bath Solution Exchange 1: B1 ($[Cl^-]$ = 140 mM)/P1 → B2 ($[Cl^-]$ = 27 mM).

The deactivation of the anionic channels was also studied in these experimental conditions. The parameters in Table 14 were obtained from the I/V curves constructed with the current density obtained immediately after the test potential was applied (as previously explained in page 80). As in *Control* experimental conditions, it is possible to observe a weak outward rectification of these curves, and an unexpected shift of the V_{rev} to more positive V_m in I_{Cl1} and I_{before}.

Table 14. WC deactivation current parameters calculated for Bath Solution Exchange 1 (B1/P1 → B2). Parameters $\mathbf{g_B}$, $\mathbf{g_F}$, $\mathbf{g_F/g_B}$, $\mathbf{V_{rev}}$, and $\mathbf{I_{Cl1}}$, as described in Table 11. Parameters $\mathbf{I_{before}}$, and $\mathbf{I_{after}}$ as described in Table 13. Data are represented as mean ± SE. *, refer to significant differences ($p < 0.05$).

	Bath Solution Exchange 1 (B1/P1 → B2)				
	g_B (nS)	**g_F (nS)**	**g_F/g_B**	**V_{rev} (mV)**	**n**
I_{Cl1}	0.086 ± 0.037	0.198 ± 0.042	3 ± 1*	5.5 ± 2.4*	4
I_{before}	0.297 ± 0.075	0.397 ± 0.143	1 ± 0	21.8 ± 16.5*	4
I_{after}	0.125 ± 0.018	0.194 ± 0.063	2 ± 0	87.1 ± 19.2*	5

5.1.4. The putative plasma membrane channels are two times more permeable to NO_3^- than to Cl^-

In order to further characterize the anionic currents found in pollen grain protoplasts, the relative permeability of the channels to Cl^- and NO_3^- (P_{NO3}/P_{Cl}) was determined by exchanging the bath solution, after the rundown was over. During the bath solution exchange 2 (BSE2: B1/P1 → B3; Table 7 in Experimental Procedures, page 62), the initial $[Cl^-]_{out}$ of 140 mM was partially replaced by NO_3^- ($[Cl^-]$ = 31 mM + $[NO_3^-]$ = 110 mM). The reverse experiment was also performed, in which NO_3^--based external and internal

solutions were used, and the initial $[NO_3^-]_{out}$ of 140 mM was partially replaced in the bath solution by Cl^- ($[NO_3^-]$ = 140 mM + $[Cl^-]$ = 5 mM → $[NO_3^-]$ = 31 mM + $[Cl^-]$ = 110 mM; Bath Solution Exchange 3: B4 /P4 → B5, Table 7 in Experimental Procedures, page 62). Since both solution exchanges were performed after the rundown occurred, these experiments only reveal the P_{NO3}/P_{Cl} of the current populations I_{Cl2} and I_{Cl3}.

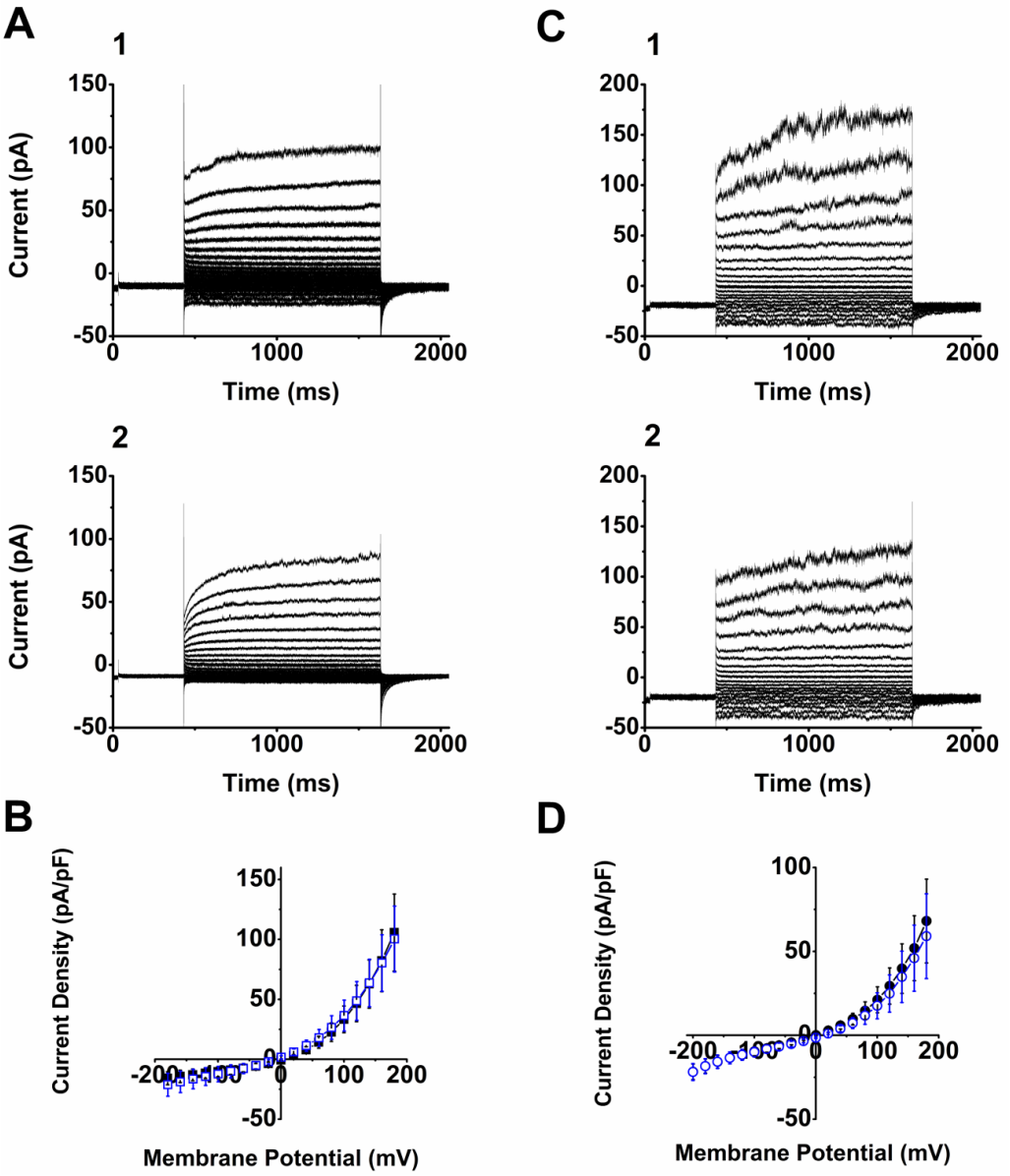

Figure 21. A: Typical anionic WC currents from a pollen grain protoplast of *Arabidopsis thaliana*, measured before (**1**) and after (**2**) Bath Solution Exchange 2 (B1/P1 → B3). **B:** Average I/V curves obtain before (■; B1, $[Cl^-]$ = 140 mM + $[NO_3^-]$ = 5 mM) and after the substitution of the external solution (□; B3, $[Cl^-]$ = 31 mM + $[NO_3^-]$ = 110 mM; n=6). **C:** Typical anionic WC currents from a pollen grain protoplast of *Arabidopsis thaliana*, measured before (**1**) and after (**2**) Bath Solution Exchange 3 (B4/P4 → B5). **D:** Average I/V curves obtain before (●; B4, $[NO_3^-]$ = 140 mM + $[Cl^-]$ = 5 mM) and after the substitution of the external solution (○; B5, $[NO_3^-]$ = 31 mM + $[Cl^-]$ = 110 mM; n=6). All currents were elicited from a holding potential of -100 mV with the voltage protocol depicted in Figure 10A.

Figure 21A and C illustrate two typical raw data of the WC currents elicited in each previously described experimental conditions. In both cases it is possible to observe a slight decrease in the current intensity and a change in the shape of the curves. Figure 21B and D display the average I/V curves obtained before and after the substitution of the bath solution in the experimental conditions B1/P1 → B3 and B4/P4 → B5, respectively. It is possible to observe a lack of significant change both in current intensity, in conductivity (g_B and g_F) and in the level of rectification of the currents (g_F/g_B) during the experiment.

Table 15 confirms these observations. Also the parameters V_h and V_s suffered no significant modification after the bath solutions were exchanged, leading to the conclusion that this did not affect the sensitivity of the channels to the V_m.

Table 15. Steady-state anionic currents' parameters calculated before and after Bath Solution Exchange 2 (BSE2: B1/P1 → B3) and Bath Solution Exchange 3 (BSE3: B4/P4 → B5). Parameters **$I_{(-160\ mV)}$**, **$I_{(+160\ mV)}$**, **g_B**, **g_F**, **g_F/g_B**, **V_h**, **V_s**, **V_{rev}**, **Activation**, **Deactivation**, **τ_1**, **τ_2**, and **%ΔSubst** as described in Table 13. **I_1**, **I_{before}** and **I_{after}** refer to the current lost during Rundown, to the currents before and after bath solution substitution, respectively. Data are represented as mean ± SE. *, refer to significant differences between comparable elements in the same experimental group. ¥, refer to significant differences between comparable elements in different experimental groups ($p < 0.05$).

	BSE2: $[Cl^-]$=140mM + $[NO_3^-]$=5mM → $[Cl^-]$=31mM + $[NO_3^-]$=110mM				**BSE3: $[NO_3^-]$=140mM + $[Cl^-]$=5mM → $[NO_3^-]$ =31mM + $[Cl^-]$=110mM**			
	$I_{(-160\ mV)}$ (pA/pF)	**$I_{(+160\ mV)}$ (pA/pF)**	**V_{rev} (mV)**	**n**	**$I_{(-160\ mV)}$ (pA/pF)**	**$I_{(+160\ mV)}$ (pA/pF)**	**V_{rev} (mV)**	**n**
I_1	-20.9 ± 7.2	159.8 ± 29.5*	-0.1 ± 0.4	6	-4.9 ± 0.7*	100.3 ± 41.3*	-2.1 ± 0.8	6
I_{before}	-14.3 ± 5.2	82.2 ± 25.8	3.1 ± 2.1	6	-15.9 ± 3.8	51.9 ± 19.3	-1.1 ± 1.7	6
I_{after}	-18.9 ± 8.9	80.3 ± 23.6	-8.0 ± 10.7	6	-15.8 ± 4.0	45.9 ± 19.7	12.4 ± 1.7*	6
%ΔSubst	-44 ± 38	-57 ± 55		6	3 ± 5	16 ± 5		6
	g_B (nS)	**g_F (nS)**	**g_F/g_B**	**n**	**g_B (nS)**	**g_F (nS)**	**g_F/g_B**	**n**
I_1	0.092 ± 0.026	1.337 ± 0.169	20 ± 4	6	0.053 ± 0.017*	1.470 ± 0.743*	39 ± 13*	6
I_{before}	0.073 ± 0.020	1.075 ± 0.303	22 ± 8¥	6	0.138 ± 0.023	0.712 ± 0.259	5 ± 1¥	6
I_{after}	0.121 ± 0.045	0.915 ± 0.197	14 ± 4¥	6	0.139 ± 0.026	0.605 ± 0.250	4 ± 1¥	6
	V_h (mV)	**V_s (mV)**	**P_{NO3}/P_{Cl}**	**n**	**V_h (mV)**	**V_s (mV)**	**P_{NO3}/P_{Cl}**	**n**
I_1	82 ± 20*	50 ± 6		6	124 ± 19	51 ± 3		6
I_{before}	140 ± 8¥	53 ± 5	2.3 ± 0.9	6	167 ± 5¥	49 ± 7	1.7 ± 0.1	6
I_{after}	143 ± 5¥	65 ± 8		6	158 ± 6¥	44 ± 8		6
	Activation		**Deactivation**		**n**	**Activation**		**Deactivation**		**n**
	τ_1 (ms)	**τ_2 (ms)**	**τ_1 (ms)**	**τ_2 (ms)**		**τ_1 (ms)**	**τ_2 (ms)**	**τ_1 (ms)**	**τ_2 (ms)**	
I_1	600 ± 75*¥	31 ± 2*¥	127 ± 8	12 ± 1*	6	355 ± 45¥	57 ± 3¥	136 ± 10	15 ± 1	6
I_{before}	381 ± 42	43 ± 2*¥	128 ± 6¥	18 ± 1	6	619 ± 35*	97 ± 39*¥	190 ± 19*¥	16 ± 1	6
I_{after}	436 ± 147	64 ± 9*¥	121 ± 5	20 ± 2¥	6	400 ± 57	-	141 ± 17	-	6

The response time of the channels to the test voltage changed with the substitution of the bath solutions. After bath solution exchange 2 (BSE 2), activation τ_2 significantly increased, while after bath solution exchange 3 (BSE 3), activation τ_1 significantly decreased while τ_2 completely disappeared. The same occurred for deactivation τ_1 and τ_2 after BSE3 (Table 15). The values for τ_1 and τ_2 present in this table were averaged from the data obtained from all V_m, as was previously explained.

Using the variation in V_{rev} before and after the exchange of the bath solution and Equation 1 (Experimental Procedures, page 70) it was possible to calculate the combined permeability ratio P_{NO3}/P_{Cl} of the current populations $I_{Cl2} + I_{Cl3}$. In BSE2 P_{NO3}/P_{Cl} = 2.3 ± 0.9, and in BSE3 P_{NO3}/P_{Cl} = 1.7 ± 0.1, indicating that these channels are 2 times more permeable to NO_3^- than to Cl^-. Another way of determine the ionic selectivity of a population of channels is by comparing the intensity of the currents before and after the bath solution exchange. Unfortunately, the data gathered were inconclusive, since for BSE2 (B1/P1 → B3) of the 6 protoplasts tested, 3 suffered an increase in current intensity, 2 suffered a decrease, and there was no change in 1. While, for BSE3 (B4/P4 → B5) of the 6 protoplasts tested, 3 suffered a decrease in current intensity and the other 3 had no change. This is reflected in the average percentage of current amplitude variation before and after bath solution exchange (%ΔSubst), and in the lack of significant variation in the average current's intensity before and after the bath solution exchange (Figure 21B and D and Table 15). This discrepancy could be due to a slight destabilization of the seal during the exchange of the bath solution.

In order to determine whether the type of anion in solution influences the behaviour of the channels, it is important to compare equivalent parameters obtained during the two different bath solution exchange experiments. In BSE2, I_{before} and I_{after} presented a significantly stronger rectification than their equivalents in BSE3, even though there was no significant difference in relation to the respective parameters g_F and g_B between the two experimental groups (Table 15). Thus said, one should notice that in BSE2, g_F parameters from I_{before} and I_{after} are higher, while g_B parameter from I_{before} is smaller.

The Boltzmann parameter V_h from I_{before} was significantly smaller in BSE2 than in BSE3. This difference indicates that the channels' behaviour with V_m is regulated by the type of ion initially present in solution, since the potential to which the channels reach 50% of their

maximum conductivity is different. This phenomenon is confirmed by the values for V_h relatively to I_1 in both BSE2 and BSE3 (Table 15), although this difference was not statistically significant. V_h from I_{after} was also smaller in BSE2, confirming the previous result.

Activation τ_1 from I_1 in BSE2 was significantly higher than its equivalent in BSE3, while activation τ_2 was significantly lower. Activation τ_2 from I_{before} in BSE2 was significantly lower than its equivalent in BSE3, and τ_2 from I_{after} was significantly higher in BSE2, since its counterpart in BSE3 disappeared. Deactivation τ_1 from I_{before} in BSE2 was significantly lower, and τ_2 from I_{after} was significantly higher in BSE 2 (Table 15).

5.1.5. The Anionic Currents are regulated by $[Ca^{2+}]_{in}$

In growing pollen tubes both Cl^- and Ca^{2+} present oscillatory fluxes at the tip. Since Ca^{2+} is a well know regulator of channel activity, including anion channels (e.g. Skerrett and Tyerman, 1994), the regulation by $[Ca^{2+}]_{in}$ of the anionic currents present in pollen grain protoplasts was tested by increasing the $[Ca^{2+}]_{free}$ in the pipette solution. This was achieved by manipulating the concentrations of Ca^{2+} and EGTA (Experimental Procedures, page 62). In the *Control* experimental condition (B1/P1) the $[Ca^{2+}]_{free}$ was estimated to be 6.04 nM. Two other estimated $[Ca^{2+}]_{free}$ were tested: 8.50 μM and 0.54 mM, following the same experimental approach as in Control conditions (Figure 11 in Experimental Procedures, page 67), These new experimental conditions were designated by μCa Test Group (B1/P2) and mCa Test Group (B1/P3), respectively. The current parameters for these three experimental groups are summarized in Table 16.

Table 16. Steady-state chloride currents' parameters calculated with different $[Ca^{2+}]_{in}$. Experimental groups: Control (B1/P1 - nCa), µCa Test Group (B1/P2) and mCa Test Group (B1/P3). Parameters $\mathbf{I_{(-160\ mV)}}$, $\mathbf{I_{(+160\ mV)}}$, $\mathbf{g_B}$, $\mathbf{g_F}$, $\mathbf{g_F/g_B}$, $\mathbf{V_h}$, $\mathbf{V_s}$, $\mathbf{V_{rev}}$, **Activation**, **Deactivation**, τ_1, τ_2, $\mathbf{I_{Cl1}}$, $\mathbf{I_{Cl2}}$, $\mathbf{I_{Cl3}}$, **%Rundown**, **%Inhibition**, $\mathbf{[NPPB]_{mean}}$, and $\mathbf{[NPPB]_{max}}$ as described in Table 11. Data are represented as mean ± SE. *****, refer to significant differences between comparable elements in the same experimental group. **¥**, refer to significant differences between comparable elements in different experimental groups ($p < 0.05$).

	Control Group (B1/P1 – nCa)				µCa Test Group (B1/P2)				mCa Test Group (B1/P3)			
	$\mathbf{I_{(-160\ mV)}}$ (pA/pF)	$\mathbf{I_{(+160\ mV)}}$ (pA/pF)	$\mathbf{V_{rev}}$ (mV)	n	$\mathbf{I_{(-160\ mV)}}$ (pA/pF)	$\mathbf{I_{(+160\ mV)}}$ (pA/pF)	$\mathbf{V_{rev}}$ (mV)	n	$\mathbf{I_{(-160\ mV)}}$ (pA/pF)	$\mathbf{I_{(+160\ mV)}}$ (pA/pF)	$\mathbf{V_{rev}}$ (mV)	n
$\mathbf{I_{Cl1}}$	-4.4 ± 1.0¥	60.8 ± 9.5*¥	-1.0 ± 0.7	17	-8.3 ± 1.7	97.6 ± 16.0*¥	-1.3 ± 0.9	14	-10.9 ± 4.2	165.0 ± 30.2¥	-0.7 ± 0.8	5
$\mathbf{I_{Cl2}}$	-5.2 ± 0.7	26.6 ± 3.4*¥	-5.0 ± 0.8*	16	-7.4 ± 1.6	42.4 ± 12.5*¥	-0.7 ± 1.5¥	12	-7.8 ± 2.2	106.1 ± 19.4¥	-4.8 ± 1.3	5
$\mathbf{I_{Cl3}}$	-0.8 ± 0.3*	16.0 ±2.8*	-1.1 ± 1.1	16	-0.7 ± 0.3*	15.6 ± 4.5*	-2.8 ± 2.6	12	-1.5 ± 0.8*	41.9 ± 10.5*¥	-1.7 ± 1.7	5
%Rundown	43 ± 5	56 ± 5		17	51 ± 6	65 ± 7		14	49 ± 14	56 ± 8		5
%Inhibition	22 ± 4	36 ± 4		16	18 ± 7	28 ± 3		12	22 ± 6	32 ± 3		5
$\mathbf{[NPPB]_{mean}}$		100 ± 0 µM		16		300 ± 30 µM		12		700 ± 187 µM		5
$\mathbf{[NPPB]_{max}}$		100 µM				500 µM				1400 µM		
	$\mathbf{g_B}$ (nS)	$\mathbf{g_F}$ (nS)	$\mathbf{g_F/g_B}$	n	$\mathbf{g_B}$ (nS)	$\mathbf{g_F}$ (nS)	$\mathbf{g_F/g_B}$	n	$\mathbf{g_B}$ (nS)	$\mathbf{g_F}$ (nS)	$\mathbf{g_F/g_B}$	n
$\mathbf{I_{Cl1}}$	0.018 ± 0.005¥	0.600 ± 0.098*¥	47 ± 5¥	17	0.031 ± 0.011	1.006 ± 0.158*¥	72 ± 16	14	0.030 ± 0.008	1.832 ± 0.293¥	79 ± 22	5
$\mathbf{I_{Cl2}}$	0.032 ± 0.004	0.315 ± 0.039*	12 ± 2*	16	0.040 ± 0.008	0.530 ± 0.162*	20 ± 8*	12	0.035 ± 0.017	1.114 ± 0.210¥	61 ± 21¥	5
$\mathbf{I_{Cl3}}$	0.007 ± 0.002*	0.202 ± 0.035*	53 ± 11	16	0.004 ± 0.001*	0.222 ± 0.055*	78 ± 17	12	0.007 ± 0.002*	0.563 ± 0.139*¥	98 ± 33	5
	$\mathbf{V_h}$ (mV)	$\mathbf{V_s}$ (mV)		n	$\mathbf{V_h}$ (mV)	$\mathbf{V_s}$ (mV)		n	$\mathbf{V_h}$ (mV)	$\mathbf{V_s}$ (mV)		n
$\mathbf{I_{Cl1}}$	88 ± 7*	55 ± 2		17	96 ± 8*	58 ± 3		14	93 ± 15*	54 ± 4		5
$\mathbf{I_{Cl2}}$	142 ± 6	59 ± 3		16	133 ± 4	50 ± 4		12	139 ± 7	62 ± 2		5
$\mathbf{I_{Cl3}}$	137 ± 11	64 ± 5		16	133 ± 5	53 ± 5		12	118 ± 10	50 ± 4		5
	Activation		Deactivation		Activation		Deactivation		Activation		Deactivation	
	τ_1 (ms)	τ_2 (ms)	τ_1 (ms)	τ_2 (ms)	τ_1 (ms)	τ_2 (ms)	τ_1 (ms)	τ_2 (ms)	τ_1 (ms)	τ_2 (ms)	τ_1 (ms)	τ_2 (ms)
$\mathbf{I_{Cl1}}$	455 ± 34	67 ± 3*	200 ± 15*	30 ± 3¥	247 ± 30*¥	67 ± 4*	129 ± 8¥	25 ± 2*¥	514 ± 50	41 ± 2¥	265 ± 40*	15 ± 1¥
$\mathbf{I_{Cl2}}$	488 ± 56	36 ± 1*	133 ± 8	21 ± 2*	748 ± 65*¥	29 ± 1*	118 ± 11	35 ± 4¥	545 ± 48	44 ± 3¥	159 ± 17*	18 ± 3
$\mathbf{I_{Cl3}}$	240 ± 5*¥	49 ± 1*¥	164 ± 14	33 ± 2	320 ± 13*	41 ± 2*	171 ± 19*	37 ± 4	369 ± 20*	40 ± 3	127 ± 10*¥	24 ±3*¥
	n				16				12			

The three populations of currents I_{Cl1}, I_{Cl2} and I_{Cl3} were present with all tested $[Ca^{2+}]$ and were differently regulated by $[Ca^{2+}]_{in}$. As it can be observed in Table 16 and in Figure 22, both negative and positive I_{Cl1} currents increased in intensity with increasing $[Ca^{2+}]_{in}$; the negative I_{Cl2} current increased in µCa Test Group and then stabilized in mCa Test Group, while the positive I_{Cl2} current increased with increasing $[Ca^{2+}]_{in}$; both negative and positive I_{Cl3} currents were stable in µCa Test Group and then increased for mCa Test Group.

The conductance parameters g_B, g_F and g_F/g_B followed the same trend as the current intensity (Table 16).

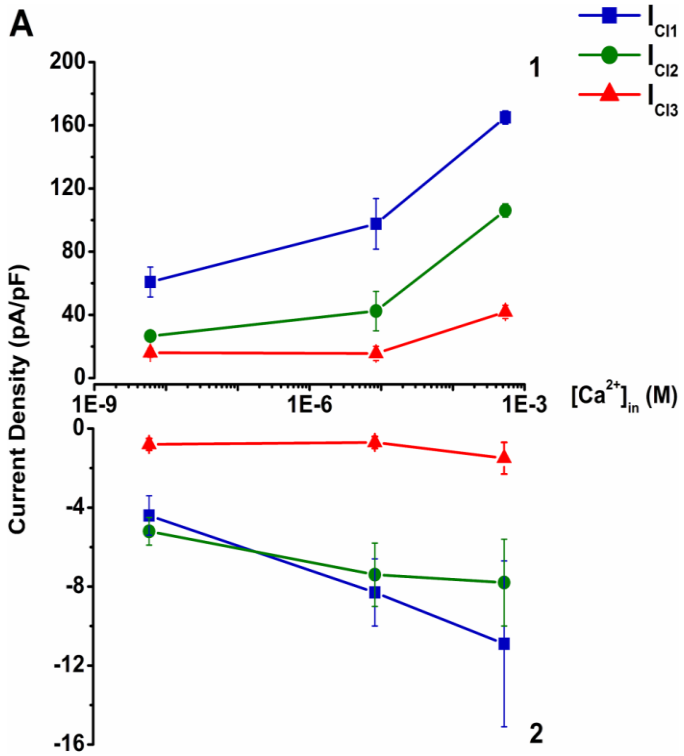

Figure 22. A: Variation of the average current density with the tested $[Ca^{2+}]_{in}$. **1** refers to the positive currents elicited at +160 mV, and **2** refers to the negative currents elicited at -160 mV. Blue squares refer to I_{Cl1} (■), dark green circles refer to I_{Cl2} (●), and red triangles refer to I_{Cl3} (▲).

Both the values of %Rundown and the %Inhibition did not vary significantly with $[Ca^{2+}]_{in}$, but the minimum values of [NPPB] necessary to achieve maximum inhibition increased with $[Ca^{2+}]_{in}$. These were 100 ± 0 µM, 300 ± 30 µM and 700 ± 187 µM, for Control, µCa and mCa Test Groups, respectively, indicating that the mechanism of inhibition might be regulated by Ca^{2+} or that Ca^{2+} might change the apparent affinity of the channels to NPPB. As in *Control* experimental conditions, the %Rundown in µCa and in mCa Test Groups, increased for negative V_m, in a statistically significant manner, and was constant for

positive V_m, while %Inhibition increased significantly with V_m for both positive and negative potentials.

Some characteristics of these current populations were kept unchanged when the $[Ca^{2+}]_{in}$ was varied. These were the weaker outward rectification of I_{Cl2} in relation to I_{Cl1} and I_{Cl3}, and the lower values of V_h from I_{Cl1}, which indicates that these characteristics are not regulated by Ca^{2+}.

As it can be observed in Table 16 and in Figure 23, the activation and deactivation time constants τ_1 and τ_2 were differently modulated by the three $[Ca^{2+}]_{in}$ tested. Activation τ_1 in I_{Cl1} had its lowest value in µCa Test Group; in I_{Cl2}, had its highest value in µCa Test Group; and in I_{Cl3} had its highest value in mCa Test Group. Activation τ_2 was significantly different in all three current populations in Control and in µCa Test Group. In both these test groups the values for activation τ_2 were highest in I_{Cl1} and lowest in I_{Cl2}. In the mCa Test Group, the values of activation τ_2 for the three current populations were not significantly different. Deactivation τ_1 in I_{Cl1} decreases in µCa Test Group; and in I_{Cl3} it decreases in mCa Test Group. Deactivation τ_2 in I_{Cl1} decreases with $[Ca^{2+}]_{in}$; in I_{Cl2} it increases in µCa Test Group; and in I_{Cl3} it decreases in mCa Test Group.

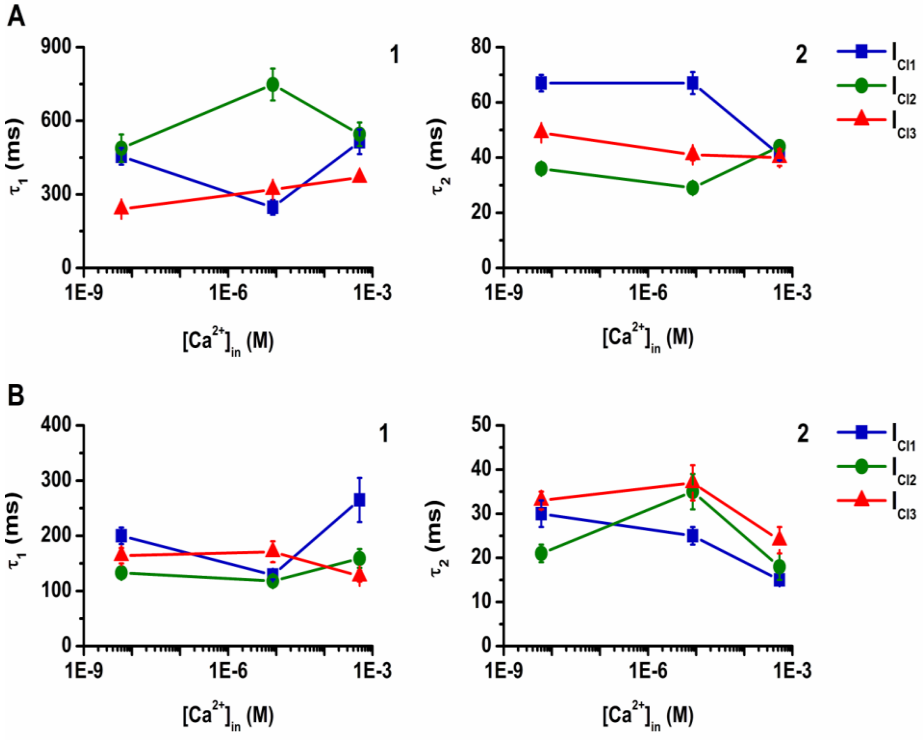

Figure 23. Variation of the activation (**A**) and deactivation (**B**) averaged time constants τ_1 (**1**) and τ_2 (**2**) with the tested $[Ca^{2+}]_{in}$. Blue squares refer to I_{Cl1} (■), dark green circles refer to I_{Cl2} (●), and red triangles refer to I_{Cl3} (▲).

5.1.6. Summary of the results

1. Anionic currents were found in pollen grain protoplasts, using Cl^--based solutions:
    a. Cl^- was the main permeable ion;
    b. $V_{rev} \approx E_{Cl^-}$;
    c. When $[Cl^-]_{ext}$ was lowered, the positive currents intensity decreased (59 ± 7 %) and the V_{rev} shifted to a more positive value (25.8 ± 2.2 mV), as expected;
    d. The currents were partially inhibited by NPPB.
    e. The currents present outward rectification:
        i. The positive currents (Cl^- entering the cell) are larger than the negative currents (Cl^- exiting the cell) - $g_F > g_B$;
2. The anionic currents are characterized by a time dependent, depolarization-induced activation and by a time-dependent, hyperpolarization-induced deactivation:
    a. Both the activation and the deactivation currents can be described by two time dependent current components I_1 and I_2, characterized by τ_1 and τ_2 respectively, with τ_1 greater than τ_2.
3. There are three different populations of outward rectified anionic currents; I_{Cl1} - the current lost during rundown; I_{Cl2} - the current resistant to NPPB; and I_{Cl3} - the current inhibited by NPPB.
    a. I_{Cl2} has a significantly weaker rectification than I_{Cl1} and I_{Cl3} (g_F/g_B = 12 ± 2);
    b. I_{Cl1} has a significantly lower V_h (88 ± 7 mV), presenting different sensitivity to variations in V_m;
    c. Activation τ_1 was significantly lower in I_{Cl3}, and activation τ_2 was significantly different in all three current populations, presenting its highest value in I_{Cl1} and its lowest in I_{Cl2};
    d. Deactivation τ_1 and τ_2 were significantly lower for I_{Cl1} and I_{Cl2}, respectively;
    e. I_{Cl1}, I_{Cl2} and I_{Cl3} were differently regulated by $[Ca^{2+}]_{in}$.
4. The channels responsible for the observed currents are regulated by $[Ca^{2+}]_{in}$.
    a. I_{Cl1} currents increased in intensity with increasing $[Ca^{2+}]_{in}$;
    b. the negative I_{Cl2} current increased in µCa Test Group and then stabilized in mCa Test Group, while the positive I_{Cl2} current increased with increasing $[Ca^{2+}]_{in}$;

c. I_{Cl3} currents were stable in µCa Test Group and then increased for mCa Test Group;
d. Cytoplasmic Ca^{2+} regulates the response time of the channels to V_m:
    i. Activation τ_1 from I_{Cl1} significantly decreases in µCa Test Group;
    ii. Activation τ_1 from I_{Cl2} significantly increases in µCa Test Group;
    iii. Activation τ_1 from I_{Cl3} significantly increases in mCa Test Group;
    iv. Activation τ_2 from I_{Cl1} significantly decreases in mCa Test Group;
    v. Activation τ_2 from I_{Cl2} significantly increases in mCa Test Group;
    vi. Activation τ_2 from I_{Cl3} has its highest value in Control Group;
    vii. Deactivation τ_1 from I_{Cl1} significantly decreases in µCa Test Group;
    viii. Deactivation τ_1 from I_{Cl3} significantly decreases in mCa Test Group;
    ix. Deactivation τ_2 from I_{Cl1} significantly decreases with $[Ca^{2+}]_{in}$;
    x. Deactivation τ_2 from I_{Cl2} significantly increases in µCa Test Group;
    xi. Deactivation τ_2 from I_{Cl3} significantly decreases in mCa Test Group.

5. The channels responsible for the currents are regulated by $[Cl^-]_{out}$:
    a. In BSE 1 the negative currents also suffered a reduction in intensity (51 ± 9 %);
    b. The parameters τ_1 and τ_2 for the activation and deactivation currents suffered a significant decrease.

6. These channels are 2 times more permeable to NO_3^- than to Cl^-:
    a. In BSE 2, P_{NO3}/P_{Cl} = 2.3 ± 0.9;
    b. In BSE 3, P_{NO3}/P_{Cl} = 1.7 ± 0.1.

7. The channels are regulated by the type of anion initially present in solution:
    a. V_h from I_{before} was significantly smaller in BSE 2 than in BSE 3;
    b. V_h from I_1 and I_{after} were also smaller in BSE 2, although this difference was not statistically significant;
    c. Activation τ_1 from I_1 was significantly higher in BSE 2 than in BSE 3, while activation τ_2 was significantly lower;
    d. Activation τ_2 from I_{before} was significantly lower in BSE 2 than in BSE 3;
    e. Activation τ_2 from I_{after} was significantly higher in BSE 2, since its counterpart in BSE 3 disappeared;

f. Deactivation τ_1 from I_{before} was significantly lower in BSE 2;

g. Deactivation τ_2 from I_{after} was significantly higher in BSE 2.

5.2. Anionic currents in pollen grain protoplasts from **Lilium longiflorum**

5.2.1. Three different activities of outward-rectifying, depolarization-activated anionic currents were found

The presence of anionic currents in pollen grain protoplasts from *Lilium longiflorum* was also investigated, under the same experimental conditions as for *Arabidopsis thaliana*. The pollen of *L. longiflorum* was tested in order to investigate if the phenomenon discovered in the *A. thaliana* was preserved across different species. This species was chosen because of the facility in obtaining pollen, which could be preserved and latter used, unlike the pollen from Arabidopsis that had to be collected fresh, and also because *L. longiflorum* has been regularly used in sexual plant reproduction studies, namely in the study of pollen tube growth and development (e.g. Obermeyer and Kolb, 1993; Zonia *et al.*, 2002).

Similarly to the anion currents found at the plasma membrane of the pollen grain protoplasts from *Arabidopsis thaliana*, under *Control* conditions (B1/P1 - symmetrical $[Cl^-]$ and $[Ca^{2+}]_{in}$= 6.04 nM), the pollen grain protoplasts from *L. longiflorum* also presented three different populations of steady-state anion currents showing outward rectification: I_{Cl1} - current lost during Rundown; I_{Cl2} – current insensitive to NPPB; and I_{Cl3} – current inhibited by NPPB (Figure 24 A-4, 3 and 5, respectively). These currents were also characterized by a time-dependent activation at positive V_m. They were fitted with Equation 6, showing one instantaneous component I_{inst} and two time dependent current components I_1 and I_2, characterized by τ_1 and τ_2 respectively, with τ_1 = 896 ± 188, 440 ± 38, and 608 ± 78 msec for I_{Cl1}, I_{Cl2} and I_{Cl3}, respectively; and τ_2 < 150 msec. Like in *A. thaliana* currents, τ_1 and τ_2 did not vary significantly with V_m.

Figure 24 B shows the I/V curves obtained by plotting the elicited steady-state currents (average from the final 50 ms – orange line) against the corresponding V_m. These curves refer to $I_{initial}$ (black squares - ■), I_{final} (orange circles - ●), and I_{Cl2} (green triangles - ▲), and it is possible not only to observe the decrease in the currents amplitude before and after rundown, but also the reduction caused by the inhibitor NPPB, for both positive and negative V_m, suggesting, as in *A. thaliana*, that these channels allow the passage of current in both directions (inwardly and outwardly).

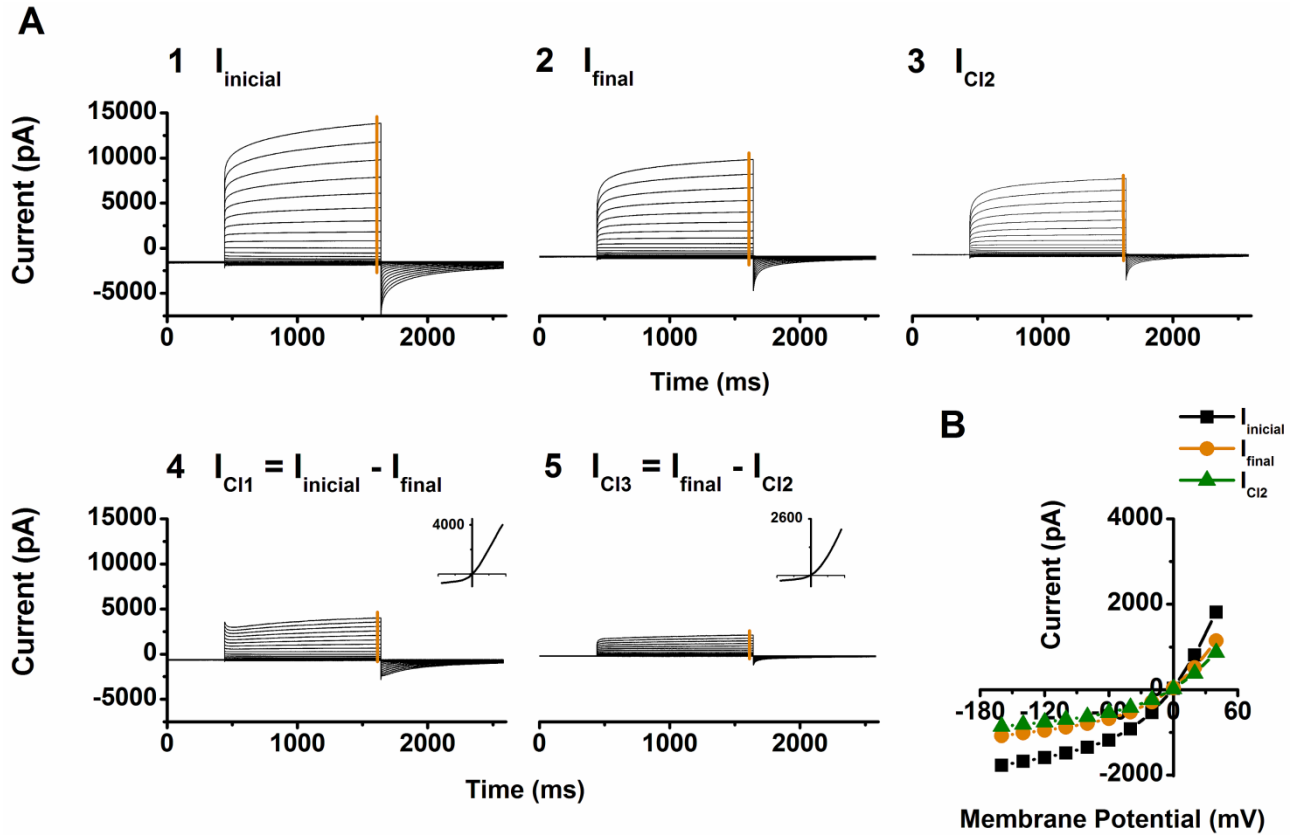

Figure 24. Typical chloride whole-cell currents from a pollen grain protoplast of *Lilium longiflorum*, measured with B1/P1 solutions (control group, nM $[Ca^{2+}]_{in}$). The currents were elicited from a holding potential of -100 mV with the voltage protocol depicted in Figure 10A. **A1 - 5** portray the raw data obtained for these currents: **A1** represents the Initial current recorded immediately after entering whole-cell configuration ($I_{initial}$); **A2**, the current recorded after Rundown (I_{final}); **A3**, the current recorded after inhibition by 500 µM NPPB (I_{Cl2}); **A4**, the current lost during rundown (I_{Cl1}) obtained by subtraction of **A1** and **A2**; and **A5**, the Inhibited Current (I_{Cl3}) obtained by subtraction of **A2** and **A3**. **B** represents the Current-Potential (I/V) relationships of $I_{initial}$ (■), I_{final} (●), and I_{Cl2} (▲). The data to construct this curve was averaged from the last 50 ms of the respective raw data (orange line). The inserts in **A4** and **A5** represent the respective I/V curves.

Under control conditions the percentage of anionic current lost during rundown (%Rundown) was constant for negative V_m, and decreased for positive V_m in a statistically significant manner indicating that the effector that regulates these currents may be sensitive to changes in the electric field that surrounds the plasma membrane. Nevertheless, as in *A. thaliana*, in order to simplify the comparative analysis of this factor in different experimental groups, only the %Rundown obtained for representative V_m (-160 mV and +160 mV) were considered. Its values were 37±7 % and 27±5 % for -160 and +160 mV, respectively (Table 17). The %Rundown was lower in these currents than in *A. thaliana*, probably reflecting slightly different intracellular contents. A maximum inhibition of the chloride currents was obtained for 500 µM [NPPB], a value 5 times higher than the one needed to inhibit the anionic currents elicited in the same conditions in *A. thaliana*. Unlike

the %Rundown, the percentage of inhibited current (%Inhibition) did not vary significantly with V_m. The values for -160 and +160 mV were 24±5 % and 28±6 %, respectively (Table 17). These are similar to the ones obtained in *A. thaliana*.

Table 17. Steady-state chloride currents' parameters obtained in *Control* experimental conditions (B1/P1 - nCa). $\mathbf{I_{(-160\ mV)}}$ and $\mathbf{I_{(+160\ mV)}}$ correspond to the current (pA) elicited by V_m of -160 mV and +160 mV respectively. Parameters $\mathbf{g_B}$, $\mathbf{g_F}$, $\mathbf{g_F/g_B}$, $\mathbf{V_h}$ $\mathbf{V_s}$, $\mathbf{I_{Cl1}}$, $\mathbf{I_{Cl2}}$, $\mathbf{I_{Cl3}}$, **%Rundown**, **%Inhibition**, $\mathbf{[NPPB]_{mean}}$ and $\mathbf{[NPPB]_{max}}$ as described in Table 11. Data are represented as mean ± SE. *, refer to significant differences ($p < 0.05$). Significant differences in the current intensities ($I_{(-160\ mV)}$ and $I_{(+160\ mV)}$), V_{rev} and conductances (g_B, g_F, g_F/g_B) were determined with the Wilcoxon test with SPSS software.

	Control Group (B1/P1 – nCa)			
	$\mathbf{I_{(-160\ mV)}}$ **(pA)**	$\mathbf{I_{(+160\ mV)}}$ **(pA)**	$\mathbf{V_{rev}}$ **(mV)**	**n**
$\mathbf{I_{Cl1}}$	-432 ± 190	2086 ± 866	0.1 ± 0.6	7
$\mathbf{I_{Cl2}}$	-451 ± 189	3314 ± 1318	-1.3 ± 0.9	7
$\mathbf{I_{Cl3}}$	-77 ± 28*	688 ± 204*	-7.3 ± 3.8	7
%Rundown	37 ± 7	27 ± 5		11
%Inhibition	24 ± 5	28 ± 6		7
$\mathbf{[NPPB]_{max}}$		500 µM		
	$\mathbf{g_B}$ **(nS)**	$\mathbf{g_F}$ **(nS)**	$\mathbf{g_F/g_B}$	**n**
$\mathbf{I_{Cl1}}$	0.72 ± 0.23	13.79 ± 5.28	26 ± 10	7
$\mathbf{I_{Cl2}}$	1.62 ± 0.67	33.14 ± 12.82*	35 ± 16	7
$\mathbf{I_{Cl3}}$	0.40 ± 0.14*	6.56 ± 1.91	32 ± 9	7
	$\mathbf{V_h}$ **(mV)**		$\mathbf{V_s}$ **(mV)**	**n**
$\mathbf{I_{Cl1}}$	14 ± 13*		50 ± 4*	7
$\mathbf{I_{Cl2}}$	103 ± 7		62 ± 1	7
$\mathbf{I_{Cl3}}$	94 ± 10		61 ± 3	7

Table 17 summarizes the steady-state chloride current parameters obtained in *Control* experimental conditions (B1/P1 - nCa). The values for $I_{(-160\ mV)}$ and $I_{(+160\ mV)}$ are in pAmperes, since the error associated to the mean I/V curves obtained with the measured currents normalized to their respective capacity values (varying between 18-100 pF) was greater than the error associated to the non-normalized currents.

As expected, the V_{rev} for I_{Cl1}, I_{Cl2} and I_{Cl3} (0.1±0.6, -1.3±0.9 and -7.3±3.8 mV, respectively) were approximate to the calculated E_{Cl-} (-0.92 mV), further confirming the nature of the currents. The values for the ratio g_F/g_B confirm the outward rectification of these three current populations. Although these values were not significantly different, g_F from I_{Cl2} was significantly higher, while g_B from I_{Cl3} was significantly lower.

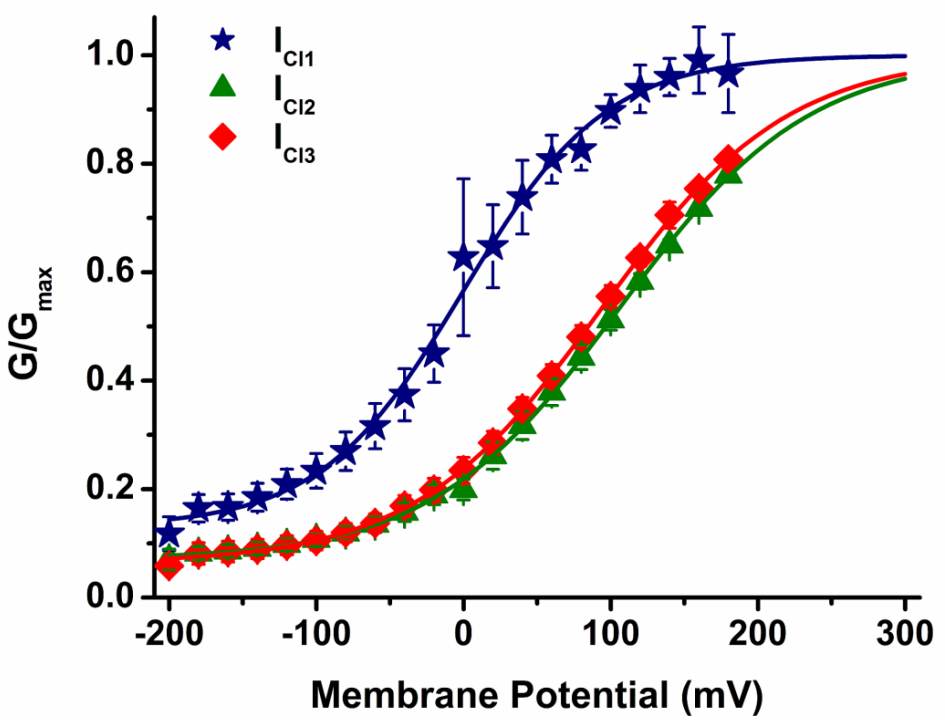

Figure 25. Voltage dependence of the averaged normalized chord conductances (G/G_{max}), obtained in *Control* experimental conditions (B1/P1 - nCa), for I_{Cl1} (*), I_{Cl2} (▲), and I_{Cl3} (♦).

Figure 25 illustrates the voltage dependence of the averaged G/G_{max} for the three current populations. The data was fitted with a Boltzmann equation (Equation 2 and Equation 3 in Experimental Procedures, page 71) and the characterizing parameters V_h and V_s are summarized in Table 17. According to this data, I_{Cl1} not only has a higher sensitivity to variations in V_m, but also has a lower value for the V_m that marks the shift between the minimum and maximum conductance states, presenting significantly lower V_h and V_s (14±13 mV and 50±4 mV, respectively). The values for V_h from the three current populations in *L. longiflorum* were significantly smaller than in *A. thaliana*, while the values for V_s were similar in both species, which indicates that although the channels responsible for these currents have a similar sensitivity to variations in the membrane potential in both species, the V_m that marks the shift between the minimum and maximum conductance states is lower in *L. longiflorum*., a possible indication that we are in the presence of two isoforms of the same channel or reflecting different intracellular environments between the two species.

5.2.2. The three populations of currents are deactivated by hyperpolarization

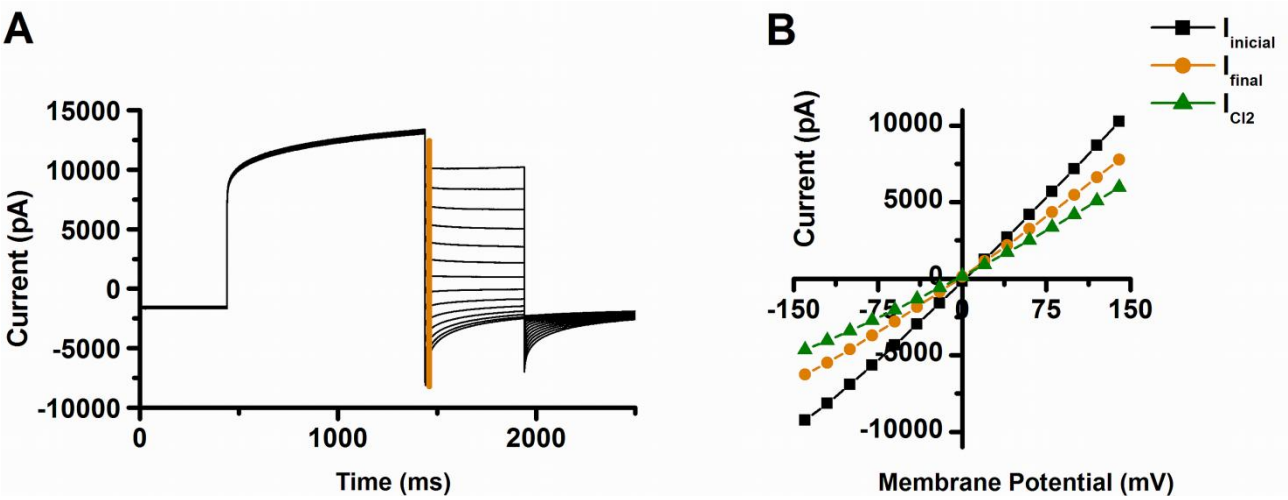

Figure 26. A: Typical raw data for the WC deactivation current ($I_{initial}$). **B:** I/V curve of $I_{initial}$ (■), I_{final} (●), and I_{Cl2} (▲), which was constructed from the current values obtained immediately after the test potential was applied (orange line). Currents were measured with protocol B (see Figure 10-B in Experimental Procedure), in *Control* experimental conditions (B1/P1 - nCa).

Figure 26A shows the typical raw data for the WC deactivation current elicited by protocol B (Figure 10-B in Experimental Procedures, page 64). It is possible to observe from the raw data that the channels responsible for these currents have a time-dependent, hyperpolarization induced deactivation. Figure 26B depicts the I/V curves obtained by plotting the current obtained immediately after the test potential is applied (orange line) against the V_m. The curves refer to one cell, and correspond to $I_{initial}$ (black squares - ■), I_{final} (orange circles - ●), and I_{Cl2} (green triangles - ▲). As expected these curves present no rectification, indicating that at +180 mV the channels are close to their maximum conductivity state (Figure 25) and, with exception of I_{Cl1}, a V_{rev} close to 0 mV, near E_{Cl^-}, which is expected under symmetric [Cl^-] conditions (Table 18). As in *A. thaliana* this shift in I_{Cl1}'s V_{rev} to more positive values could be explained either by the leakage of cations, such as Ca^{2+}, Mg^{2+} or H^+, from the pipette into the bath solution, or by the passage of H^+ through transporters, such as a H^+ - anion antiporter. Furthermore, the deactivation currents of I_{Cl1}, I_{Cl2} and I_{Cl3} also undergo rundown and inhibition by NPPB, confirming the nature of the Cl^- currents.

Table 18. WC deactivation current parameters calculated for *Control* experimental group (B1/P1 - nCa). Parameters g_B, g_F, g_F/g_B, V_{rev}, I_{Cl1}, I_{Cl2}, and I_{Cl3} as described in Table 11. Data are represented as mean ± SE. *, refer to significant differences ($p < 0.05$). Significant differences in the current intensities ($I_{(-160\ mV)}$ and $I_{(+160\ mV)}$), V_{rev} and conductances (g_B, g_F, g_F/g_B) were determined with the Wilcoxon test with SPSS software.

Control Group (B1/P1 – nCa)					
	g_B (nS)	g_F (nS)	g_F/g_B	V_{rev} (mV)	n
I_{Cl1}	16.17 ± 4.59	15.77 ± 4.39	1 ± 0	15.3 ± 2.0	7
I_{Cl2}	37.88 ± 6.63*	41.13 ± 6.63*	1 ± 0	-1.4 ± 2.6	7
I_{Cl3}	6.9 ± 3.4	8.5 ± 4.8	1 ± 0	-13.3 ± 15.4	7

5.2.3. The magnitude of the outward current is dependent on external [Cl^-]

To confirm the nature of the Cl^- currents a lower $[Cl^-]_{out}$ (27 mM) was tested. The result was the expected reduction in the outward currents (reduced entrance of chloride into the cell), while the inward currents remained relatively unchanged, and a shift of the V_{rev} to more positive potentials (19.7 ± 2.3 mV). This is the usual behaviour when the chemical gradient of the permeable ion is changed.

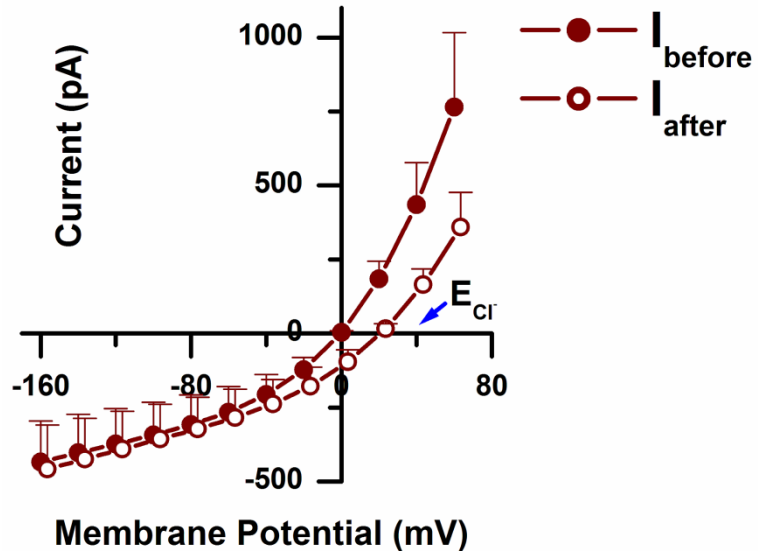

Figure 27. Average I/V curves obtain before (●, B1 - [Cl^-] = 140 mM + [NO_3^-] = 5 mM) and after the substitution of the external solution (○, B2 - [Cl^-] = 27 mM + [NO_3^-] = 5 mM ;n=6). The blue Arrow shows the E_{Cl^-} for the B2/P1 combination.

Figure 27 shows the average curves, obtained after rundown, for the current measured under control conditions ([Cl^-] = 140 mM; [NO_3^-] = 5 mM) and after exchanging to a bath solution containing only 27 mM Cl^- (B1/P1→B2: [Cl^-] = 27 mM + [NO_3^-] = 5 mM). The reversal potential of the whole-cell currents became more positive in comparison to the symmetrical conditions (P1/B1). Nevertheless, it did not reach the expected value for the

E_{Cl-} (+40.5 mV). On average, the reversal potential was +19.7±2.3 mV (n = 6). The deviation is most likely due to the contribution of the NO_3^- (E_{NO3-} = 0 mV), which under these conditions (low $[Cl^-]_{out}$) may gain relevance.

Table 19 summarises the parameters of the currents obtained in this experimental group. It is possible to observe that the reduction in the intensity of the positive current is accompanied by an also expected reduction in g_F and in the g_F/g_B ratio. There was no significant change on the Boltzmann parameters V_h and V_s, which indicates that the decrease in $[Cl^-]_{out}$ does not affect the channels' sensitivity to V_m, a difference in relation to the anionic currents found in *A. thaliana* pollen grain protoplasts.

Table 19. Steady-state anion current parameters calculated before and after Bath Solution Exchange 1 (B1/P1 to B2). **$I_{(-160\ mV)}$**, **$I_{(+160\ mV)}$**, **g_B**, **g_F**, and **g_F/g_B**, **V_h** and **V_s** ,**$I_{140mM\ Cl^-}$**, **$I_{27mM\ Cl^-}$**, **%ΔSubst** as described in Table 13. Data are represented as mean ± SE. *, refer to significant differences ($p < 0.05$). Significant differences in the current intensities ($I_{(-160\ mV)}$ and $I_{(+160\ mV)}$), V_{rev} and conductances (g_B, g_F, g_F/g_B) were determined with the Wilcoxon test with SPSS software.

	Bath Solution Exchange 1 (B1/P1 → B2)			
	$I_{(-160\ mV)}$ (pA)	**$I_{(+160\ mV)}$ (pA)**	**V_{rev} (mV)**	**n**
$I_{140mM\ Cl^-}$	-434 ± 139	3629 ± 1186*	-2.0 ± 1.3*	6
$I_{27mM\ Cl^-}$	-459 ± 149	1941 ± 650*	19.7 ± 2.3*	6
%ΔSubst	5 ± 9	24 ± 4		
	g_B (nS)	**g_F (nS)**	**g_F/g_B**	**n**
$I_{140mM\ Cl^-}$	1.55 ± 0.52	37.83 ± 12.05*	28 ± 4*	6
$I_{27mM\ Cl^-}$	1.85 ± 0.61	20.08 ± 6.38*	14 ± 3*	6
	V_h (mV)		**V_s (mV)**	**n**
$I_{140mM\ Cl^-}$	105 ± 10		67 ± 4	6
$I_{27mM\ Cl^-}$	105 ± 19		68 ± 7	6

5.2.4. Relative permeability of putative plasma membrane channels to Cl^- and NO_3^- is similar

To determine the relative permeability of the channels to Cl^- and NO_3^- (P_{NO3}/P_{Cl}), the initial $[Cl^-]_{out}$ of 140 mM was partially replaced by NO_3^- ($[Cl^-]$ = 31 mM + $[NO_3^-]$ = 110 mM) in the bath solution (Bath Solution Exchange 2: B1/P1 → B3; Table 7 in Experimental Procedures, page 62). The reverse experiment was also preformed, in which the starting point were NO_3^--based solutions followed by the partial replacement of the NO_3^- in the bath solution by Cl^- ($[NO_3^-]$ = 140 mM + $[Cl^-]$ = 5 mM → $[NO_3^-]$ = 31 mM + $[Cl^-]$ = 110 mM; Bath Solution Exchange 3: B4/P4 → B5; Table 7 in Experimental Procedures, page 62). Both exchanges of the bath solutions were performed after complete rundown occurred.

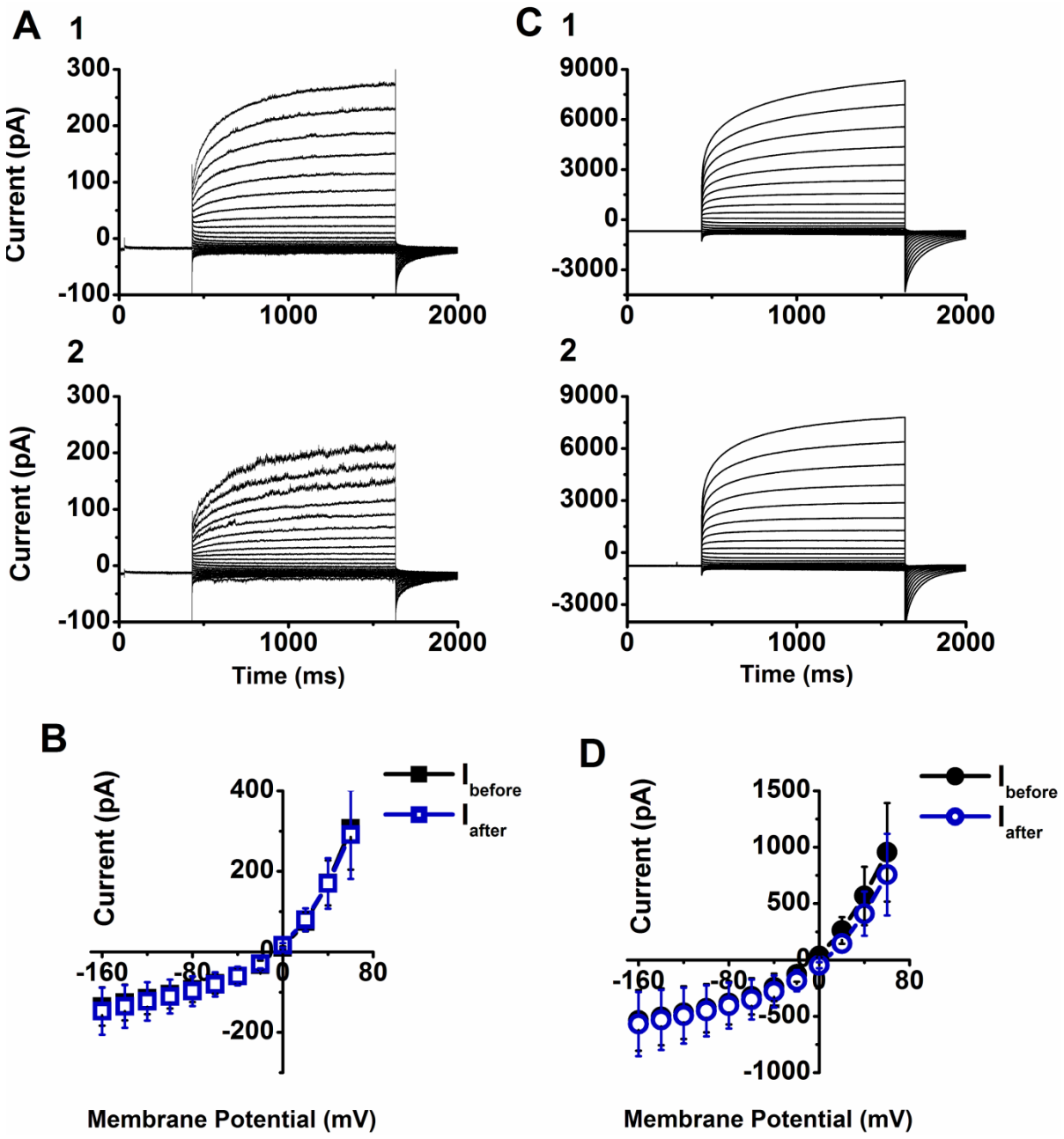

Figure 28. A. Typical anionic WC currents from a pollen grain protoplast, measured before (**1**) and after (**2**) Bath Solution Exchange 2 (B1/P1 → B3). **B:** Average I/V curves obtain before (■, B1 - [Cl^-] = 140 mM + [NO_3^-] = 5 mM) and after the substitution of the external solution (□, B3 - [Cl^-] = 31 mM + [NO_3^-] = 110 mM; n=9). **C:** Typical anionic WC currents from a pollen grain protoplast, measured before (**1**) and after (**2**) Bath Solution Exchange 3 (B4/P4 → B5). **D:** Average I/V curves obtain before (●, B4 - [NO_3^-] = 140 mM + [Cl^-] = 5 mM) and after the substitution of the external solution (○, B5 - [NO_3^-] = 31 mM + [Cl^-] = 110 mM; n=4). All currents were elicited from a holding potential of -100 mV with the voltage protocol depicted in Figure 10A.

Figure 28-A and C depicts the raw data obtained for two different cells, each illustrating one of the above described experiments. After the rundown, the average amplitude of the currents measured under symmetrical Cl^- (P1/B1) and NO_3^- (P4/B4) and the corresponding

forward and backward conductances were not significantly different (Table 20), which indicates that these channels do not discriminate between the two anions. On the other hand I_1 (current lost during rundown) had a significantly stronger outward rectification with NO_3^- - based solutions (Table 20), mainly due to the contribution of g_F, which may indicate that this population of channels is more permeable to NO_3^-.

Table 20. Steady-state anionic currents' parameters calculated before and after Bath Solution Exchange 2 (B1/P1 → B3) and Bath Solution Exchange 3 (B4/P4 → B5). Parameters $\mathbf{I_{(-160\ mV)}}$, $\mathbf{I_{(+160\ mV)}}$, $\mathbf{g_B}$, $\mathbf{g_F}$, $\mathbf{g_F/g_B}$, $\mathbf{V_h}$, $\mathbf{V_s}$, $\mathbf{V_{rev}}$, and **%ΔSubst** as described in Table 13. $\mathbf{I_1}$, $\mathbf{I_{before}}$ and $\mathbf{I_{after}}$ as described in Table 15. Data are represented as mean ± SE. *, refer to significant differences between comparable elements in the same experimental group. ¥, refer to significant differences between comparable elements in different experimental groups ($p < 0.05$). Significant differences in the current intensities ($I_{(-160\ mV)}$ and $I_{(+160\ mV)}$), V_{rev} and conductances (g_B, g_F, g_F/g_B) were determined with the Wilcoxon test with SPSS software.

	Bath Solution Exchange 2 (B1/P1 → B3)				**Bath Solution Exchange 3 (B4/P4 → B5)**			
	$\mathbf{I_{(-160\ mV)}}$ **(pA)**	$\mathbf{I_{(+160\ mV)}}$ **(pA)**	$\mathbf{V_{rev}}$ **(mV)**	**n**	$\mathbf{I_{(-160\ mV)}}$ **(pA)**	$\mathbf{I_{(+160\ mV)}}$ **(pA)**	$\mathbf{V_{rev}}$ **(mV)**	**n**
$\mathbf{I_1}$	-112 ± 19	969 ± 233	-1.1 ± 1.1	9	-300 ± 258	2812 ± 1275	-0.9 ± 2.3	4
$\mathbf{I_{before}}$	-136 ± 48	1720 ± 627	-4.6 ± 0.9	9	-536 ± 269	4185 ± 1860	-6.3 ± 1.7	4
$\mathbf{I_{after}}$	-147 ± 58	1427 ± 557	-7.7 ± 1.6¥	9	-569 ± 285	3806 ± 1788	3.3 ± 1.1¥	4
%ΔSubst	5 ± 9	24 ± 4		9	-4 ± 3	17 ± 7		4
	$\mathbf{g_B}$ **(nS)**	$\mathbf{g_F}$ **(nS)**	$\mathbf{g_F/g_B}$	**n**	$\mathbf{g_B}$ **(nS)**	$\mathbf{g_F}$ **(nS)**	$\mathbf{g_F/g_B}$	**n**
$\mathbf{I_1}$	0.36 ± 0.11	7.72 ± 2.40¥	29 ± 7¥	9	0.36 ± 0.15	23.37 ± 9.27¥	75±24¥	4
$\mathbf{I_{before}}$	0.51 ± 0.23	20.66 ± 7.69¥	49 ± 10	9	1.60 ± 0.84	41.62 ± 18.18¥	38±10	4
$\mathbf{I_{after}}$	0.61 ± 0.29	17.10 ± 6.82¥	31 ± 6	9	1.83 ± 0.94	40.71 ± 18.65¥	30±9	4
	$\mathbf{V_h}$ **(mV)**	$\mathbf{V_s}$ **(mV)**	$\boldsymbol{P_{NO3}/P_{Cl}}$	**n**	$\mathbf{V_h}$ **(mV)**	$\mathbf{V_s}$ **(mV)**	$\boldsymbol{P_{NO3}/P_{Cl}}$	**n**
$\mathbf{I_1}$	25 ± 14*	39 ± 2*		9	42 ± 15*	48 ± 6*		4
$\mathbf{I_{before}}$	116 ± 3	65 ± 2	1.1 ± 0.1	9	107 ± 12	70 ± 2	1.5 ± 0.1	4
$\mathbf{I_{after}}$	120 ± 5	73 ± 3		9	123 ± 9	74 ± 1		4

From Figure 28-B and D it is possible to observe that no considerable changes occurred to the reversal potential of the average I/V curves, a further indication of the currents being dominated by the passage of anions. The value found for P_{NO3}/P_{Cl} determined from the deviation of the averaged V_{rev} (Equation 1 in Experimental Procedures, page 70), was 1.1±0.1 (n = 9) and 1.5±0.1 (n = 4) for BSE2 and BSE3, respectively, indicating that these channels are in average 1.2 times more permeable to NO_3^- than to Cl^-.

The Boltzmann parameters obtained from the cord conductances are similar for the situations before and after anionic substitution (Cl^- → NO_3^- and NO_3^- → Cl^-; Table 20), showing that the dependence of the anionic conductance to the membrane potential was not altered by the presence of the different anions.

5.2.5. I_{Cl1}, I_{Cl2} and I_{Cl3} are modulated by different ranges of $[Ca^{2+}]_{in}$

As before, the possible effect of $[Ca^{2+}]_{in}$ was investigated on three independent groups of cells by replacing the $[Ca^{2+}]_{in}$ from a nM concentration (6 nM, control, P1/B1) to 8.5 µM (P2/B1) or 0.5 mM (P3/B1) concentrations. The current parameters for these three experimental groups are summarized in Table 21.

The three populations of currents I_{Cl1}, I_{Cl2} and I_{Cl3} were differently regulated by $[Ca^{2+}]_{in}$: the amplitude of I_{Cl1} increases with growing $[Ca^{2+}]_{in}$ from nM up to 0.5 mM, while I_{Cl2} and I_{Cl3} showed their maximum value with µM intracellular concentrations (Figure 29). The corresponding averaged values for the backward and forward conductances follow the same trend.

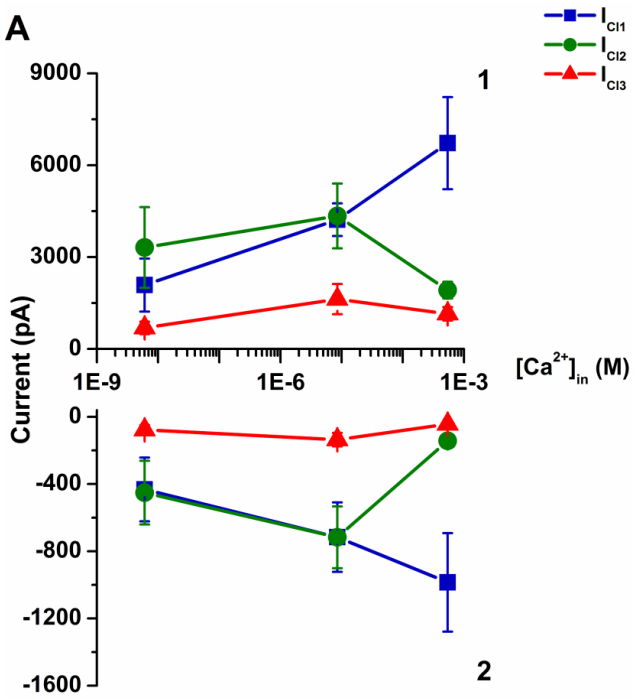

Figure 29. A: Variation of the average current density with the tested $[Ca^{2+}]_{in}$. **1** refers to the positive currents elicited at +160 mV, and **2** refers to the negative currents elicited at -160 mV. Blue squares refer to I_{Cl1} (■), dark green circles refer to I_{Cl2} (●), and red triangles refer to I_{Cl3} (▲).

As in the Control experimental group, the percentages of anionic current lost during rundown in the µCa Test Group and the mCa Test Group (%Rundown) were constant for negative V_m, and decreased for positive V_m in a statistically significant manner. The %Rundown also increased significantly with increasing $[Ca^{2+}]_{in}$ (Table 21).

For all $[Ca^{2+}]_{in}$ tested, G/G_{max} from I_{Cl1} displayed a different potential for the half-maximal chord conductance (V_h) from the other two currents, with a shift for less depolarizing

potentials. This population of current also presented a significantly higher sensitivity to variations in V_m (V_s) in nCa and µCa Test Groups. The values of V_s and V_h for I_{Cl2} and I_{Cl3} didn't vary significantly in the same experimental group. Nevertheless V_h for I_{Cl1} was significantly lower in µCa than in mCa Test Group, V_h for I_{Cl2} was significantly lower in µCa, and V_s for I_{Cl2} was significantly higher in µCa indicating that Ca^{2+} may affect directly the kinetic behaviour of the channels responsible for these currents.

The maximum inhibition with NPPB was attained at 500 µM for the control group (P1/B1). For the other two experimental groups, larger concentrations of inhibitor were required to obtain the maximum inhibitory effect (1750 and ≥2000 µM for increasing $[Ca^{2+}]_{in}$). The relative amplitude of I_{Cl2} and I_{Cl3} was constant for all three calcium concentrations tested, showing that NPPB inhibited the same population of channels. We observed some degree of variation between cells within each experimental group. Corresponding control experiments with DMSO were performed with nM (n = 7) and µM Ca (n = 6). We observed that for concentrations of NPPB above 500 µM, the effect of the solvent could not be neglected.

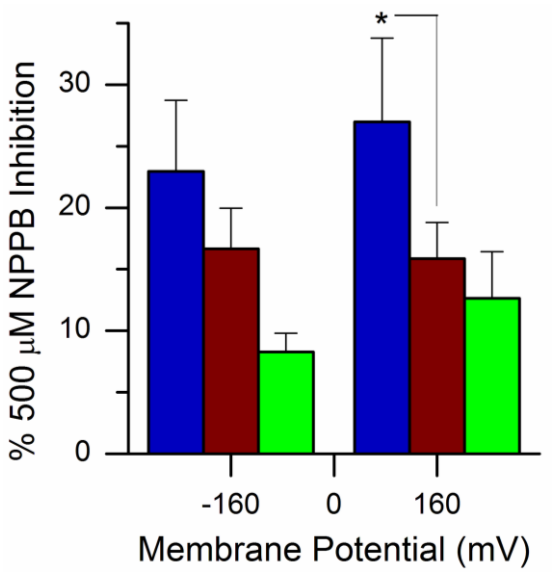

Figure 30. % Inhibition with 500 µM [NPPB] for the three experimental groups. Control Group (B1/P1 – nCa, ■), µCa Test Group (B1/P2, ■), and mCa Test Group (B1/P3, ■).

Figure 30 shows the average percentage of inhibition obtained with 500 µM NPPB for the three experimental groups. Higher effect was obtained in the presence of lower $[Ca^{2+}]_{in}$ (control).

Table 21. Steady-state chloride currents' parameters calculated with different $[Ca^{2+}]_{in}$. Experimental groups: Control (B1/P1 - nCa), µCa Test Group (B1/P2) and mCa Test Group (B1/P3). Parameters $\mathbf{I_{(-160\ mV)}}$, $\mathbf{I_{(+160\ mV)}}$, $\mathbf{g_B}$, $\mathbf{g_F}$, $\mathbf{g_F/g_B}$, $\mathbf{V_h}$, $\mathbf{V_s}$, $\mathbf{V_{rev}}$, **Activation**, **Deactivation**, τ_1, τ_2, $\mathbf{I_{Cl1}}$, $\mathbf{I_{Cl2}}$, $\mathbf{I_{Cl3}}$, **%Rundown**, **%Inhibition**, and $\mathbf{[NPPB]_{max}}$ as described in Table 11. Data are represented as mean ± SE. *****, refer to significant differences between comparable elements in the same experimental group. **¥**, refer to significant differences between comparable elements in different experimental groups ($p < 0.05$). Significant differences in the current intensities ($I_{(-160\ mV)}$ and $I_{(+160\ mV)}$), V_{rev} and conductances (g_B, g_F, g_F/g_B) were determined with the Wilcoxon test with SPSS software.

	Control Group (B1/P1 – nCa)				**µCa Test Group (B1/P2)**				**mCa Test Group (B1/P3)**			
	$I_{(-160\ mV)}$ (pA)	**$I_{(+160\ mV)}$ (pA)**	**V_{rev} (mV)**	**n**	**$I_{(-160\ mV)}$ (pA)**	**$I_{(+160\ mV)}$ (pA)**	**V_{rev} (mV)**	**n**	**$I_{(-160\ mV)}$ (pA)**	**$I_{(+160\ mV)}$ (pA)**	**V_{rev} (mV)**	**n**
I_{Cl1}	-432 ± 190	2086 ± 866	0.1 ± 0.6	11	-716 ± 207	4220 ± 532	1.4 ± 0.8	10	-985 ± 293	6721 ± 1505	-0.7 ± 0.3	3
I_{Cl2}	-451 ± 189	3314 ± 1318	-1.3 ± 0.9	7	-717 ± 184	4342 ± 1058	-5.7 ± 4.3	6	-143 ± 18	1919 ± 272	-13.8 ± 1.9	3
I_{Cl3}	-77 ± 28*	688 ± 204*	-7.3 ± 3.8	7	-136 ± 40*	1626 ± 493*	-2.0 ± 1.4	6	-43 ± 9*	1148 ± 219	-1.0 ± 1.7	3
%Rundown	37 ± 7¥	27 ± 5¥		11	56±7¥	46±7¥		10	81±7¥	67±7¥		3
%Inhibition	24 ± 5	28 ± 6		7	22 ± 5	33 ± 5		6	23 ± 3	37 ± 6		3
$[NPPB]_{max}$		500 µM				1750 µM				>2000 µM		
	g_B (nS)	**g_F (nS)**	**g_F/g_B**	**n**	**g_B (nS)**	**g_F (nS)**	**g_F/g_B**	**n**	**g_B (nS)**	**g_F (nS)**	**g_F/g_B**	**n**
I_{Cl1}	0.72 ± 0.23	13.79 ± 5.28	26 ± 10	11	1.79 ± 0.46	27.45 ± 4.3 8	24 ± 7	9	2.38 ± 0.92	53.95 ± 13.45*	30 ± 9*	3
I_{Cl2}	1.62 ± 0.67	33.14 ± 12.82*	35 ± 16	7	2.18 ± 0.65	40.42 ± 10.03*	23 ± 3	9	0.23 ± 0.03	20.69 ± 3.66	87 ± 5¥	3
I_{Cl3}	0.40 ± 0.14*	6.56 ± 1.91	32 ± 9	7	0.65 ± 0.21*	16.29 ± 5.27	35 ± 8	9	0.15 ± 0.06	13.50 ± 2.96	132 ± 61¥	3
	V_h (mV)	**V_s (mV)**		**n**	**V_h (mV)**	**V_s (mV)**		**n**	**V_h (mV)**	**V_s (mV)**		**n**
I_{Cl1}	14 ± 13*	50 ± 4*		11	-14 ± 9*¥	38 ± 5*		9	30 ± 7*¥	50 ± 8		3
I_{Cl2}	103 ± 7	65 ± 1		7	77 ± 4¥	70 ± 2¥		8	110 ± 9	61 ± 3		3
I_{Cl3}	94 ± 10	61 ± 3		7	77 ± 14	53 ± 6		8	121 ± 4	59 ± 3		3

5.2.6. Summary of the results

1. Anionic currents were found in pollen grain protoplasts:
    a. Cl^- was the main permeable ion;
    b. $V_{rev} \approx E_{Cl^-}$;
    c. When $[Cl^-]_{ext}$ was lowered, the positive current's intensity decreased (24 ± 4 %) and the V_{rev} shifted to a more positive value (19.7 ± 2.3 mV), as expected;
    d. Currents were partially inhibited by NPPB.
    e. The currents present an outward rectification:
        i. The positive currents (Cl^- entering the cell) are larger than the negative currents (Cl^- exiting the cell) - $g_F > g_B$.
2. The anionic currents characterized by a time dependent, depolarization-induced activation and by a time-dependent, hyperpolarization-induced deactivation:
    a. Both the activation and the deactivation currents can be described by two time dependent current components I_1 and I_2, characterized by τ_1 and τ_2 respectively, with τ_1 greater than τ_2.
3. There are three different populations of outward rectified anionic currents; I_{Cl1} - the current lost during rundown; I_{Cl2} - the current resistant to NPPB; and I_{Cl3} - the current inhibited by NPPB:
    a. I_{Cl1} has a significantly lower V_h and V_s (14 ± 13 mV and 50 ± 4, respectively), presenting different sensitivity to variations in V_m;
    b. I_{Cl1}, I_{Cl2} and I_{Cl3} were differently regulated by $[Ca^{2+}]_{in}$.
4. The channels responsible for the observed currents are regulated by $[Ca^{2+}]_{in}$:
    a. I_{Cl1} currents increased in intensity with increasing $[Ca^{2+}]_{in}$;
    b. I_{Cl2} and I_{Cl3} showed their maximum value with µM $[Ca^{2+}]_{in;}$
    c. Cytoplasmic Ca^{2+} regulates the sensitivity of the channels to V_m:
        i. V_h from I_{Cl1} was significantly lower in µCa than in mCa Test Group;
        ii. V_h from I_{Cl2} was significantly lower in µCa Test Group;
        iii. V_s from I_{Cl2} was significantly higher in µCa Test Group.

5. These channels are 1.2 times more permeable to NO_3^- than to Cl^-:
    a. In BSE 2, $P_{NO3}/P_{Cl} = 1.1 \pm 0.1$;
    b. In BSE 3, $P_{NO3}/P_{Cl} = 1.5 \pm 0.1$.

5.3. Identification of the channel or channels responsible for the anionic currents found in pollen grain protoplasts from **Arabidopsis thaliana**

From the analysis of *Arabidopsis thaliana*'s pollen grain transcriptomic (Becker and Feijo, 2007) six putative anion channel candidates have risen: ALMT12, SLAH2 and SLAH3 (SLAC1 homologues), CaCC (a TMEM16 homolog), CLCc and CLCd (Table 22). In a second phase, the best candidates, based on available physiological data, were chosen for further analysis, namely the study of the anionic currents from pollen grain protoplasts from KO plants.

Table 22. Channel candidates for the anionic currents found in the transcriptome of pollen grains from *Arabidopsis thaliana*.

Name of Protein	Gene	Additional information
CLC-c	At5g49890	Belong to the Chloride Channel family; Has been localized in the tonoplast; Only one to be over expressed in pollen.
CLC-d	At5g26240	Belong to the Chloride Channel family; Has been localized in the trans-Golgi network vesicles.
MSL10	At5g12080	Mechanosensitive channel of small conductance.
SLAH2	At4g27970	SLAC1 homologue 2.
SLAH3	At5g24030	SLAC1 homologue 3.
ALMT12	At4g17970.1	Belongs to the Al^{3+}-activated Malate Transporter family; Responsible for the R-type currents found in guard cells.
CaCC	At1g73020	Mammalian TMEM16 family homologue.

5.3.1. CLCc and CLCc

The transporters CLCc and CLCd were included in this list because *CLCc* is the only gene in this list to be overexpressed in pollen, and because, when co-transfected with CPK34, CLCc is allocated to the plasma membrane of the growing pollen tube (Konrad K, personal communication). Regardless of these observations, it has been well established that both CLCc and CLCd are localized in the endomembranar system, namely the vacuole and the TGN, respectively.

5.3.2. MSL10

This channel has been found to be activated by a convex curvature of the plasma membrane, and was associated with the increase of cell volume during cell growth or during a hypo-osmotic shock (Haswell *et al.*, 2008; Peyronnet *et al.*, 2008). These channels have only been characterized in the single-channel configuration and therefore the WC currents are unknown and cannot be compared with the ones reported here. Nevertheless MSL10 could not be responsible for the observed steady state currents here described since there is evidence that these channels are not regulated by cytosolic Ca^{2+} nor by voltage.

5.3.3. SLAH2 and SLAH3

The inclusion of the channels SLAH2 and SLAH3 in this list is due to the fact that these proteins are homologs of the SLAC1 channel, which has an extremely important role in the efflux of Cl^- and mal^{2-} during stomata closure. Since these proteins have not been electrophysiologically characterized so far, it is impossible to comment on their similarity with the anionic currents found in pollen grain protoplasts. Nevertheless it would be interesting to test whether these proteins were involved by means of electrophysiologically characterizing pollen grain protoplasts from mutant knock-out plants for SLAH2 and/or SLAH3.

5.3.4. ALMT12

ALMT12 has been recently associated with the R-type currents found in guard cells (Meyer *et al.*, 2010). The currents through this channel depend on $[mal^{2-}]_{ext}$, which shifts the threshold for voltage activation towards more hyperpolarized potentials. These channels are voltage dependent and have a characteristic bell-shaped I/V curve. They are activated by and permeate SO_4^{2-}, and the addition of 10 mM mal^{2-} into the external medium maximizes the inward currents (positive currents). Similarly to the currents found in pollen grain protoplasts, ALMT12 channels present strong voltage dependence, are activated by depolarization and the amplitude of their current appears to be depend on $[Cl^-]_{ext}$.

In order to test whether our currents were due to the ALMT12 channel, the depolarizing ramp voltage protocol described in Schroeder and Keller, (1992) was used and 5 mM of mal^{2-} was tested on the anion currents elicited in *Control* conditions (B1/P1) in pollen grain

protoplasts from *Arabidopsis thaliana*. Figure 31 shows the I/V curves that resulted from the ramp voltage protocol. Unlike the currents through ALMT12, these did not present the characteristic bell-shaped I/V curve, and the positive currents were inhibited by 5 mM mal^{2-}. Higher concentrations of mal^{2-} in the bath solution cause the Giga-seal to destabilize and then to be lost altogether. The addition of 5 mM mal^{2-} also caused the anion currents to lose their strong outward rectification, and changed their sensitivity to V_m, with V_h shifting to less positive V_m (Table 23).

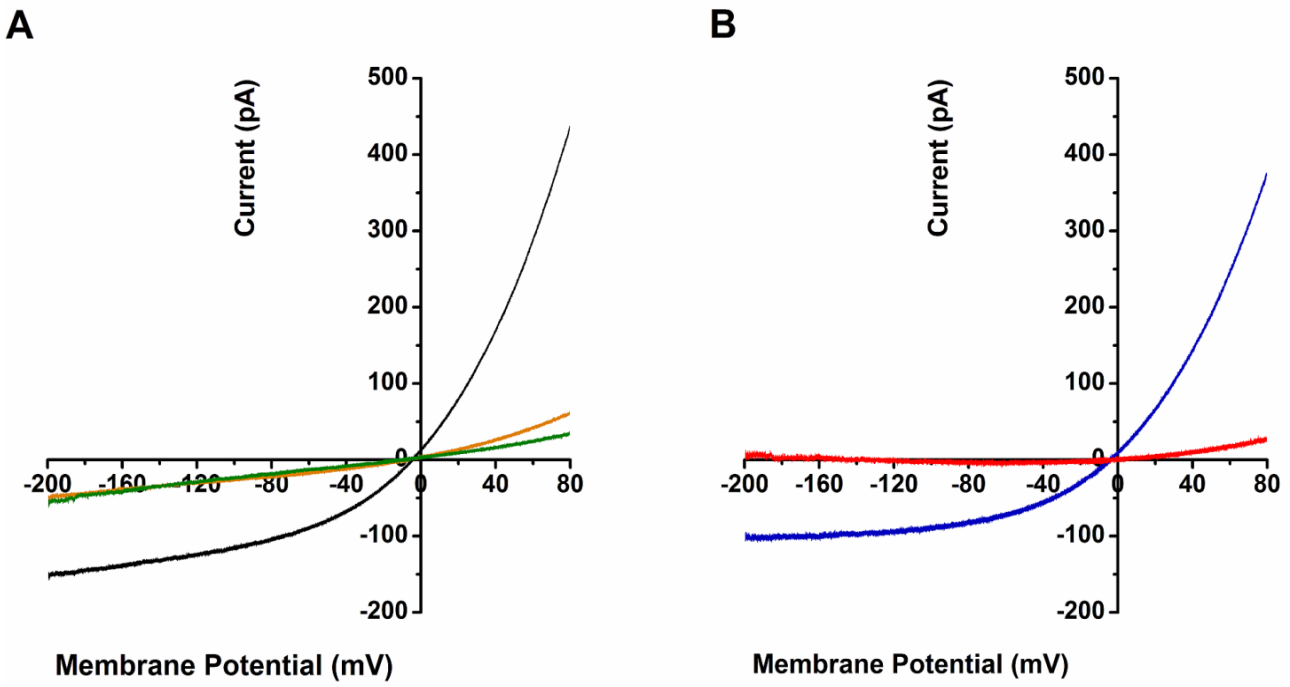

Figure 31. I/V curves obtained with a depolarizing 10 sec voltage ramp protocol from one protoplast. The protoplasts, obtained from *Arabidopsis thaliana* pollen grains, were kept at a holding potential of -100mV, then the membrane was clamped from -200 mV to +80mV. **A:** black line – $I_{initial}$; orange line - I_{final}; dark green line – Current resistant to 5 mM Malate. **B:** blue line – I_{Cl1}; red line current inhibited by 5 mM Malate.

These results lead to the conclusion that the anion currents present in pollen grain protoplasts from *Arabidopsis thaliana* are unlikely to be due to the ALMT12 channel.

Table 23. Steady-state anionic currents' parameters calculated before and after the addition of 5 mM Malate to the BS (B1/P1). Parameters $I_{(-160\ mV)}$, $I_{(+160\ mV)}$, g_B, g_F, g_F/g_B, V_h, V_s, V_{rev}, and **%Inhibition** as described in Table 13. $I_{140mM\ Cl^-}$ and $I_{5mM\ Mal^{2-}}$ refer to the currents before and after 5 mM Malate addition, respectively. Data are represented as mean ± SE. *, refer to significant differences between comparable elements in the same experimental group ($p < 0.05$).

	Addition of 5 mM Malate			
	$I_{(-160\ mV)}$	$I_{(+160\ mV)}$	V_{rev}	**n**
$I_{140mM\ Cl^-}$	-5.2 ± 1.9	41.4 ± 20.2	-14.8 ± 8.3	3
$I_{5mM\ Mal^{2-}}$	-5.3 ± 4.6	11.1 ± 4.6*	-6.6 ± 2.0	3
%Inhibition	-5 ± 5	72 ± 11		
	g_B	g_F	g_F/g_B	**n**
$I_{140mM\ Cl^-}$	0.038 ± 0.016	0.477 ± 0.244	14 ± 4	3
$I_{5mM\ Mal^{2-}}$	0.035 ± 0.016	0.089 ± 0.040*	2 ± 1*	3
	V_h		V_s	**n**
$I_{140mM\ Cl^-}$	150 ± 4		65 ± 8	**3**
$I_{5mM\ Mal^{2-}}$	85 ± 29*		72 ± 14	**3**

5.3.5. TMEM16

The gene At1g73020 is a plant homologue to the TMEM16A family, possessing an Anoctamin domain. Because of this similarity the resulting protein is here designated as CaCC. TMEM16A proteins were first electrophysiologically characterized in 2008 both in Axolotl oocyte system (Schroeder *et al.*, 2008) and in mammalian cells (Caputo *et al.*, 2008; Yang *et al.*, 2008). This family of Ca^{2+}-activated Cl^- channels (CaCC) is characterized by a strong outward rectification at submaximal [Ca^{2+}] levels, and by a linear I/V relationship at high [Ca^{2+}]. xTMEM16A (Xenopus TMEM16A) were shown to be inhibited by DIDS, NA, and less effectively by NPPB and DPC but resistant to tamoxifen (Schroeder *et al.*, 2008), while mouse TMEM16A is inhibited by DIDS, NPPB, fluoxetine, tamoxifen, n-phenyl-anthranilic acid, and mefloquine (Yang *et al.*, 2008). Human TMEM16A was inhibited by NA and NPPB, but insensitive to diphenylamine carboxylate and CFTRinh-172 (Caputo *et al.*, 2008). TMEM16 channels exhibit greater permeability for larger anions than for chloride, as can be seen by their permeability sequence: NO_3^- ≈ SCN^- (2.20) > I^- (1.85).> Br^- (1.74) > Cl^- (1.0) > F^- (0.43). These proteins were shown to have multiple current components that arise from multiple open states, which differ not only in kinetics but also in anion selectivity (Schroeder *et al.*, 2008). TMEM16A was found to be alternatively spliced, generating multiple protein isoforms with various combinations of

alternative protein segments a, b, c, and d. These isoforms presented variations in intensity of the Cl^- channel activity and kinetics (Caputo *et al.*, 2008).

The anion currents reported here share several characteristics with the TMEM16 family: they are Ca^{2+} regulated, although they never showed a linear rectification with very high [Ca^{2+}]; they are inhibited by NPPB; they are twice more permeable to NO_3^- that to Cl^- (in *Arabidopsis thaliana*); and also show multiple current components. Furthermore, the WC currents from the TMEM16 family are identical to the ones reported here: they show a strong outward rectification, have a time dependent, depolarization induced activation, and a time dependent, hyperpolarization induced deactivation (Caputo *et al.*, 2008; Schroeder *et al.*, 2008).

Due to these similarities, the *Arabidopsis thaliana* knock-out mutant line FLAG_526A10 – ecotype Wassilewskija (Ws), with a T-DNA insertion in the fourth exon of the *At1g73020* gene, coding for a putative TMEM16A protein homologue – was chosen to test whether the protein CaCC was responsible for the currents found in the pollen grain protoplasts, as the negative control.

In a first step, these plants were genotyped, and 3 of the 6 plants tested were homozygous for the T-DNA insert (Figure 32).

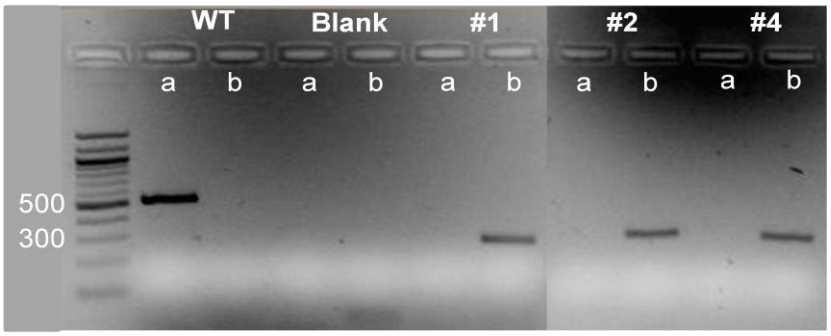

Figure 32. Fragments produced by PCR during the analysis of the genomic DNA. Two primer combinations were used in this analysis: FLAG_526A10_F + FLAG_526A10_R **(a)** was designed specifically to detect the absence of T-DNA insert, while FLAG_526A10_F + LB4 **(b)** was designed to detect the presence of the insert. **WT** refers to wild type, **Blank** refers to the negative control, **#1, #2 and #4** refer to 3 different tested plants from the FLAG_526A10 line. As predicted the fragments had 500 and 300 bp (see Experimental Procedure).

The transcription of the gene *At1g73020* was then checked on all three homozygous plants. During the analysis, by agarose gel electrophoresis, of the RT-PCR products, obtained with AT1G73020_F and AT1G73020_R primers (see section 3.2.2 of the

Experimental Procedures, page 56), an unexpected fragment with approximately 400 bp was found in the homozygous mutant cDNA sample (**-/-** in Figure 33). This fragment was sequenced along with the 400 bp fragment obtained for the WT cDNA sample. Both sequences matched the predicted cDNA sequence for the At1g73020 available on line at *The Arabidopsis Information Resource*.

It is possible that in this case the T-DNA insert was interpreted by the cellular machinery as an intron and excised, thus not interrupting the production of mRNA for that gene. Nevertheless, because this mRNA should represent an unnatural *splicing variant*, the protein that arises might not be functional. In order to determine whether this was the case, a new pair of primers, AT1G73020_2_F and AT1G73020_2_R (see section 3.2.2 of the Experimental Procedures, page 56), was used in the PCR described in Table 4 (Experimental Procedures, page 58).

The PCR performed with the primers AT1G73020_2_F and AT1G73020_2_R produced a band with ~460 bp for the cDNA of the WT sample and the homozygous *at1g73020* KO samples (Figure 33 c).

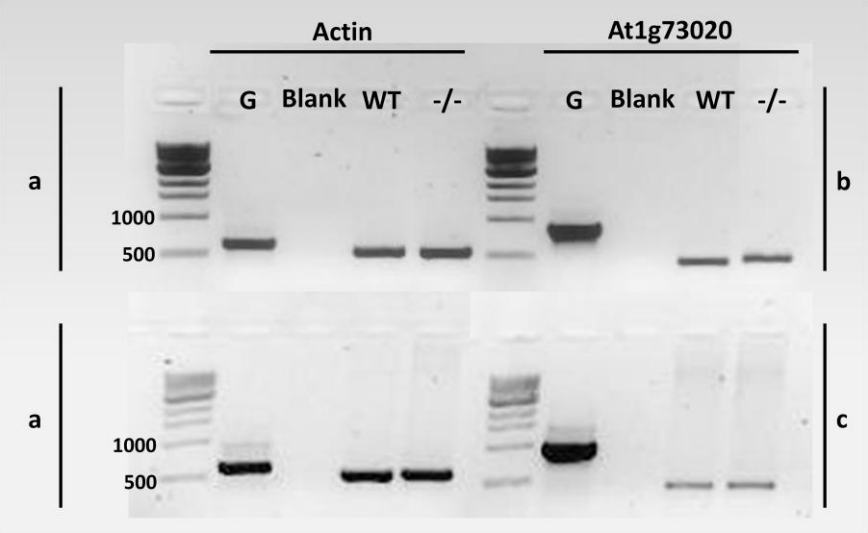

Figure 33. Analysis of the products of the RT-PCR by agarose gel electrophoresis. The first column refers to the control of the quality of the cDNA by means of the detection of the *actin* transcript. The second column refers to the study of the *at1g73020* transcript. The primers used in **(a)** were Actin_F and Actin_R; in **(b)** were AT1G73020_F and AT1G73020_R; and in **(c)** were AT1G73020_2_F and AT1G73020_2_R. **G** refers to genomic DNA (primer and PCR mix control), **Blank** refers to the negative control, **WT** refers to the cDNA sample from wild type plants, **-/-** refers to the cDNA sample from a homozygous *at1g73020* KO plant. All the fragments had the predicted size (see Experimental Procedure).

These fragments were sequenced, and both sequences matched the predicted cDNA sequence for the At1g73020 available on line at *The Arabidopsis Information Resource*, indicating that the transcription of the gene was not interrupted. Similar phenomena have been reported in plants before (Daxinger *et al.*, 2008; Mlotshwa *et al.*, 2010).

Furthermore, the grown KO plants #1, #2 and #4 had no discernable phonotypical differences in relation to the wild type of the same ecotype (Wassilewskija) (Figure 34).

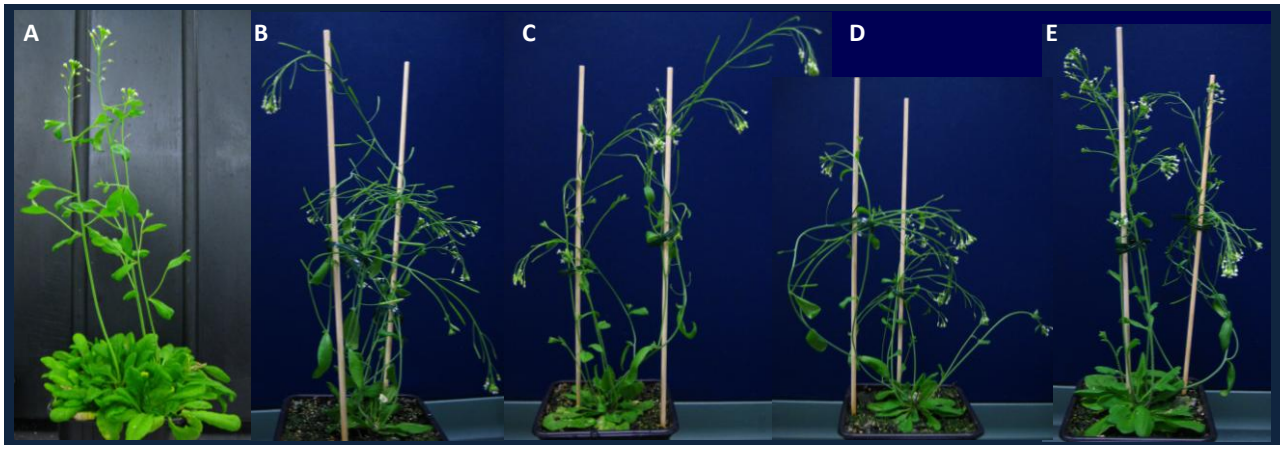

Figure 34. Flowering *Arabidopsis thaliana* of two different ecotypes, Columbia (Col-0) and Wassilewskija (Ws). **A:** Col-0 wild type (WT); **B:** Ws WT; **C:** Ws *cacc* #1; **D:** Ws *cacc* #2; **E:** Ws *cacc* #4.

When the pollen protoplasts of the KO plants #1, #2 and #4 were tested by means of the WC configuration of the patch clamp technique, some significant differences were found, namely higher current densities, higher %Rundown, and higher [NPPB] needed to reach maximum inhibition, although these proved to be differences between ecotypes and not due to the mutation of the gene (Table 24). Taken with the results on the analysis of the transcripts of these plants, these last electrophysiological results are therefore inconclusive. Different mutant lines will have to be tested or the At1g73020 cDNA will have to be heterologously transfected into animal culture cells and the resulting protein electrophysiologically characterized.

Table 24. Steady-state chloride currents' parameters obtained in *Control* experimental conditions (**B1/P1 - nCa**) with pollen protoplasts from *Arabidopsis thaliana*, ecotype Columbia, wild type (**At Col-0 WT**); from *A. thaliana*, ecotype Wassilewskija, wild type (**At Ws WT**); and from *A. thaliana*, ecotype Wassilewskija, knock-out cacc mutants (**At Ws cacc KO #1, #2 and #4**). **$I_{(-160\ mV)}$**, **$I_{(+160\ mV)}$**, **g_B, g_F, g_F/g_B**, **Activation, Deactivation**, **I_{Cl1}**, **I_{Cl2}** and **I_{Cl3}** as described in Table 11. **%Rdw** refers to the percentage of current lost during rundown for V_m = -160 and +160 mV. **%Inhibit** refers to the percentage of inhibited current for those same V_m. **$[NPPB]_{avg}$** and **$[NPPB]_{max}$** refer to the average and maximal [NPPB] needed for maximal inhibition, respectively.

	At Col-0 WT (B1/P1 – nCa)				**At Ws WT (B1/P1 – nCa)**				**At Ws cacc KO #1, #2 and #4 (B1/P1 – nCa)**			
	Activation Currents				**Activation Currents**				**Activation Currents**			
	$I_{(-160\ mV)}$	**$I_{(+160\ mV)}$**	**V_{rev}**	**n**	**$I_{(-160\ mV)}$**	**$I_{(+160\ mV)}$**	**V_{rev}**	**n**	**$I_{(-160\ mV)}$**	**$I_{(+160\ mV)}$**	**V_{rev}**	**n**
I_{Cl1}	-4.4 ± 1.0	60.8 ± 9.5	-1.0 ± 0.7	17	-33.0 ± 14.2	306.6 ± 39.8	-2.5 ± 0.1	3	-24.7 ± 7.2	213.3 ± 47.3	-2.5 ± 0.6	7
I_{Cl2}	-5.2 ± 0.7	26.6 ± 3.4	-5.0 ± 0.8	16	-9.3 ± 7.2	63.0 ± 16.3	-5.3 ± 0.3	3	-8.1 ± 2.4	97.3 ± 38.9	-5.9 ± 0.7	7
I_{Cl3}	-0.8 ± 0.3	16.0 ±2.8	-1.1 ± 1.1	16	-1.3 ± 0.5	47.3 ± 8.6	-2.2 ± 1.5	3	-1.7 ± 0.9	43.2 ± 11.2	-1.9 ± 1.0	7
%Rdw	43 ± 5	56 ± 5		17	77 ± 4	70 ± 9		3	71 ± 7	64 ± 6		7
%Inhibit	22 ± 4	36 ± 4		16	23 ± 2	33 ± 4		**3**	21 ± 7	39 ± 5		7
$[NPPB]_{avg}$		100 ± 0 µM		16		400 ± 66 µM		3		400 ± 58 µM		**7**
$[NPPB]_{max}$		100 µM				700 µM				700 µM		
	g_B	**g_F**	**g_F/g_B**	**n**	**g_B**	**g_F**	**g_F/g_B**	**n**	**g_B**	**g_F**	**g_F/g_B**	**n**
I_{Cl1}	0.018 ± 0.005	0.600 ± 0.098	47 ± 5	17	0.106 ± 0.045	1.782 ± 0.613	23 ± 11	3	0.078 ± 0.021	1.785 ± 0.406	52 ± 29	7
I_{Cl2}	0.032 ± 0.004	0.315 ± 0.039	12 ± 2	16	0.057 ± 0.052	0.582 ± 0.182	51 ± 24	3	0.037 ± 0.013	1.094 ± 0.428	51 ± 15	7
I_{Cl3}	0.007 ± 0.002	0.202 ± 0.035	53 ± 11	16	0.004 ± 0.001	0.214 ± 0.143	49 ± 28	3	0.007 ± 0.003	0.451 ± 0.105	90 ± 15	7

	Deactivation Currents						**Deactivation Currents**						**Deactivation Currents**					
	g_B	**g_F**	**g_F/g_B**	**V_{rev}**	**n**		**g_B**	**g_F**	**g_F/g_B**	**V_{rev}**	**n**		**g_B**	**g_F**	**g_F/g_B**	**V_{rev}**	**n**
I_{Cl1}	0.217 ± 0.079	0.467 ± 0.071	4 ± 2	11.8 ± 1.4	6		0.144 ± 0.054	1.429 ± 0.249	8 ± 4	22.7 ± 14.1	3		0.469 ± 0.235	1.230 ± 0.294	6 ± 2	8.2 ± 3.8	7
I_{Cl2}	0.083 ± 0.031	0.300 ± 0.045	4 ± 1	5.4 ± 1.8	6		0.108 ± 0.053	0.409 ± 0.114	4 ± 1	14.3 ± 4.9	3		0.329 ± 0.141	0.707 ± 0.268	4 ± 1	15.3 ± 4.8	7
I_{Cl3}	0.050 ± 0.034	0.100 ± 0.037	2 ± 0	17.4 ± 13.9	6		0.138 ± 0.051	0.342 ± 0.086	4 ± 0	66.3 ± 27.5	3		0.176 ± 0.075	0.339 ± 0.095	4 ± 1	7.4 ± 1.8	7

6. Discussion

By employing the whole-cell configuration of the patch clamp technique with Cl^- based bath and pipette solutions, it was possible to identify three distinct anionic current populations (I_{Cl1}, I_{Cl2} and I_{Cl3}) based on loss of current by rundown and NPPB inhibition, regulated by $[Ca^{2+}]_{in}$ and sharing a strong outward rectification, in two distinct plant species, *Arabidopsis thaliana* and *Lilium longiflorum*. All I/V curves presented V_{rev} close to the expected E_{Cl^-} and the positive currents diminished in intensity when the $[Cl^-]_{out}$ was reduced, with the corresponding expected shift of V_{rev} towards positive potentials. Under these experimental conditions, these are all strong indications that Cl^- is the major contributor to these currents. Tail analysis further confirmed the anionic nature of the currents, with the I/V curves being linear (in *Lilium longiflorum*), reversing at the equilibrium potential expected for Cl^- and NO_3^-, undergoing rundown, and being partially inhibited by NPPB (both in Lilium and in Arabidopsis).

In the presence of NO_3^--based solutions, the currents kept the general kinetic features and voltage dependency, an indication that different anions may permeate these channels.

Due to the strong outward rectification of the anionic current populations, it could be suggested that the putative channels only allowed the influx of anions. But, since the negative currents measured in both species underwent rundown and a portion was inhibited by NPPB, it is possible to conclude that the anionic channels responsible for the currents described here display the ability of conducting anions both inwardly and outwardly, according to the anionic electrochemical gradient found under natural conditions.

The two plant species studied shared several anionic transport characteristics, such as a time-dependent depolarization-induced activation, and a time-dependent hyperpolarization-induced deactivation, both displaying an instantaneous component and two time-dependent components. A similar phenomenon was reported by Marten *et al.* (1999). These authors detected whole-cell K^+ currents by means of the heterologous expression of AKT3 (a potassium channel from vascular tissue of *Arabidopsis thaliana*) in *Xenopus* oocytes which presented instantaneous and time dependent components. A similar inhibition profile and rundown behaviour to the ones reported here, was also described for

both current components through the potassium channel (Marten *et al.*, 1999). In addition, the heterologous expression of the Ca^{2+}-activated channel mTMEM16A in HEK293 cells produced whole-cell currents with a similar profile to the ones detected here, with a fast and slower activation components (Schroeder *et al.*, 2008).

Under control conditions (P1/B1) I_{Cl1} was identified as the current lost by rundown, possibly being modulated by an unknown intracellular regulator which is diluted into the pipette solution; I_{Cl3} was identified as the current which is inhibited by NPPB; and I_{Cl2} is the current remaining after the loss of I_{Cl1} and which is insensitive to NPPB. Throughout this work I_{Cl1}, I_{Cl2} and I_{Cl3} were treated as individual anionic current populations, which displayed distinctive features. In *Arabidopsis thaliana*, I_{Cl2} had a significantly weaker rectification, I_{Cl1} had a significantly lower V_h, and I_{Cl1}, I_{Cl2} and I_{Cl3} had different activation and deactivation time constants, while in *Lilium longiflorum*, I_{Cl1} had a significantly lower V_h and V_s. Finally I_{Cl1}, I_{Cl2} and I_{Cl3}, in both species, were differently regulated by $[Ca^{2+}]_{in}$. Likewise, the TMEM16A proteins were shown to have multiple current components that arise from multiple open states, which differed not only in kinetics but also in anion selectivity (Schroeder *et al.*, 2008; Yang *et al.*, 2008), and also different isoforms that presented variations in kinetics and in the intensity of Cl^- conductivity (Caputo *et al.*, 2008). Recently in our group it was possible to detect single channel events with three conductance substates across the membrane of pollen grain protoplasts from *Lilium longiflorum* (Tavares *et al.*, 2011a). So far it was not possible to determine if each current population represents each of these substates or if the currents belong to more than one substate or channel.

The average inhibition caused by 100 µM NPPB or 500 µM NPPB (measured with nM $[Ca^{2+}]_{in}$, +160 mV; in Arabidopsis and in Lilium, respectively) was significantly different from the inhibition values obtained for the test groups (measured with µM and mM $[Ca^{2+}]_{in}$) with the same concentration of inhibitor. It is possible that the anionic channels may present different conformations in the presence of different $[Ca^{2+}]$, with different apparent affinities to NPPB.

In *Arabidopsis thaliana*, the $[Ca^{2+}]_{in}$. regulates the response time of the channels to V_m. The same could not be said for the anionic currents found in *Lilium longiflorum*. Since the time constants did not varied with the tested $[Ca^{2+}]_{in}$, it is likely that in this species Ca^{2+}

regulates the amount of open channels contributing to the current at a given moment. This could also occur in Arabidopsis.

In *Arabidopsis thaliana*, the currents measured with symmetrical NO_3^- showed a shift of the half-maximum chord conductance (V_h) between +15 and +30 mV, indicating a different sensitivity of the channels to the potential in the presence of this anion. These currents were also regulated by $[Cl^-]_{out}$, presenting a decrease in the negative currents and in the time constants, when $[Cl^-]_{out}$ was lowered. Again, in Lilium, these changes did not occur. Furthermore, in *Arabidopsis thaliana* the channels are 2 times more permeable to NO_3^- than to Cl^-, while in *Lilium longiflorum* the channels are only slightly more permeable to NO_3^- than to Cl^- ($P_{NO3}/P_{Cl} \approx 1.2$), and the values for V_h from the three current populations in *L. longiflorum* were significantly smaller than in *A. thaliana*. The differences between the anionic currents found in these species could be the result of the different natural physiological environments, where the putative anion channels are integrated and have evolved different isoforms. A similar observation can be made in relation to the S-type anion channels found in the guard cells of different species. Although with very similar characteristics, these channels differ in their sensitivity to known anion channel blockers (Table 1 in Introduction, page 36). Also, the TMEM16A Ca^{2+}-activated Cl^- channel from the Xenopus oocyte and from the mouse also displayed different sensitivity to anion channel blockers (Schroeder *et al.*, 2008; Yang *et al.*, 2008).

It was consistently observed that the currents suffered rundown over time (~90 mins). Binder *et al.* (2003) observed a similar behaviour while studying the Cl^- currents in protoplasts from the marine alga *Valonia utricularis* and attributed it to a retarded equilibration of the cytosol with the pipette solution, as indicated by alterations of the V_{rev} of the detected currents, until it stabilized near the predicted E_{Cl}^-. In this study, no drifts of the V_{rev} of the measured currents from E_{Cl}^- were observed, which may indicate that the equilibration is faster in these protoplasts. This is also applied to the currents measured with symmetrical NO_3^-. Alternatively, the natural intracellular anion concentration may be similar to those in the pipette solution, thus explaining the lack of shift of the V_{rev} while the cytoplasm and its contents, such as any regulatory effectors, are equilibrated with the pipette solution. It has been debated that pollen tube germination does not require extracellular anions (Weisenseel and Jaffe, 1976). The results presented here, in Zonia *et al.* (2002) and in Breygina *et al.* (2009a) suggest that pollen grains may present

considerable anionic reserves, readily available for transport across the membrane. If this is the case, the channels responsible for the anionic currents observed in pollen grain protoplasts could be involved in the efflux of anions during the grain hydration and the tube growth processes.

In 2004 Dutta and Robinson reported the absence of Cl^- channels in outside-out patches from the plasma membrane of pollen protoplasts from *Lilium longiflorum*. The authors also reported, in the same paper, a complete absence of hyperpolarization-activated Ca^{2+} channels that were subsequently found by several other authors in the plasma membrane of pollen protoplasts from *Lilium davidii* D., *Arabidopsis thaliana* and *Pyrus pyrifolia* (Qu *et al.*, 2007; Shang *et al.*, 2005; Wu *et al.*, 2007). Thus, one can infer that the configuration of the patch clamp technique used by Dutta and Robinson, might not be the most appropriate one to study the ion currents present in such a poorly known system as the plasma membrane of the pollen grain or pollen tube protoplasts. Recently, it was observed in our group that it was possible to measure whole-cell currents of very small amplitude (~200 pA for +160 mV) from outside-out patches using high resistance pipettes (Tavares *et al.*, 2011a). It is therefore possible that Dutta and Robinson may have misinterpreted the macroscopic even current levels with the absence of channel activity. Although uncommon, macroscopic currents have been observed from outside-out patches (e.g. Artigas and Gadsby, 2002). Another experimental difference that could explain the absence of Cl^- channels was the use of extremely high $[Ca^{2+}]_{out}$ (40 mM) by Dutta and Robinson (2004). There is evidence of inward K^+ currents in *Arabidopsis* pollen grain protoplasts regulated by $[Ca^{2+}]_{out}$ (Fan *et al.*, 2001).

The existence of Ca^{2+} domains has been demonstrated by means of imaging techniques, with intracellular nM values for $[Ca^{2+}]_{in}$ in most of the tube, and an increasing concentration gradient towards the tip up to µM concentrations. There are, inclusively, suggestions that $[Ca^{2+}]_{in}$ may reach mM domains close to the plasma membrane at the tip (Holdaway-Clarke *et al.*, 1997; Malho *et al.*, 1995; Messerli *et al.*, 2000; Michard *et al.*, 2008; Miller *et al.*, 1992; Pierson *et al.*, 1994; Pierson *et al.*, 1996; Rathore *et al.*, 1991; Reiss and Herth, 1985; reviewed in Holdaway-Clarke and Hepler, 2003, see Figure 1 in Introduction, page 26). From the results presented here, one can speculate that the channels responsible for the anionic currents found in pollen grain protoplasts, may be involved in the anionic apical effluxes detected at the tip of growing tubes (Zonia *et al.*, 2002) where the $[Ca^{2+}]_{in}$ reaches

its maximum. On the other hand, one cannot exclude that the anionic currents from Arabidopsis and Lilium protoplasts may additionally be distinctly regulated by other intracellular or extracellular effectors, reflecting the different stages of pollen physiology. For instance, it has been already shown that Inositol 3,4,5,6-Tetra*kis*phosphate modulates the oscillatory Cl^- efflux at the pollen tube apex (Zonia *et al.*, 2002). Another example of distinct modes of channel regulation can be found in a recent publication (Chen *et al.*, 2010), based on concurrent measurements, in guard cells, of anionic currents and $[Ca^{2+}]_{in}$ *in vivo*, that suggests the existence of three modes by which anionic S-type currents may be regulated, one of which is Ca^{2+}-dependent. Additionally, both Ca^{2+}-dependent and Ca^{2+}-independent currents detected showed an extra regulation involving protein de-phosphorylation, assessed by okadaic acid, a protein phosphatase antagonist.

Under physiological conditions it is expected that the membrane potential of hydrated grain and of the pollen tube to be intrinsically negative (Breygina *et al.*, 2009b; Feijo *et al.*, 1995; Mouline *et al.*, 2002). Using the values of the initial current ($I_{initial}$) obtained in the Control experimental group and in the µCa and mCa test groups it was possible to calculate, by means of Equation 5 (in Experimental Procedures, page 71), the anion fluxes that the currents found in pollen grain protoplasts from *A. thaliana* and *L. longiflorum*, could generate. Table 25 and Table 26 summarize the calculated fluxes, from *A. thaliana* and *L. longiflorum*, respectively, for different V_m. It is possible to observe that, by simply oscillating the cytosolic $[Ca^{2+}]$ and the V_m, it is possible to generate oscillations in the anionic fluxes. In the case of *Lilium longiflorum*, the values for the currents could not be normalized with C_m. Therefore, the fluxes were estimated by assuming a spherical shape for the membrane surface and calculating the corresponding current density in ($pA.cm^{-2}$). The generated oscillations in the anionic fluxes in Lilium were compatibles with the ones observed in growing pollen tubes by Zonia *et al.* (2002). So far it was not possible to measure, in our group, the Cl^- fluxes in growing pollen tubes from *A. thaliana*, and such a similar comparison cannot be performed. Nevertheless, the apical effluxes found in tobacco and lily pollen tubes (400 – 1200 pmol cm^{-2} s^{-1} and 50 – 8000 pmol cm^{-2} s^{-1}, respectively), diminished in intensity with diminishing average pollen tube radius (14 - 20 µm and 10 µm for Lilium and tobacco, respectively). If this trend is kept in Arabidopsis, then one could also accept the values calculated as plausible.

Table 25. Anionic fluxes calculated with Equation 5, using the $I_{initial}$ values from Control (B1/P1 - nCa), µCa Test (B1/P2) and mCa Test (B1/P3) experimental conditions, expected at different V_m.

	Average Anionic Fluxes (pmol cm^{-2} s^{-1})		
Vm (mV)	**nCa**	**µCa**	**mCa**
-199.9	118 ± 15	197 ± 26	234 ± 32
-179.9	107 ± 14	181 ± 23	222 ± 30
-159.9	98 ± 13	165 ± 21	209 ± 29
-139.9	90 ± 13	153 ± 19	198 ± 27
-119.9	82 ± 12	142 ± 18	186 ± 26
-99.9	75 ± 11	131 ± 16	173 ± 25
-79.9	67 ± 10	116 ± 15	158 ± 23
-59.9	57 ± 9	99 ± 13	138 ± 20
-39.9	44 ± 7	77 ± 11	109 ± 16

Table 26. Anionic fluxes calculated with Equation 5, using the $I_{initial}$ values from Control (B1/P1 - nCa), µCa Test (B1/P2) and mCa Test (B1/P3) experimental conditions, expected at different V_m, and the average oscillatory efflux observed at the tip of *Lilium longiflorum* growing pollen tubes.

	Average Calculated Anionic Fluxes (pmol cm^{-2} s^{-1})					
	r = 10 µm			**r = 3 µm**		
Vm (mV)	**nCa**	**µCa**	**mCa**	**nCa**	**µCa**	**mCa**
-179.9	829 ± 212	1543 ± 123	1014 ± 244	9215 ± 2357	17140 ± 1370	11264 ± 2712
-159.9	790 ± 202	1468 ± 116	966 ± 229	8783 ± 2241	16310 ± 1294	10736 ± 2539
-139.9	753 ± 191	1392 ± 109	923 ± 215	8363 ± 2127	15463 ± 1215	10251 ± 2387
-119.9	711 ± 180	1315 ± 102	876 ± 201	7895 ± 1999	14607 ± 1132	9735 ± 2229
-99.9	662 ± 167	1226 ± 94	823 ± 186	7351 ± 1853	13626 ± 1042	9148 ± 2068
-79.9	603 ± 151	1117 ± 84	760 ± 168	6698 ± 1676	12417 ± 936	8442 ± 1871
-59.9	521 ± 129	972 ± 72	665 ± 144	5788 ± 1439	10796 ± 801	7394 ± 1596
-39.9	405 ±100	764 ± 57	528 ± 109	4502 ± 1110	8487 ± 629	5868 ± 1206

Average observed oscillatory efflux at the tip of growing pollen tubes from *Lilium longiflorum*:
50 to 8000 pmol s^{-1} cm^{-2}

The currents reported here were measured from protoplasts of hydrated pollen grains, before the onset of germination. These results, together with the single channel currents recently measured by our group, in *Lilium longiflorum*, under the same experimental conditions (Tavares *et al.*, 2011a) demonstrate the existence of anionic fluxes across channels in the plasma membrane of ungerminated grains. Additionally, our group has also found anionic currents from germinated pollen from *Lilium longiflorum* which are most likely due to the same kind of putative channels (Tavares *et al.*, 2011a). Taken together with the similarity between the observed apical effluxes and the calculated fluxes, it is reasonable to

propose that the channels responsible for the anionic currents presented here, are also responsible for the observed Cl^- fluxes in growing pollen tubes.

Several anion channels have been reported in plasma membrane of plant cells. These have been associated with various processes in plants such as stomata closure, hormone signaling, membrane excitability, cellular osmoregulation, growth regulation and anionic nutrition (as reviewed in Barbier-Brygoo *et al.*, 2000; De Angeli *et al.*, 2007; Roberts, 2006; Tavares *et al.*, 2011b). Most of the described anion channels are inward rectifiers (channels through which the exit of anions from the cell is greater than its entrance). Some outward rectifiers have been detected in root cells and were suggested to be involved in repolarization of the membrane potential after sodium uptake by roots in saline soils. The anionic selectivity of the channels found in plant membranes to NO_3^- and Cl^-, as well as their pharmacology and regulation, varies according to species and cell type (Table 1 in Introduction, page 36).

The currents described here share some similarities with the few outwardly rectifying depolarization-activated anion channels (ORAC) already described in plants. Nevertheless, the kinetic properties of the currents studied here are distinctive from the others. The ORAC found in protoplasts derived from wheat root has a significantly faster activation kinetics, activating in less than 100 msec (Skerrett and Tyerman, 1994). The outwardly rectifying channels in roots of *L. albus* display a slower kinetics (seconds) which is dependent on the holding potential (Zhang *et al.*, 2004a). The currents presented here, both from Arabidopsis and from Lilium protoplasts, are not dependent on the holding potential (-100, 0 and +100 mV, data not shown). The ORAC so far described are believed to be involved in stabilization of the plasma membrane voltage in different ionic environments, namely in the uptake of Cl^- in high salinity conditions, in order to maintain a negative membrane potential after the influx of Na^+; or in the adaptation to phosphorus deficiency.

The channels that present the greatest similarity with the currents presented here are the animal TMEM16A (Ca^{2+} regulation, inhibition by NPPB, more permeable to NO_3^- that to Cl^-, multiple current components, a strong outward rectification, a time dependent, depolarization induced activation, and a time dependent, hyperpolarization induced deactivation). Unfortunately it was not possible to ascertain whether this was the case or not. The other most probable candidates are the SLAH2 and SLAH3, mainly because of

the similarities between the osmotic regulation known to occur in guard cells and in growing pollen tubes. Since these channels have yet to be electrophysiologically characterized, a functional comparison is impossible.

Due to its fast growth rate, pollen tubes must have a tight control on the flow of water. It has already been established that growing pollen tubes possess strong ionic fluxes and that these are essential for the growing process. It is possible to establish a parallel between what is known about turgor regulation in guard cells, and events that take place during pollen tube growth. As in stomata closing, the pollen tube tips present a tremendous efflux of Cl^- and K^+, an influx of Ca^{2+}, an elevation of $[Ca^{2+}]_{in}$, and a probable depolarization of the plasma membrane (Holdaway-Clarke *et al.*, 1997; Michard *et al.*, 2008; Zonia *et al.*, 2002). It is therefore reasonable to hypothesize that water flows out of the pollen tube at the tip following the osmotic potential from Cl^-. A similar parallel can be constructed with the events leading to the stomata opening. It has been established recently that, during rehydration, pollen grains' plasma membrane hyperpolarise, this event is accompanied by an acidification of the extracellular medium and is blocked by vanadate, indicating the involvement of the plasma membrane H^+ ATPase, which is modulated by 14-3-3 proteins (Breygina *et al.*, 2009b; Pertl *et al.*, 2010). In the growing pollen tube, the plasma membrane is hyperpolarized at the shank, where influxes of Cl^- and K^+ were found (Zonia *et al.*, 2002; Feijó JA, personal communication; Konrad K, personal communication). This, as in guard cells, may indicate the point of influx of water, this time driven initially by K^+, with the anions entering the cell to balance the positive charges (Figure 35).

Figure 35 represents the schematic hypothetical parallel between the events leading to stomata aperture regulation and the growing of the pollen tube. In this proposed model, the events leading to entrance and exit of water, which in the guard cells are separated in time, are in the pollen tube separated in space, with water entering in the tube shank and exiting at the tip.

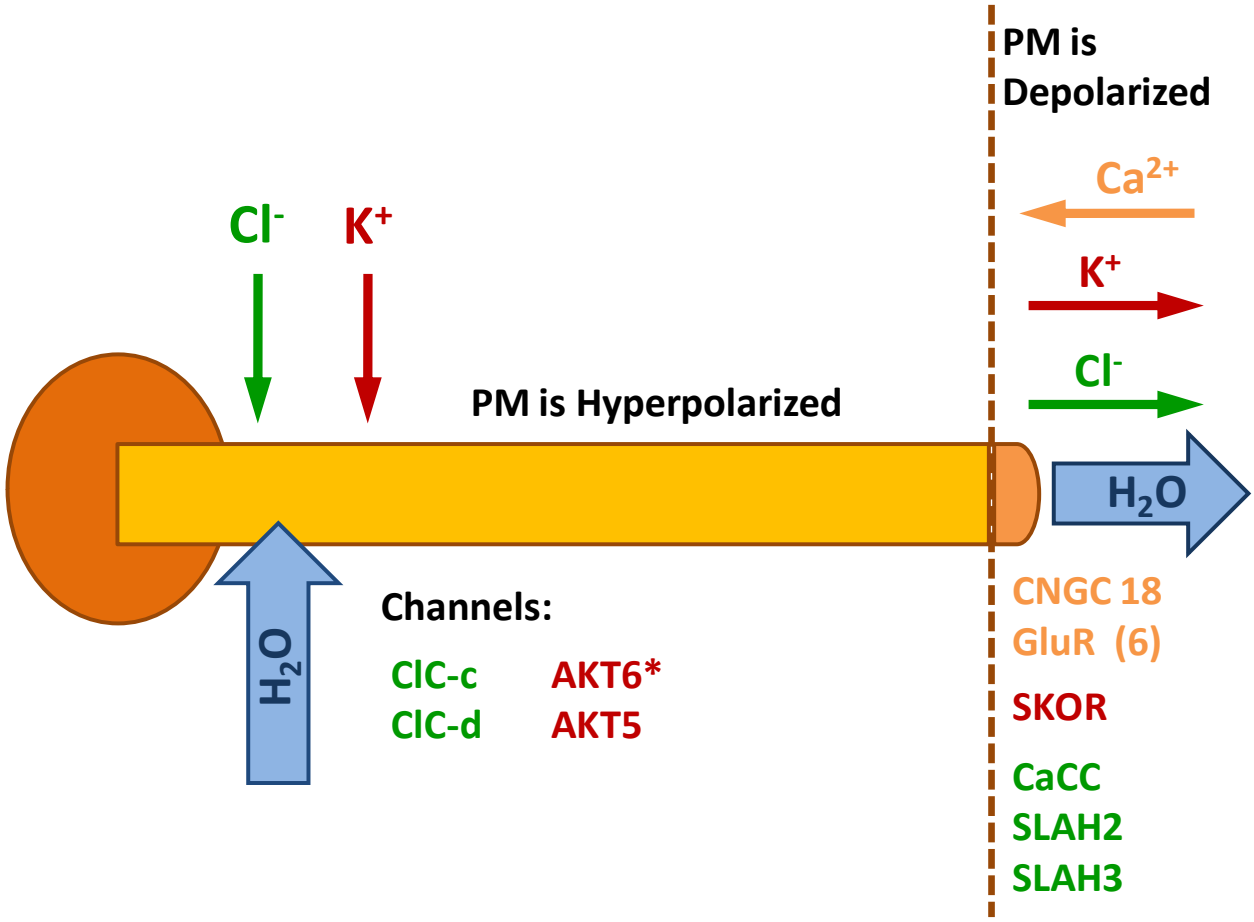

Figure 35. Schematic hypothetical parallel between the events leading to stomata aperture regulation and the growing of the pollen tube. Green arrows indicate Cl^- fluxes, red arrows indicate K^+ fluxes, orange arrow indicates Ca^{2+} influx, and blue arrows indicate water movements. The channels indicated are known to be transcribed in pollen and, taken with the data known from the Guard Cell Model, could be responsible for the observed fluxes. AKT6 is specifically transcribed in pollen and CNGC18 has been implicated in pollen tube growth. Of the GluR (glutamate receptor) and CNGC genes known in Arabidopsis, 6 elements of each family are transcribed in pollen (CNGC7 to 10, 16, and 18; AtGLR2.1, AtGLR1.3, AtGLR3.5, AtGLR3.7, AtGLR2.4, and AtGLR1.2). SKOR - stellar K^+ outward rectifying channel like GORK. SLAH – SLAC1 homolog. CaCC – homologue to the animal TEM16A channel. Although CLC-c and CLC-d have been localized in intracellular membranes, it has been shown that when co-transcribed with CPK34, CLC-c goes to the plasma membrane (Konrad, personal communication).

Overall the correspondence between the observed Cl^- fluxes and the calculated fluxes in Lilium, and the similarity between the anionic currents from pollen grains and from germinated pollen (Tavares *et al.*, 2011a), all indicate that the anionic currents described here have a significant physiological role.

7. Final remarks

Anion channels, sharing their main features, were functionally characterized, for the first time, in pollen grain protoplasts from *Arabidopsis thaliana* and *Lilium longiflorum*. These could be responsible for the observed chloride effluxes present at the tip of growing pollen tubes.

Despite the fact that the discovery of the molecular identity of the anionic channel or channels responsible for the currents found in pollen grain protoplasts from *Arabidopsis thaliana* was not achieved, the work reported here is of worth, for not only was a experimental protocol specifically tuned to study anionic currents in this difficult and interesting cellular system, but also a thorough first characterization of these currents was performed, both of which will facilitate future research in this area.

In the future, a major breakthrough will be the molecular identification of the channel or channels responsible for these currents. This will allow the localization of the protein and the correlation with other known cellular mechanisms such as the Cl^- fluxes already characterized.

Since the protocols for the isolation and characterization of these currents are already established, a more thorough portrayal of the intra and extracellular regulation of these currents will be possible.

8. Bibliography

Ache P, Bauer H, Kollist H, Al-Rasheid KA, Lautner S, Hartung W, Hedrich R. **2010**. Stomatal action directly feeds back on leaf turgor: new insights into the regulation of the plant water status from non-invasive pressure probe measurements. *Plant J* **62**, 1072-1082.

Ache P, Becker D, Ivashikina N, Dietrich P, Roelfsema MR, Hedrich R. **2000**. GORK, a delayed outward-rectifier expressed in guard cells of *Arabidopsis thaliana*, is a K^+-selective, K^+-sensing ion channel. *FEBS Lett* **486**, 93-98.

Alekov AK, Fahlke C. **2008**. Anion channels: regulation of ClC-3 by an orphan second messenger. *Current Biology* **18**, R1061-1064.

Amtmann A, Laurie S, Leigh R, Sanders D. **1997**. Multiple inward channels provide flexibility in Na^+/K^+ discrimination at the plasma membrane of barley suspension culture cells. *J Exp Bot* **48**, 481-497.

Artigas P, Gadsby DC. **2002**. Ion channel-like properties of the Na^+/K^+ Pump. *Ann N Y Acad Sci* **976**, 31-40.

Axon Instruments I. **1993**. *The Axon Guide for Electrophysiology & Biophysics Laboratory Techniques*. Foster City, USA: Axon Instruments, Inc.

Barbara JG, Stoeckel H, Takeda K. **1994**. Hyperpolarization-activated inward chloride current in protoplasts from suspension-cultured carrot cells. *Protoplasma* **180**, 136-144.

Barbier-Brygoo H, Vinauger M, Colcombet J, Ephritikhine G, Frachisse J, Maurel C. **2000**. Anion channels in higher plants: functional characterization, molecular structure and physiological role. *Biochimica Et Biophysica Acta* **1465**, 199-218.

Becker D, Geiger D, Dunkel M, Roller A, Bertl A, Latz A, Carpaneto A, Dietrich P, Roelfsema MRG, Voelker C, Schmidt D, Mueller-Roeber B, Czempinski K, Hedrich R. **2004**. AtTPK4, an Arabidopsis tandem-pore K^+ channel, poised to control the pollen membrane voltage in a pH- and Ca^{2+}-dependent manner. *Proc Natl Acad Sci U S A* **101**, 15621-15626.

Becker JD, Feijo JA. **2007**. How many genes are needed to make a pollen tube? Lessons from transcriptomics. *Ann Bot* **100**, 1117-1123.

Becq F. **1996**. Ionic channel rundown in excised membrane patches. *Biochimica Et Biophysica Acta* **1286**, 53-63.

Binder KA, Wegner LH, Heidecker M, Zimmermann U. **2003**. Gating of Cl^- currents in protoplasts from the marine alga *Valonia utricularis* depends on the transmembrane Cl^- gradient and is affected by enzymatic cell wall degradation. *J Membr Biol* **191**, 165-178.

Boavida LC, Becker JD, Feijo JA. **2005a**. The making of gametes in higher plants. *Int J Dev Biol* **49**, 595-614.

Boavida LC, Vieira AM, Becker JD, Feijo JA. **2005b**. Gametophyte interaction and sexual reproduction: how plants make a zygote. *Int J Dev Biol* **49**, 615-632.

Breygina MA, Matveeva NP, Ermakov IP. **2009a**. The role of Cl^- in pollen germination and tube growth. *Russian Journal of Developmental Biology* **39**, 157-164.

Breygina MA, Smirnova AV, Maslennikov MV, Matveeva NP, Yermakov IP. **2010**. Effects of anion channel blockers NPPB and DIDS on tobacco pollen tube growth and its mitochondria state. *Tsitologiia* **52**, 334-341.

Breygina MA, Smirnova AV, Matveeva NP, Ermakov IP. **2009b**. Membrane potential changes during pollen germination and tube growth. *Tsitologiia* **51**, 815-823.

Brownlee C. **1987**. Microelectrode techniques and plant cells. In: Standen NB, Gray PTA, Whitaker MJ, eds. *Microelectrode Techniques - The Plymouth Workshop Handbook*. Cambridge, UK: The Company of Biologists Ld., 187 - 198.

Caputo A, Caci E, Ferrera L, Pedemonte N, Barsanti C, Sondo E, Pfeffer U, Ravazzolo R, Zegarra-Moran O, Galietta LJ. **2008**. TMEM16A, a membrane protein associated with calcium-dependent chloride channel activity. *Science* **322**, 590-594.

Carew MA, Yang X, Schultz C, Shears SB. **2000**. *myo*-Inositol 3,4,5,6-tetra*kis*phosphate inhibits an apical calcium-activated chloride conductance in polarized monolayers of a cystic fibrosis cell line. *J Biol Chem* **275**, 26906-26913.

Cenis JL. **1992**. Rapid extraction of fungal DNA for PCR amplification. *Nucleic Acids Research* **20**, 2380.

Cerana R, Colombo R. **1992**. K^+ and Cl^- conductance of *Arabidopsis thaliana* plasma membrane at depolarised voltages. *Botanica Acta* **105**, 273-277.

Certal AC, Almeida RB, Carvalho LM, Wong E, Moreno N, Michard E, Carneiro J, Rodriguez-Leon J, Wu HM, Cheung AY, Feijo JA. **2008**. Exclusion of a proton ATPase from the apical membrane is associated with cell polarity and tip growth in *Nicotiana tabacum* pollen tubes. *Plant Cell* **20**, 614-634.

Chen ZH, Hills A, Lim CK, Blatt MR. **2010**. Dynamic regulation of guard cell anion channels by cytosolic free Ca^{2+} concentration and protein phosphorylation. *Plant J* **61**, 816-825.

Cho MH, Spalding EP. **1996**. An anion channel in Arabidopsis hypocotyls activated by blue light. *Proc Natl Acad Sci U S A* **93**, 8134-8138.

Colmenero-Flores JM, Martinez G, Gamba G, Vazquez N, Iglesias DJ, Brumos J, Talon M. **2007**. Identification and functional characterization of cation-chloride cotransporters in plants. *Plant J* **50**, 278-292.

Cosgrove DJ, Hedrich R. **1991**. Stretch-activated Chloride, Potassium, and Calcium channels coexisting in plasma membranes of guard-cells of *Vicia faba* L. *Planta* **186**, 143-153.

Daxinger L, Hunter B, Sheikh M, Jauvion V, Gasciolli V, Vaucheret H, Matzke M, Furner I. **2008**. Unexpected silencing effects from T-DNA tags in Arabidopsis. *Trends in Plant Science* **13**, 4-6.

De Angeli A, Monachello D, Ephritikhine G, Frachisse JM, Thomine S, Gambale F, Barbier-Brygoo H. **2006**. The nitrate/proton antiporter AtCLCa mediates nitrate accumulation in plant vacuoles. *Nature* **442**, 939-942.

De Angeli A, Thomine S, Frachisse J-M, Ephritikhine G, Gambale F, Barbier-Brygoo H. **2007**. Anion channels and transporters in plant cell membranes. *FEBS Lett* **581**, 2367–2374.

Diatloff E, Roberts M, Sanders D, Roberts SK. **2004**. Characterization of anion channels in the plasma membrane of Arabidopsis epidermal root cells and the identification of a citrate-permeable channel induced by phosphate starvation. *Plant Physiol* **136**, 4136-4149.

Dietrich P, Hedrich R. **1998**. Anions permeate and gate GCAC1, a voltage-dependent guard cell anion channel. *The Plant Journal* **15**, 479–487.

Dieudonne S, Forero ME, Llano I. **1997**. Two different conductances contribute to the anion currents in *Coffea arabica* protoplasts. *J Membr Biol* **159**, 83-94.

Duran C, Thompson CH, Xiao Q, Hartzell HC. **2010**. Chloride channels: often enigmatic, rarely predictable. *Annu Rev Physiol* **72**, 95-121.

Dutta R, Robinson KR. **2004**. Identification and characterization of stretch-activated ion channels in pollen protoplasts. *Plant Physiol* **135**, 1398-1406.

Edwards K, Johnstone C, Thompson C. **1991**. A simple and rapid method for the preparation of plant genomic DNA for PCR analysis. *Nucleic Acids Research* **19**, 1349.

Elzenga J, Van Volkenburgh E. **1997a**. Characterization of a light-controlled anion channel in the plasma membrane of mesophyll cells of pea. *Plant Physiol* **113**, 1419-1426.

Elzenga JT, Van volkenburgh E. **1997b**. Kinetics of Ca^{2+}- and ATP-dependent, voltage-controlled anion conductance in the plasma membrane of mesophyll cells of *Pisum sativum*. *Planta* **201**, 415-423.

Fairley K, Laver D, Walker NA. **1991**. Whole-cell and single-channel currents across the plasmalemma of corn shoot suspension cells. *J Membr Biol* **121**, 11-22.

Falke LC, Edwards KL, Pickard BG, Misler S. **1988**. A stretch-activated anion channel in tobacco protoplasts. *FEBS Lett* **237**, 141-144.

Fan LM, Wang YF, Wang H, Wu WH. **2001**. *In vitro* Arabidopsis pollen germination and characterization of the inward potassium currents in Arabidopsis pollen grain protoplasts. *J Exp Bot* **52**, 1603-1614.

Fan LM, Wang YF, Wu WH. **2003**. Outward K^+ channels in *Brassica chinensis* pollen protoplasts are regulated by external and internal pH. *Protoplasma* **220**, 143-152.

Fan LM, Wu WH, Yang HY. **1999**. Identification and characterization of the inward K^+ channel in the plasma membrane of Brassica pollen protoplasts. *Plant and Cell Physiology* **40**, 859-865.

Feijo JA. **2010**. The mathematics of sexual attraction. *J Biol* **9**, 18.

Feijo JA, Malho R, Obermeyer G. **1995**. Ion Dynamics and Its Possible Role during in-Vitro Pollen Germination and Tube Growth. *Protoplasma* **187**, 155-167.

Feijo JA, Sainhas J, Hackett GR, Kunkel JG, Hepler PK. **1999**. Growing pollen tubes possess a constitutive alkaline band in the clear zone and a growth-dependent acidic tip. *Journal of Cell Biology* **144**, 483-496.

Feijo JA, Sainhas J, Holdaway-Clarke T, Cordeiro MS, Kunkel JG, Hepler PK. **2001**. Cellular oscillations and the regulation of growth: the pollen tube paradigm. *Bioessays* **23**, 86-94.

Forestier C, Bouteau F, Leonhardt N, Vavasseur A. **1998**. Pharmacological properties of slow anion currents in intact guard cells of Arabidopsis. Application of the discontinuous single-electrode voltage-clamp to different species. *Pflugers Arch* **436**, 920-927.

Frachisse JM, Colcombet J, Guern J, Barbier-Brygoo H. **2000**. Characterization of a nitrate-permeable channel able to mediate sustained anion efflux in hypocotyl cells from *Arabidopsis thaliana*. *Plant J* **21**, 361-371.

Frachisse JM, Thomine S, Colcombet J, Guern J, Barbier-Brygoo H. **1999**. Sulfate is both a substrate and an activator of the voltage-dependent anion channel of Arabidopsis hypocotyl cells. *Plant Physiol* **121**, 253-262.

Frelet-Barrand A, Kolukisaoglu HU, Plaza S, Ruffer M, Azevedo L, Hortensteiner S, Marinova K, Weder B, Schulz B, Klein M. **2008**. Comparative mutant analysis of Arabidopsis ABCC-type ABC transporters: AtMRP2 contributes to detoxification, vacuolar organic anion transport and chlorophyll degradation. *Plant and Cell Physiology* **49**, 557-569.

Frietsch S, Wang YF, Sladek C, Poulsen LR, Romanowsky SM, Schroeder JI, Harper JF. **2007**. A cyclic nucleotide-gated channel is essential for polarized tip growth of pollen. *Proc Natl Acad Sci U S A* **104**, 14531-14536.

Garrill A, Tyerman SD, Findlay GP. **1994**. Ion channels in the plasma membrane of protoplasts from the halophytic angiosperm *Zostera muelleri*. *J Membr Biol* **142**, 381-393.

Geiger D, Scherzer S, Mumm P, Marten I, Ache P, Matschi S, Liese A, Wellmann C, Al-Rasheid KA, Grill E, Romeis T, Hedrich R. **2010**. Guard cell anion channel SLAC1 is regulated by CDPK protein kinases with distinct Ca^{2+} affinities. *Proc Natl Acad Sci U S A* **107**, 8023-8028.

Geiger D, Scherzer S, Mumm P, Stange A, Marten I, Bauer H, Ache P, Matschi S, Liese A, Al-Rasheid KA, Romeis T, Hedrich R. **2009**. Activity of guard cell anion channel SLAC1 is controlled by drought-stress signaling kinase-phosphatase pair. *Proc Natl Acad Sci U S A* **106**, 21425-21430.

Gobert A, Isayenkov S, Voelker C, Czempinski K, Maathuis FJ. **2007**. The two-pore channel TPK1 gene encodes the vacuolar K^+ conductance and plays a role in K^+ homeostasis. *Proc Natl Acad Sci U S A* **104**, 10726-10731.

Gogelein H. **1988**. Chloride channels in epithelia. *Biochimica Et Biophysica Acta* **947**, 521-547.

Grabov A, Leung J, Giraudat J, Blatt MR. **1997**. Alteration of anion channel kinetics in wild-type and abi1-1 transgenic *Nicotiana benthamiana* guard cells by abscisic acid. *Plant J* **12**, 203-213.

Griessner M, Obermeyer G. **2003**. Characterization of whole-cell K^+ currents across the plasma membrane of pollen grain and tube protoplasts of *Lilium longiflorum*. *Journal of Membrane Biology* **193**, 99-108.

Gu Y, Fu Y, Dowd P, Li SD, Vernoud V, Gilroy S, Yang ZB. **2005**. A Rho family GTPase controls actin dynamics and tip growth via two counteracting downstream pathways in pollen tubes. *Journal of Cell Biology* **169**, 127-138.

Halliwell JV, Plant TD, Standen NB. **1987**. Voltage clamp techniques. In: Standen NB, Gray PTA, Whitaker MJ, eds. *Microelectrode Techniques - The Plymouth Workshop Handbook*. Cambridge, UK: The Company of Biologists, Ld, 13 - 28.

Hamilton DW, Hills A, Kohler B, Blatt MR. **2000**. Ca^{2+} channels at the plasma membrane of stomatal guard cells are activated by hyperpolarization and abscisic acid. *Proc Natl Acad Sci U S A* **97**, 4967-4972.

Harada H, Kuromori T, Hirayama T, Shinozaki K, Leigh RA. **2004**. Quantitative trait loci analysis of nitrate storage in Arabidopsis leading to an investigation of the contribution of the anion channel gene, AtCLC-c, to variation in nitrate levels. *J Exp Bot* **55**, 2005-2014.

Haswell ES, Peyronnet R, Barbier-Brygoo H, Meyerowitz EM, Frachisse JM. **2008**. Two MscS homologs provide mechanosensitive channel activities in the Arabidopsis root. *Current Biology* **18**, 730-734.

Hechenberger M, Schwappach B, Fischer WN, Frommer WB, Jentsch TJ, Steinmeyer K. **1996**. A family of putative chloride channels from Arabidopsis and functional complementation of a yeast strain with a CLC gene disruption. *J Biol Chem* **271**, 33632-33638.

Hedrich R. **1995**. Thechical approaches to studying specific properties of ion channels in plants. In: Sakmann B, Neher E, eds. *Single-Channel Recording*. New York, USA: Springer, 277 - 306.

Hedrich R, Becker D. **1994**. Green circuits - the potential of plant specific ion channels. *Plant Molecular Biology* **26**, 1637-1650.

Hedrich R, Busch H, Raschke K. **1990**. Ca^{2+} and nucleotide dependent regulation of voltage dependent anion channels in the plasma membrane of guard cells. *Embo Journal* **9**, 3889-3892.

Hedrich R, Marten I. **1993**. Malate-induced feedback regulation of plasma membrane anion channels could provide a CO_2 sensor to guard cells. *Embo Journal* **12**, 897-901.

Hedrich R, Marten I, Lohse G, Dietrich P, Winter H, Lohaus G, Heldt HW. **1994**. Malate-sensitive anion channels enable guard-cells to sense changes in the ambient CO_2 concentration. *Plant Journal* **6**, 741-748.

Heidecker M, Wegner LH, Zimmermann U. **1999**. A patch-clamp study of ion channels in protoplasts prepared from the marine alga *Valonia utricularis*. *J Membr Biol* **172**, 235-247.

Helling D, Possart A, Cottier S, Klahre U, Kost B. **2006**. Pollen tube tip growth depends on plasma membrane polarization mediated by tobacco PLC3 activity and endocytic membrane recycling. *Plant Cell* **18**, 3519-3534.

Hoekenga OA, Maron LG, Pineros MA, Cancado GM, Shaff J, Kobayashi Y, Ryan PR, Dong B, Delhaize E, Sasaki T, Matsumoto H, Yamamoto Y, Koyama H, Kochian LV. **2006**.

AtALMT1, which encodes a malate transporter, is identified as one of several genes critical for aluminum tolerance in Arabidopsis. *Proc Natl Acad Sci U S A* **103**, 9738-9743.

Holdaway-Clarke TL, Feijo JA, Hackett GR, Kunkel JG, Hepler PK. **1997**. Pollen tube growth and the intracellular cytosolic calcium gradient oscillate in phase while extracellular calcium influx is delayed. *Plant Cell* **9**, 1999-2010.

Holdaway-Clarke TL, Hepler PK. **2003**. Control of pollen tube growth: role of ion gradients and fluxes. *New Phytologist* **159**, 539-563.

Hosy E, Vavasseur A, Mouline K, Dreyer I, Gaymard F, Poree F, Boucherez J, Lebaudy A, Bouchez D, Very AA, Simonneau T, Thibaud JB, Sentenac H. **2003**. The Arabidopsis outward K^+ channel GORK is involved in regulation of stomatal movements and plant transpiration. *Proc Natl Acad Sci U S A* **100**, 5549-5554.

Hwang JU, Gu Y, Lee YJ, Yang ZB. **2005**. Oscillatory ROP GTPase activation leads the oscillatory polarized growth of pollen tubes. *Molecular Biology of the Cell* **16**, 5385-5399.

Jentsch TJ. **2008**. CLC chloride channels and transporters: from genes to protein structure, pathology and physiology. *Crit Rev Biochem Mol Biol* **43**, 3-36.

Katz B, Miledi R. **1970**. Membrane noise produced by acetylcholine. *Nature* **226**, 962-963.

Katz B, Miledi R. **1971**. Further observations on acetylcholine noise. *Nat New Biol* **232**, 124-126.

Keller BU, Hedrich R, Raschke K. **1989**. Voltage-dependent anion channels in the plasma membrane of guard cells. *Nature* **341**, 450-453.

Kollmeier M, Dietrich P, Bauer CS, Horst WJ, Hedrich R. **2001**. Aluminium activates a citrate-permeable anion channel in the aluminium-sensitive zone of the maize root apex. A comparison between an aluminium-sensitive and an aluminium-resistant cultivar. *Plant Physiol* **126**, 397-410.

Kourie JI. **1994**. Transient Cl^- and K^+ currents during the action potential in *Chara inflata* (effects of external sorbitol, cations, and ion channel blockers). *Plant Physiol* **106**, 651-660.

Kovermann P, Meyer S, Hortensteiner S, Picco C, Scholz-Starke J, Ravera S, Lee Y, Martinoia E. **2007**. The Arabidopsis vacuolar malate channel is a member of the ALMT family. *Plant J* **52**, 1169-1180.

Kunkel JG, Lin LY, Prado AM, Feijo J, Hwang PP, Hepler PK. **2001**. The strategic use of good buffers to measure proton gradients about growing pollen tubes. *In "Cell Biology of Plant and Fungal Tip Growth" (A. Geitman, Ed.), pp. 14pp. IOS Press, Amsterdam.*

Kwak JM, Mori IC, Pei ZM, Leonhardt N, Torres MA, Dangl JL, Bloom RE, Bodde S, Jones JD, Schroeder JI. **2003**. NADPH oxidase AtrbohD and AtrbohF genes function in ROS-dependent ABA signaling in Arabidopsis. *Embo Journal* **22**, 2623-2633.

Kwak JM, Murata Y, Baizabal-Aguirre VM, Merrill J, Wang M, Kemper A, Hawke SD, Tallman G, Schroeder JI. **2001**. Dominant negative guard cell K^+ channel mutants reduce inward-rectifying K^+ currents and light-induced stomatal opening in Arabidopsis. *Plant Physiol* **127**, 473-485.

Lee SC, Lan W, Buchanan BB, Luan S. **2009**. A protein kinase-phosphatase pair interacts with an ion channel to regulate ABA signaling in plant guard cells. *Proc Natl Acad Sci U S A* **106**, 21419-21424.

Lew RR. **1991**. Substrate regulation of single potassium and chloride ion channels in Arabidopsis plasma membrane. *Plant Physiol* **95**, 642-647.

Linder B, Raschke K. **1992**. A slow anion channel in guard-cells, activating at large hyperpolarization, may be principal for stomatal closing. *FEBS Lett* **313**, 27-30.

Lu Y, Chanroj S, Zulkifli L, Johnson MA, Uozumi N, Cheung A, Sze H. **2011**. Pollen Tubes Lacking a Pair of K+ Transporters Fail to Target Ovules in Arabidopsis. *Plant Cell* **11**, 677-690.

Lv Q-d, Tang R-j, Liu H, Gao X-s, Li Y-z, Zheng H-q, Zhang H-x. **2009**. Cloning and molecular analyses of the *Arabidopsis thaliana* chloride channel gene family. *Plant Science* **176**, 650-651.

Malho R, Liu Q, Monteiro D, Rato C, Camacho L, Dinis A. **2006**. Signalling pathways in pollen germination and tube growth. *Protoplasma* **228**, 21-30.

Malho R, Read ND, Trewavas AJ, Pais MS. **1995**. Calcium channel activity during pollen tube growth and reorientation. *Plant Cell* **7**, 1173-1184.

Marmagne A, Vinauger-Douard M, Monachello D, de Longevialle AF, Charon C, Allot M, Rappaport F, Wollman FA, Barbier-Brygoo H, Ephritikhine G. **2007**. Two members of the Arabidopsis CLC (chloride channel) family, AtCLCe and AtCLCf, are associated with thylakoid and Golgi membranes, respectively. *J Exp Bot* **58**, 3385-3393.

Marten I, Hoth S, Deeken R, Ache P, Ketchum KA, Hoshi T, Hedrich R. **1999**. AKT3, a phloem-localized K^+ channel, is blocked by protons. *Proc Natl Acad Sci U S A* **96**, 7581-7586.

Marten I, Lohse G, Hedrich R. **1991**. Plant growth hormones control voltage-dependent activity of anion channels in plasma membrane of guard cells. *Nature* **353**, 758 - 762.

Marty A, Neher E. **1995**. Tight-seal whole-cell recording. In: Sakmann B, Neher E, eds. *Single Channel Recording*. New York: Plenum, 31-52.

Matveyeva NP, Andreyuk DS, Yermakov IP. **2003**. Transport of Cl^- across the plasma membrane during pollen grain germination in tobacco. *Biochemistry-Moscow* **68**, 1247-1251.

Messerli MA, Creton R, Jaffe LF, Robinson KR. **2000**. Periodic increases in elongation rate precede increases in cytosolic Ca^{2+} during pollen tube growth. *Developmental Biology* **222**, 84-98.

Messerli MA, Danuser G, Robinson KR. **1999**. Pulsatile influxes of H^+, K^+ and Ca^{2+} lag growth pulses of *Lilium longiflorum* pollen tubes. *Journal of Cell Science* **112 (Pt 10)**, 1497-1509.

Messerli MA, Smith PJS, Lewis RC, Robinson KR. **2004**. Chloride fluxes in lily pollen tubes: a critical re-evaluation. *Plant Journal* **40**, 799-812.

Meyer S, Mumm P, Imes D, Endler A, Weder B, Al-Rasheid KA, Geiger D, Marten I, Martionia E, Hedrich R. **2010**. AtALMT12 represents an R-type anion channel required for stomatal movement in Arabidopsis guard cells. *Plant J*.

Michard E, Alves F, Feijo JA. **2009**. The role of ion fluxes in polarized cell growth and morphogenesis: the pollen tube as an experimental paradigm. *Int J Dev Biol* **53**, 1609-1622.

Michard E, Dias P, Feijo JA. **2008**. Tobacco pollen tubes as cellular models for ion dynamics: improved spatial and temporal resolution of extracellular flux and free cytosolic concentration of calcium and protons using pHluorin and YC3.1 CaMeleon. *Sexual Plant Reproduction* **21**, 169-181.

Miller DD, Callaham DA, Gross DJ, Hepler PK. **1992**. Free Ca^{2+} Gradient in Growing Pollen Tubes of Lilium. *Journal of Cell Science* **101**, 7-12.

Mindell JA, Maduke M. **2001**. ClC chloride channels. *Genome Biology* **2**, REVIEWS3003.

Mitchell J, Wang X, Zhang G, Gentzsch M, Nelson DJ, Shears SB. **2008**. An expanded biological repertoire for Ins(3,4,5,6)P4 through its modulation of ClC-3 function. *Current Biology* **18**, 1600-1605.

Mlotshwa S, Pruss GJ, Gao Z, Mgutshini NL, Li J, Chen X, Bowman LH, Vance V. **2010**. Transcriptional silencing induced by Arabidopsis T-DNA mutants is associated with 35S promoter siRNAs and requires genes involved in siRNA-mediated chromatin silencing. *Plant J* **64**, 699-704.

Monachello D, Allot M, Oliva S, Krapp A, Daniel-Vedele F, Barbier-Brygoo H, Ephritikhine G. **2009**. Two anion transporters AtClCa and AtClCe fulfil interconnecting but not redundant roles in nitrate assimilation pathways. *New Phytol* **183**, 88-94.

Mori IC, Murata Y, Yang Y, Munemasa S, Wang YF, Andreoli S, Tiriac H, Alonso JM, Harper JF, Ecker JR, Kwak JM, Schroeder JI. **2006**. CDPKs CPK6 and CPK3 function in ABA regulation of guard cell S-type anion- and Ca^{2+}-permeable channels and stomatal closure. *Plos Biology* **4**, e327.

Mouline K, Very AA, Gaymard F, Boucherez J, Pilot G, Devic M, Bouchez D, Thibaud JB, Sentenac H. **2002**. Pollen tube development and competitive ability are impaired by disruption of a Shaker K^+ channel in Arabidopsis. *Genes & Development* **16**, 339-350.

Neher E, Sakmann B. **1976**. Single-channel currents recorded from membrane of denervated frog muscle fibres. *Nature* **260**, 799-802.

Niemeyer MI, Cid LP, Yusef YR, Briones R, Sepulveda FV. **2009**. Voltage-dependent and -independent titration of specific residues accounts for complex gating of a ClC chloride channel by extracellular protons. *J Physiol* **587**, 1387-1400.

Obermeyer G, Blatt MR. **1995**. Electrical properties of intact pollen grains of *Lilium longiflorum*: characteristics of the non-germinating pollen grain. *J Exp Bot* **46**, 803-813.

Obermeyer G, Kolb HA. **1993**. K^+ channels in the plasma membrane of lily pollen protoplasts. *Botanica Acta* **106**, 26-31.

Obermeyer G, Weisenseel MH. **1991**. Calcium channel blocker and calmodulin antagonists affect the gradient of free calcium ions in lily pollen tubes. *European Journal of Cell Biology* **56**, 319-327.

Padmanaban S, Chanroj S, Kwak JM, Li X, Ward JM, Sze H. **2007**. Participation of endomembrane cation/H^+ exchanger AtCHX20 in osmoregulation of guard cells. *Plant Physiol* **144**, 82-93.

Parton RM, Fischer-Parton S, Trewavas AJ, Watahiki MK. **2003**. Pollen tubes exhibit regular periodic membrane trafficking events in the absence of apical extension. *Journal of Cell Science* **116**, 2707-2719.

Pei ZM, Murata Y, Benning G, Thomine S, Klusener B, Allen GJ, Grill E, Schroeder JI. **2000**. Calcium channels activated by hydrogen peroxide mediate abscisic acid signalling in guard cells. *Nature* **406**, 731-734.

Pei ZM, Ward JM, Harper JF, Schroeder JI. **1996**. A novel chloride channel in *Vicia faba* guard cell vacuoles activated by the serine/threonine kinase, CDPK. *Embo Journal* **15**, 6564-6574.

Peiter E, Maathuis FJ, Mills LN, Knight H, Pelloux J, Hetherington AM, Sanders D. **2005**. The vacuolar Ca^{2+}-activated channel TPC1 regulates germination and stomatal movement. *Nature* **434**, 404-408.

Penner R. **1995**. A practical guide to patch clamping. In: Sakmann B, Neher E, eds. *Single-Channel Recording*. New York, USA: Springer, 3-30.

Pertl H, Pockl M, Blaschke C, Obermeyer G. **2010**. Osmoregulation in Lilium pollen grains occurs via modulation of the plasma membrane H^+-ATPase activity by 14-3-3 proteins. *Plant Physiol*.

Peyronnet R, Haswell ES, Barbier-Brygoo H, Frachisse JM. **2008**. AtMSL9 and AtMSL10: Sensors of plasma membrane tension in Arabidopsis roots. *Plant Signal Behav* **3**, 726-729.

Pierson ES, Miller DD, Callaham DA, Shipley AM, Rivers BA, Cresti M, Hepler PK. **1994**. Pollen tube growth is coupled to the extracellular calcium ion flux and the intracellular calcium gradient: effect of BAPTA-type buffers and hypertonic media. *Plant Cell* **6**, 1815-1828.

Pierson ES, Miller DD, Callaham DA, van Aken J, Hackett G, Hepler PK. **1996**. Tip-localized calcium entry fluctuates during pollen tube growth. *Developmental Biology* **174**, 160-173.

Pina C, Pinto F, Feijo JA, Becker JD. **2005**. Gene family analysis of the Arabidopsis pollen transcriptome reveals biological implications for cell growth, division control, and gene expression regulation. *Plant Physiol* **138**, 744-756.

Pineros MA, Kochian LV. **2001**. A patch-clamp study on the physiology of aluminum toxicity and aluminum tolerance in maize. Identification and characterization of Al^{3+}-induced anion channels. *Plant Physiol* **125**, 292-305.

Qi Z, Kishigami A, Nakagawa Y, Iida H, Sokabe M. **2004**. A mechanosensitive anion channel in *Arabidopsis thaliana* mesophyll cells. *Plant and Cell Physiology* **45**, 1704-1708.

Qu HY, Shang ZL, Zhang SL, Liu LM, Wu JY. **2007**. Identification of hyperpolarization-activated calcium channels in apical pollen tubes of *Pyrus pyrifolia*. *New Phytol* **174**, 524-536.

Raichaudhuri A, Peng M, Naponelli V, Chen S, Sanchez-Fernandez R, Gu H, Gregory JF, 3rd, Hanson AD, Rea PA. **2009**. Plant vacuolar ATP-binding cassette transporters that translocate folates and antifolates in vitro and contribute to antifolate tolerance *in vivo*. *J Biol Chem* **284**, 8449-8460.

Rathore KS, Cork RJ, Robinson KR. **1991**. A cytoplasmic gradient of Ca^{2+} is correlated with the growth of Lily pollen tubes. *Developmental Biology* **148**, 612-619.

Rato C, Monteiro D, Hepler PK, Malho R. **2004**. Calmodulin activity and cAMP signalling modulate growth and apical secretion in pollen tubes. *Plant Journal* **38**, 887-897.

Rea PA. **2007**. Plant ATP-binding cassette transporters. *Annual Review of Plant Biology* **58**, 347-375.

Reiss HD, Herth W. **1985**. Nifedipine-sensitive calcium channels are involved in polar growth of Lily pollen tubes. *Journal of Cell Science* **76**, 247-254.

Roberts SK. **2006**. Plasma membrane anion channels in higher plants and their putative functions in roots. *New Phytologist* **169**, 647-666.

Robertson WR, Clark K, Young JC, Sussman MR. **2004**. An *Arabidopsis thaliana* plasma membrane proton pump is essential for pollen development. *Genetics* **168**, 1677-1687.

Roelfsema MR, Levchenko V, Hedrich R. **2004**. ABA depolarizes guard cells in intact plants, through a transient activation of R- and S-type anion channels. *Plant J* **37**, 578-588.

Roelfsema MRG, Staal M, Prins HBA. **1998**. Blue light-induced apoplastic acidification of *Arabidopsis thaliana* guard cells: Inhibition by ABA is mediated through protein phosphatases. *Physiologia Plantarum* **103**, 466-474.

Roelfsema MRG, Steinmeyer R, Staal M, Hedrich R. **2001**. Single guard cell recordings in intact plants: light-induced hyperpolarization of the plasma membrane. *Plant Journal* **26**, 1-13.

Roy SJ, Holdaway-Clarke TL, Hackett GR, Kunkel JG, Lord EM, Hepler PK. **1999**. Uncoupling secretion and tip growth in lily pollen tubes: evidence for the role of calcium in exocytosis. *Plant J* **19**, 379-386.

Sanchez-Fernandez R, Davies TG, Coleman JO, Rea PA. **2001**. The *Arabidopsis thaliana* ABC protein superfamily, a complete inventory. *J Biol Chem* **276**, 30231-30244.

Schauf CL, Wilson KJ. **1987**. Properties of single K^+ and Cl^- channels in *Asclepias tuberosa* protoplasts. *Plant Physiol* **85**, 413-418.

Schiott M, Romanowsky SM, Baekgaard L, Jakobsen MK, Palmgren MG, Harper JF. **2004**. A plant plasma membrane Ca^{2+} pump is required for normal pollen tube growth and fertilization. *Proc Natl Acad Sci U S A* **101**, 9502-9507.

Schmidt C, Schelle I, Liao YJ, Schroeder JI. **1995**. Strong regulation of slow anion channels and abscisic acid signaling in guard-cells by phosphorylation and dephosphorylation events. *Proc Natl Acad Sci U S A* **92**, 9535-9539.

Schmidt C, Schroeder JI. **1994**. Anion selectivity of slow anion channels in the plasma membrane of guard-cells - Large nitrate permeability. *Plant Physiol* **106**, 383-391.

Schroeder BC, Cheng T, Jan YN, Jan LY. **2008**. Expression cloning of TMEM16A as a calcium-activated chloride channel subunit. *Cell* **134**, 1019-1029.

Schroeder JI, Keller BU. **1992**. Two types of anion channel currents in guard-cells with distinct voltage regulation. *Proc Natl Acad Sci U S A* **89**, 5025-5029.

Schulz-Lessdorf B, Lohse G, Hedrich R. **1996**. GCAC1 recognizes the pH gradient across the plasma membrane: a pH-sensitive and ATP-dependent anion channel links guard cell membrane potential to acid and energy metabolism. *The Plant Journal* **10**, 993–1004.

Shang ZL, Ma LG, Zhang HL, He RR, Wang XC, Cui SJ, Sun DY. **2005**. Ca^{2+} influx into lily pollen grains through a hyperpolarization-activated Ca^{2+}-permeable channel which can be regulated by extracellular CaM. *Plant and Cell Physiology* **46**, 598-608.

Siegel R, Xue S, Murata Y, Yang Y, Nishimura N, Wang A, Schroeder J. **2009**. Calcium elevation-dependent and attenuated resting calcium-dependent abscisic acid induction of stomatal closure and abscisic acid-induced enhancement of calcium sensitivities of S-type anion and inward-rectifying K^+ channels in Arabidopsis guard cells. *Plant J* **59**, 207-220.

Sirichandra C, Wasilewska A, Vlad F, Valon C, Leung J. **2009**. The guard cell as a single-cell model towards understanding drought tolerance and abscisic acid action. *J Exp Bot* **60**, 1439-1463.

Skerrett M, Tyerman SD. **1994**. A channel that allows inwardly directed fluxes of anions in protoplasts derived from wheat roots. *Planta*, 295-305.

Song LF, Zou JJ, Zhang WZ, Wu WH, Wang Y. **2009**. Ion transporters involved in pollen germination and pollen tube tip-growth. *Plant Signal Behav* **4**, 1193-1195.

Sottocornola B, Visconti S, Orsi S, Gazzarrini S, Giacometti S, Olivari C, Camoni L, Aducci P, Marra M, Abenavoli A, Thiel G, Moroni A. **2006**. The potassium channel KAT1 is activated by plant and animal 14-3-3 proteins. *J Biol Chem* **281**, 35735-35741.

Sze H, Padmanaban S, Cellier F, Honys D, Cheng NH, Bock KW, Conejero G, Li XY, Twell D, Ward JM, Hirschi KD. **2004**. Expression patterns of a novel AtCHX gene family highlight potential roles in osmotic adjustment and K^+ homeostasis in pollen development. *Plant Physiol* **136**, 2532-2547.

Tanaka I, Kitazume C, Ito M. **1987**. The isolation and culture of Lily pollen protoplasts. *Plant Science* **50**, 205-211.

Tavares B, Dias PN, Domingos P, Moura T, Feijó JA, Bicho A. **2011a**. Calcium Regulated Anion Channels from Pollen of Lilium longiflorum. *New Phytologist*, Provisionally rejected with resubmission encouraged in 22 Oct 2010. Resubmitted 2018 Feb 2011.

Tavares B, Domingos P, Dias PN, Feijó JA, Bicho A. **2011b**. The essential role of anionic transport in plant cells - the pollen tube as a case study. *J Exp Bot*, doi:10.1093/jxb/err1036.

Taylor AR, Brownlee C. **2003**. A novel Cl^- inward-rectifying current in the plasma membrane of the calcifying marine phytoplankton *Coccolithus pelagicus*. *Plant Physiol* **131**, 1391-1400.

Terry BR, Tyerman SD, Findlay GP. **1991**. Ion channels in the plasma membrane of Amaranthus protoplasts: one cation and one anion channel dominate the conductance. *J Membr Biol* **121**, 223-236.

Thomine S, Guern J, Barbier-Brygoo H. **1997**. Voltage-dependent anion channel of Arabidopsis hypocotyls: nucleotide regulation and pharmacological properties. *J Membr Biol* **159**, 71-82.

Thomine S, Zimmermann S, Guern J, Barbier-Brygoo H. **1995**. ATP-dependent regulation of an anion channel at the plasma membrane of protoplasts from epidermal cells of Arabidopsis hypocotyls. *Plant Cell* **7**, 2091-2100.

Vahisalu T, Kollist H, Wang YF, Nishimura N, Chan WY, Valerio G, Lamminmaki A, Brosche M, Moldau H, Desikan R, Schroeder JI, Kangasjarvi J. **2008**. SLAC1 is required for plant guard cell S-type anion channel function in stomatal signalling. *Nature* **452**, 487-491.

Vahisalu T, Puzorjova I, Brosche M, Valk E, Lepiku M, Moldau H, Pechter P, Wang YS, Lindgren O, Salojarvi J, Loog M, Kangasjarvi J, Kollist H. **2010**. Ozone-triggered rapid stomatal response involves the production of reactive oxygen species, and is controlled by SLAC1 and OST1. *Plant J* **62**, 442-453.

Verrier PJ, Bird D, Burla B, Dassa E, Forestier C, Geisler M, Klein M, Kolukisaoglu U, Lee Y, Martinoia E, Murphy A, Rea PA, Samuels L, Schulz B, Spalding EJ, Yazaki K, Theodoulou FL. **2008**. Plant ABC proteins - a unified nomenclature and updated inventory. *Trends in Plant Science* **13**, 151-159.

von der Fecht-Bartenbach J, Bogner M, Dynowski M, Ludewig U. **2010**. CLC-b-mediated NO_3^-/H^+ exchange across the tonoplast of Arabidopsis vacuoles. *Plant and Cell Physiology* **51**, 960-968.

von der Fecht-Bartenbach J, Bogner M, Krebs M, Stierhof YD, Schumacher K, Ludewig U. **2007**. Function of the anion transporter AtCLC-d in the trans-Golgi network. *Plant J* **50**, 466-474.

Wang Y, Zhang WZ, Song LF, Zou JJ, Su Z, Wu WH. **2008**. Transcriptome analyses show changes in gene expression to accompany pollen germination and tube growth in Arabidopsis. *Plant Physiol* **148**, 1201-1211.

Wang YF, Fan LM, Zhang WZ, Zhang W, Wu WH. **2004**. Ca^{2+}-permeable channels in the plasma membrane of Arabidopsis pollen are regulated by actin microfilaments. *Plant Physiol* **136**, 3892-3904.

Ward JM, Maser P, Schroeder JI. **2009**. Plant ion channels: gene families, physiology, and functional genomics analyses. *Annu Rev Physiol* **71**, 59-82.

Ward JM, Schroeder JI. **1994**. Calcium-activated K^+ channels and calcium-induced calcium release by slow vacuolar ion channels in guard cell vacuoles implicated in the control of stomatal closure. *Plant Cell* **6**, 669-683.

Weisenseel MH, Jaffe LF. **1976**. Major growth current through Lily pollen tubes enters as K^+ and leaves as H^+. *Planta* **133**, 1-7.

Weisenseel MH, Nuccitelli R, Jaffe LF. **1975**. Large electrical currents traverse growing pollen tubes. *Journal of Cell Biology* **66**, 556-567.

White MM, Miller C. **1979**. A voltage-gated anion channel from the electric organ of *Torpedo californica*. *J Biol Chem* **254**, 10161-10166.

Wu Y, Xu X, Li S, Liu T, Ma L, Shang Z. **2007**. Heterotrimeric G-protein participation in Arabidopsis pollen germination through modulation of a plasma membrane hyperpolarization-activated Ca^{2+}-permeable channel. *New Phytol* **176**, 550-559.

Yang YD, Cho H, Koo JY, Tak MH, Cho Y, Shim WS, Park SP, Lee J, Lee B, Kim BM, Raouf R, Shin YK, Oh U. **2008**. TMEM16A confers receptor-activated calcium-dependent chloride conductance. *Nature* **455**, 1210-1215.

Yoon GM, Dowd PE, Gilroy S, McCubbin AG. **2006**. Calcium-dependent protein kinase isoforms in Petunia have distinct functions in pollen tube growth, including regulating polarity. *Plant Cell* **18**, 867-878.

Zhang WH, Ryan PR, Tyerman SD. **2004a**. Citrate-permeable channels in the plasma membrane of cluster roots from white lupin. *Plant Physiol* **136**, 3771-3783.

Zhang WH, Walker NA, Patrick JW, Tyerman SD. **2004b**. Pulsing Cl^- channels in coat cells of developing bean seeds linked to hypo-osmotic turgor regulation. *J Exp Bot* **55**, 993-1001.

Zifarelli G, Pusch M. **2007**. CLC chloride channels and transporters: a biophysical and physiological perspective. *Rev Physiol Biochem Pharmacol* **158**, 23-76.

Zimmermann S, Frachisse J, Thomine S, Barbier-Brygoo H, Guern J. **1998**. Elicitor-induced chloride efflux and anion channels in tobacco cell suspensions. *Plant Physiology and Biochemistry* **36**, 665-674.

Zimmermann S, Thomine S, Guern J, Barbier-Brygoo H. **1994**. An anion current at the plasma membrane of tobacco protoplasts shows ATP-dependent voltage regulation and is modulated by auxin. *The Plant Journal* **6**, 707–716.

Zonia L, Cordeiro S, Tupy J, Feijo JA. **2002**. Oscillatory chloride efflux at the pollen tube apex has a role in growth and cell volume regulation and is targeted by inositol 3,4,5,6-tetra*kis*phosphate. *Plant Cell* **14**, 2233-2249.

Zonia L, Munnik T. **2004**. Osmotically induced cell swelling versus cell shrinking elicits specific changes in phospholipid signals in tobacco pollen tubes. *Plant Physiol* **134**, 813-823.